General Disclaimer

One or more of the Following Statements may affect this Document

- This document has been reproduced from the best copy furnished by the organizational source. It is being released in the interest of making available as much information as possible.

- This document may contain data, which exceeds the sheet parameters. It was furnished in this condition by the organizational source and is the best copy available.

- This document may contain tone-on-tone or color graphs, charts and/or pictures, which have been reproduced in black and white.

- This document is paginated as submitted by the original source.

- Portions of this document are not fully legible due to the historical nature of some of the material. However, it is the best reproduction available from the original submission.

NASA-CR168077

[redacted]

APRIL 1983

[redacted]

FINAL REPORT

FOR

PHASED ARRAY-FED ANTENNA CONFIGURATION STUDY NAS 3-23252

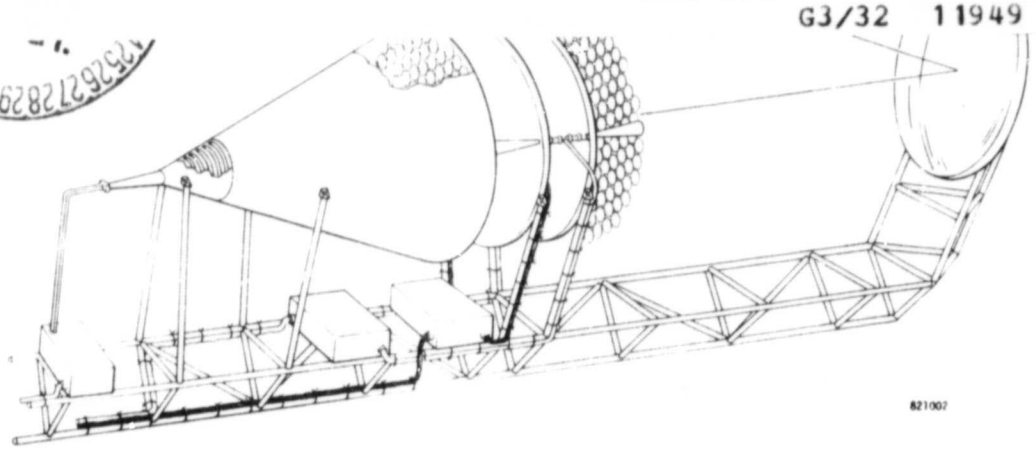

821002

PREPARED FOR

NASA LEWIS RESEARCH CENTER

HARRIS

HARRIS CORPORATION GOVERNMENT ELECTRONIC SYSTEMS DIVISION
P.O. BOX 96000, MELBOURNE, FLORIDA 32901, (305) 727-4000

APRIL 1983

FINAL REPORT

FOR

PHASED ARRAY-FED ANTENNA CONFIGURATION STUDY NAS 3-23252

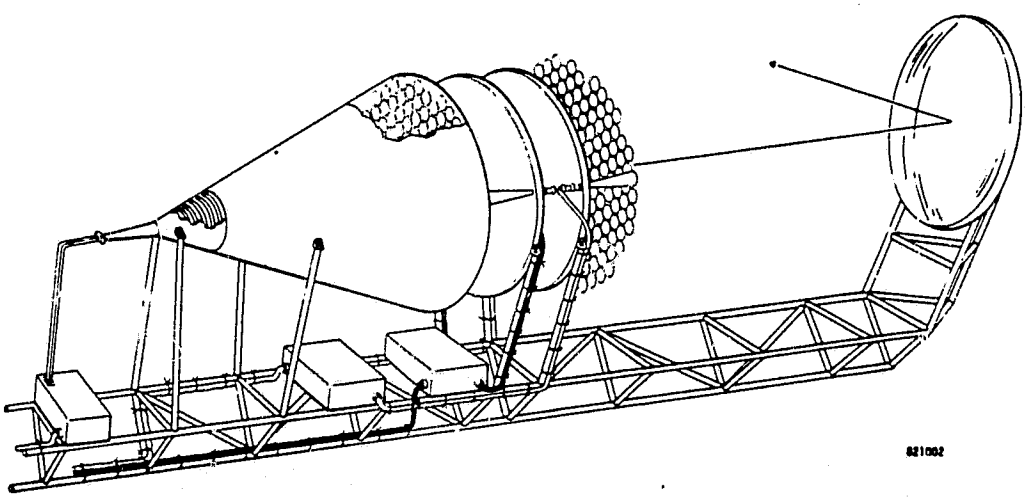

PREPARED FOR

NASA LEWIS RESEARCH CENTER

1. Report No.	2. Government Accession No.	3. Recipient's Catalog No.
CR 168077		

4. Title and Subtitle	5. Report Date
Phased Array-Fed Antenna Configuration Study Final Report	April 1983
	6. Performing Organization Code

7. Author(s)	8. Performing Organization Report No.
W.F. Croswell, D.E. Ball, R.C. Taylor	
	10. Work Unit No.

9. Performing Organization Name and Address	11. Contract or Grant No.
Harris Corporation Government Electronic Systems Division P.O. Box 37 Melbourne, FL 32901	NAS 3-23252
	13. Type of Report and Period Covered

12. Sponsoring Agency Name and Address	14. Sponsoring Agency Code
NASA Lewis Research Center Cleveland, Ohio 44135	

15. Supplementary Notes

16. Abstract

The scope of this contract entails performing a configuration study for a phased array-fed transmit antenna operating in the frequency band of 17.7 to 20.2 GHz. This initial contract provides a basis for understanding the design limitations and advantages of advanced phased array and cluster feeds (both utilizing integral MMIC modules) illuminating folded reflector optics (both near-field and focused types). Design parametric analyses are performed utilizing as constraints the objective secondary performance requirements of the Advanced Communications Technology Satellite (Table 1.0). The output of the study provides design information which serves as a data base for future active phased array-fed antenna studies such as detailed designs required to support the development of a ground tested breadboard.

In general, this study is significant because it provides the antenna community with an understanding of the basic principles which govern near-field phased scanned feed effects on secondary reflector system performance. Although several articles have been written on analysis procedures and results for these systems, the authors of this report have observed phenomenon of near-field antenna systems not previously documented. Because the physical justification for the exhibited performance is provided herein, the findings of this study add a new dimension to the available knowledge of the subject matter. Additionally, unique ways of integrating MMIC modules into the waveguide elements, heat dissipation methods of the modules in the array environment and the total array/element integration problem with bias and control line interfaces is addressed.

17. Key Words (Suggested by Author(s))	18. Distribution Statement
Multiple Beam Antenna Scanning Beam Antenna Phased Array Feed Monolithic Microwave Integrated Circuits	Distribution Unlimited

19. Security Classif. (of this report)	20. Security Classif. (of this page)	21. No. of Pages	22. Price*
Unclassified	Unclassified	157	

* For sale by the National Technical Information Service, Springfield, Virginia 22161

PHASED ARRAY-FED ANTENNA CONFIGURATION STUDY

TABLE OF CONTENTS

TABLE OF CONTENTS (Continued)

APPENDICES

1.0 INTRODUCTION

During the last decade, communication satellite technology has been directed predominantly toward expanded use of the existing spectrum 4/6 GHz and 12/14 GHz bands. Market studies performed by ITT and Western Union have shown that these frequency bands, by implementing a higher degree of frequency reuse (where, for example, the expansion is accomplished by providing a large number of beams isolated spacially and by polarization orthogonality), can provide larger amounts of useable spectrum.[1,2] Even though at first sight this appears to be a tenable approach to solving the spectrum saturation problem, the state-of-the-art in spacecraft control and antenna pointing maintainability falls short of allowing such a scheme to be realized in the near term. Hence, by developing 30/20 GHz technology in parallel with the necessary frequency reuse technology, the 30/20 GHz band can be exploited in order to provide the needed bandwidth for an expanded user base.

To date a great amount of activity and resources have been directed toward the development of an EHF communication satellite - the Advanced Communications Technology Satellite - system by the NASA Lewis Research Center. The initial thrust of this work is to develop technology and demonstrate its utility for a system which will ultimately produce 10-18 fixed trunking user beams and 6 customer premise service scanning beams in the 30 GHz receive and 20 GHz transmit bands. The proposed satellite will provide proof-of-concept information by generating 6 fixed beams and 1 scanning beam. Advanced technologies will be used for this system such as TWTA's, IF switch matrices, and others. However, it is envisioned that in the future, the advanced operating systems will utilize antenna subsystems consisting of active phased array feeds with integrated monolithic microwave integrated circuit (MMIC) receive and transmit modules. These modules provide several advantages over conventional TWTA feed systems composed of ferrite phase shifters. They include: (1) fast switching times (10 nanoseconds), which aids in accessing a large number of users via a TDMA scheme, (2) ease of beam trimming to compensate for satellite mispointing phenomena, and (3) graceful failure using a large number of MMIC modules as opposed to a single TWTA. The Base Research and Technology arms of the Advanced Communication Technology

program has been established with one of its goals to explore advanced applications of MMIC modules to future systems applications on spaceborne phased array-fed reflector antennas.

The scope of this contract entails performing a configuration study for a phased array-fed transmit antenna operating in the frequency band of 17.7 to 20.2 GHz. This initial contract provides a basis for understanding the design limitations and advantages of advanced phased array and cluster feeds (both utilizing integral MMIC modules) illuminating folded reflector optics (both near-field and focused types). Design parametric analyses are performed utilizing as constraints the objective secondary performance requirements of the Advanced Communications Technology Satellite (Table 1.0). The output of the study provides design information which serves as a data base for future active phased array-fed antenna studies such as detailed designs required to support the development of a ground tested breadboard.

In general, this study is significant because it provides the antenna community with an understanding of the basic principles which govern near-field phased scanned feed effects on secondary reflector system performance. Although several articles have been written on analysis procedures and results for these systems[3,4], the authors of this report have observed phenomenon of near-field antenna systems not previously documented. Because the physical justification for the exhibited performance is provided herein, the findings of this study add a new dimension to the available knowledge of the subject matter. Additionally, unique ways of integrating MMIC modules into the waveguide elements, heat dissipation methods of the modules in the array environment and the total array/element integration problem with bias and control line interfaces is addressed.

2.0 SYSTEM DESIGN BASELINES

The purpose of this section is to underscore the overall antenna system requirements of both the multibeam and scanning beam subsystems, and to make clear all system baseline design assumptions unique to this contract. It is important to note that, even though the multibeam and scanning beam functions may eventually be combined into one antenna system, they shall be considered separately in this study, and likewise, in the remainder of this report.

Table 1.0. Objective Requirements for Multibeam and Scanning Beam Antenna

Beam Configuration		Multibeam	Scanning Beam
Antenna Size		Shuttle	Compatible
Operation Frequency Range (GHz)	-Downlink -Uplink	17.7 - 20.2 27.5 - 30.0	17.7 - 20.2 27.5 - 30.0
Number of Beams	-Operational	10 - 18	6 Beams
Minimum Gain (dB)	-20 GHz -30 GHz	53 56	53 53
Bandwidth (MHz)	-20 GHz -30 GHz	500 500	500 500
Polarization		Linear	Linear
C/I Performance (dB)(1)		30	30
Pointing Accuracy (degrees)	-E & H Plane Polarization	0.02 0.4(2)	0.02 0.4
Power/Beam (EIRP) dBW		52 - 62	67 - 75

(1) Carrier to interference ratio for each beam relative to all other beams.

(2) Degrees rotation from reference (i.e., true satellite vertical or horizontal).

2.1 Objective Requirements and Specifications

Table 1.0 parameters are considered as design goals for the multiple scanning spot beam antenna system. There are to be six transmit beams in one 500 MHz band, operating in the frequency range of 17.7 to 20.2 GHz, each assigned to provide coverage to one of six contiguous sectors covering the continental United States (CONUS), and each independently controlled. These sectors are illustrated in Figure 2.1. Isolation between beams covering different sectors is achieved by spatial separation and polarization diversity. Frequency isolation techniques are to be used only when the above mentioned techniques cannot provide the required isolation.

Every point within a given sector, must fall within the 3 dB beam spot area for at least one beam position. Beam movement within a given sector from one position to another, is accomplished in 10 to 100 nanoseconds, with the dwell time on any one position being programmable between 10 and 100 microseconds. The control system for the scanning beams is able to allow any single beam to be independently sequenced to any one of its positions, with instructions supplied by an onboard computer.

Table 1.0 parameters are also considered as the design goals basis for the multibeam antenna system configuration, a trunking beam service application. A list of coverage sites for both the "ten city coverage" and the "eighteen city coverage" schemes appears in Table 2.1. The numerical order corresponds to the beam coverage priority. The beam-to-beam isolation requirement is to be accomplished via spatial separation, beam shaping, and/or polarization techniques. A multibeam coverage map is shown in Figure 2.2. Again, frequency isolation techniques are to be used only when beam-to-beam isolation cannot be achieved by the previously mentioned techniques.

2.1.1 MMIC Components

The component requirements outlined below are assumed as typical specifications of MMIC components to be used in developing the antenna configurations. These specifications will be used to form the initial design

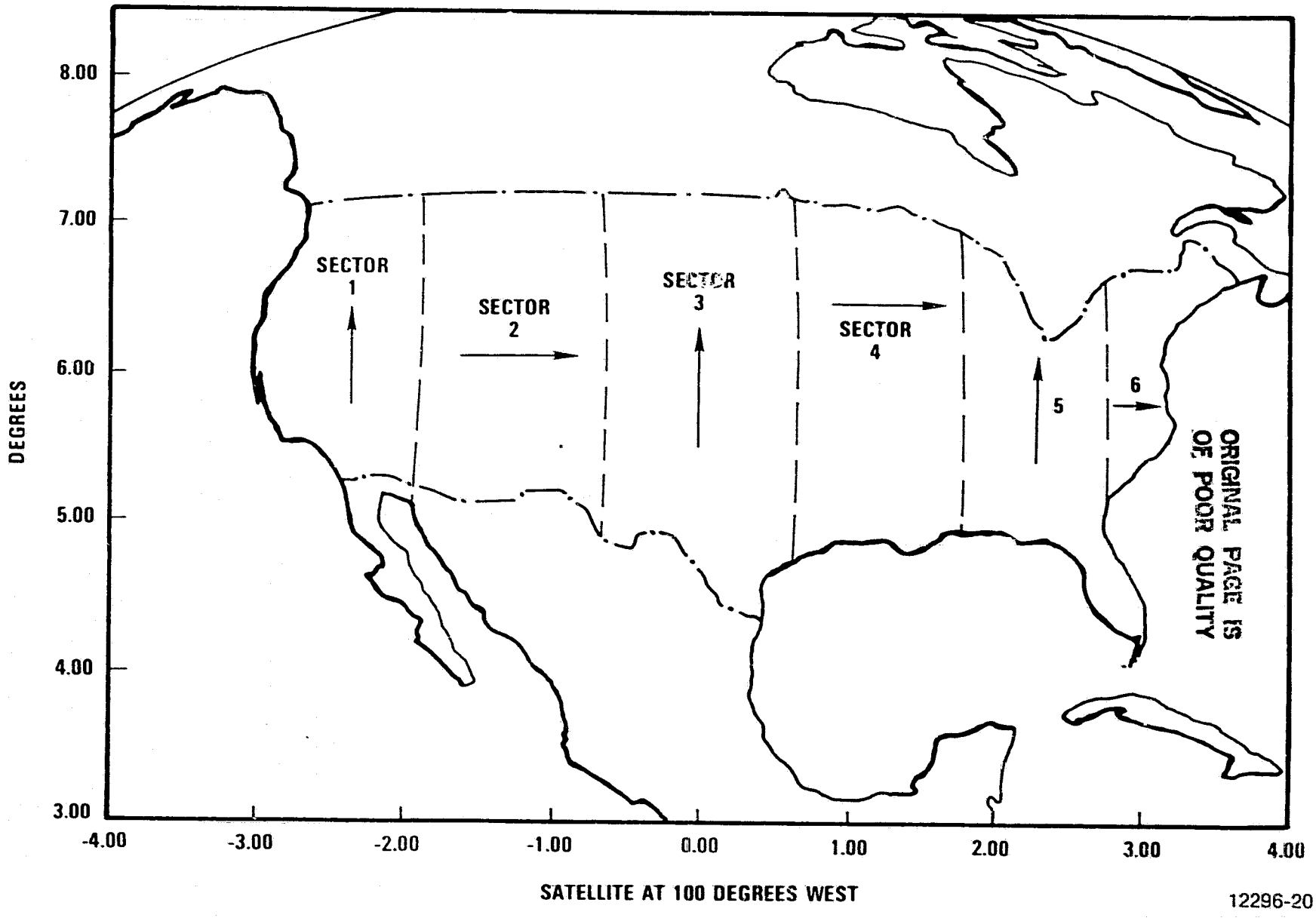

Figure 2.1. A Proposed Multiple Scanning Spot Beam Antenna Coverage Scenario

Table 2.1. Multiple Fixed Spot Beam Antenna Coverage

Spot-Beam Coverage Site	Ten-City Coverage	Eighteen-City Coverage
1. New York City	X	X
2. Washington, DC	X	X
3. Boston, MA		X
4. San Francisco, CA	X	X
5. Seattle, WA		X
6. Chicago, IL	X	X
7. Los Angeles, CA	X	X
8. Denver, CO	X	X
9. Minneapolis, MN	X	X
10. Atlanta, GA	X	X
11. Dallas, TX	X	X
12. Houston, TX	X	X
13. Detroit, MI/Cleveland, OH		X
14. Buffalo, NY/Pittsburgh, PA		X
15. St. Louis, MO		X
16. Phoenix, AZ		X
17. New Orleans, LA		X
18. Miami, FL		X

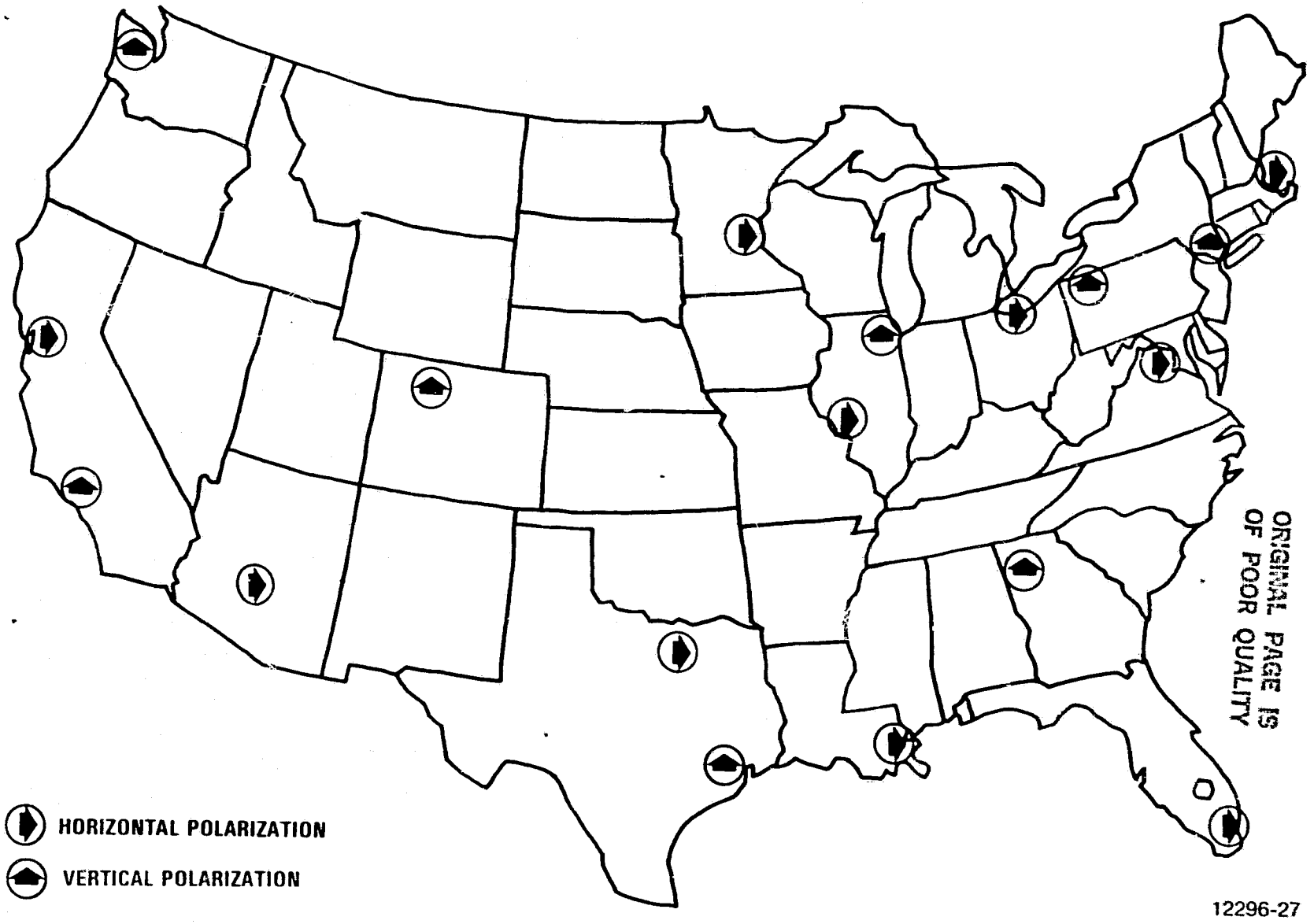

Figure 2-2. Multiple Fixed Spot Beam Coverage Map

point for parametric analysis, the final design point in the four selected configurations, and design concept refinement.

2.1.1.1 Variable Phase Transmit Module

The variable phase transmit module to be used in this study is assumed to have the specifications of Table 2.1.1.1.

The module construction is fully monolithic with no discrete components, wire bonds, or off-chip matching.

The module is designed for high reliability under synchronous orbit environment. Heat removal is by conduction to a heat sink maintained in the range of 0^{o} to $70^{o}C$.

2.1.1.2 Variable Power Amplifier Module

The variable power amplifier (VPA) module used in this study is assumed to have the specifications listed in Table 2.1.1.2.

The module construction is fully monolithic with no discrete components, wire bonds, or off-chip matching.

The module is designed for high reliability under synchronous orbit environment. Heat removal is by conduction to a heat sink maintained in the range of 0^{o} to $70^{o}C$.

2.1.1.3 MMIC Component Breakdown

Component specifications are as outlined in Section 2.1.1. For maximum flexibility in design of the phased array, however, it is assumed that the variable phase transmit module actually consists of two separate physical devices: a variable phase shift (VPS) module and a constant gain amplifier (CGA) module. The phase shift module is assumed to have 3 dB loss; while the constant gain amplifier has 19 dB gain. Thus, the total gain for the modules combined is 16 dB, as specified.

Table 2.1.1.1. Variable Phase Transmit Module

Parameter	Characteristic Value
• Frequency	17.7 - 20.2 GHz
• RF Input/Output Impedance	50 ohms (nominal)
• Input/Output VSWR	$\leq$1.3:1
• RF Output Power	$\geq$0.2 watts @ 1 dB gain compression point
• RF Gain	$\geq$16 dB
• Gain Variation	<1 dB maximum (17.7 - 20.2 GHz) <0.4 dB (over any 500 MHz band)
• Module-to-Module Gain Variation	At any given frequency, <0.5 dB between modules measured against the RMS average for all modules at that frequency
• Power Added Efficiency	$\geq$15% defined as follows: $\text{Efficiency} = \frac{\text{RF Output - RF Input}}{\text{DC Input - Logic Input}}$
• Phase Shifter Levels	5 bits as follows @ band center* 0^0 or $-180^0 \pm 3^0$ 0^0 or $-90^0 \pm 3^0$ 0^0 or $-45^0 \pm 3^0$ 0^0 or $-22.5^0 \pm 3^0$ 0^0 or $-11.25^0 \pm 3^0$
• Phase Shift Response Time	$\leq$10 nanoseconds
• Group Delay Variation	$\leq$0.2 nanoseconds peak-to-peak in any 0.5 MHz portion of the operating band

*Total phase shift is proportional to frequency in the operating band with phase error $\leq 6^0$.

Table 2.1.1.2. Variable Power Amplifier Module

Parameters	Characteristic Value
• Frequency	17.7 - 20.2 GHz
• RF Input/Output Impedance	50 ohms (nominal)
• Input/Output VSWR	≤1.3:1
• RF Output	Nominal Output Power (mW) / Minimum Gain (dB) / Efficiency (%) State 500 / 20 / 15 125 / 14 / 12 50 / 10 / 9 12.5 / 4 / 6 0 / maximum dissipation: 50 mW
• Amplitude Control	Digitally controlled providing the five output state listed above
• Amplitude Control Response Time	≤10 nanoseconds
• Number of Control Lines	≤4
• Control Line Impedance and Voltage Level	TTL Compatible
• Control Line Input Signal	Continuously available during dwell periods
• Group Delay Variation	≤0.2 nanoseconds peak-to-peak in any 0.5 MHz portion of the operating band
• Linearity	Third order intermodulation products ≤20 dBC
• Amplitude/Phase Isolation	Phase shift shall not vary by more than $\pm 5^{0}$ in response to change in amplitude state

2.2 Underlying Assumptions

Recall, that it is the objective of this study to develop phased array-fed reflector systems for communication satellite multibeam and scanning beam antennas. More specifically, the Advanced Communication Technology Satellite (ACTS) System is selected as the design goal. Several simplifying assumptions are therefore necessary, in order to concentrate more fully on the actual detailed antenna design, and alleviate the need for elaborate satellite system design optimization.

The first of these assumptions, as defined in the statement of work, is that the antenna system is to be operated on a Shuttle-launched satellite, operationally located in geosynchronous orbit at a position of $100^{0} \pm 5^{0}$ west longitude. The spacecraft is assumed to be three axis stabilitzed, with the antenna system occupying no more than 18 cubic meters, and weighing less than 230 kg.

Also provided for use in this study are the geometric parameters of a 3.7-m (12-foot), shuttle compatible, offset parabolic reflector shown in Figure 2.2a, obtained by direct scaling of the antenna configuration in Figure 2.2b, supplied by NASA. It was specified from the outset, that no shaped reflectors were to be used in this phase of the project, and that not more than one subreflector was to be considered. These limitations in reflector optics suggest that two dual-reflector antenna systems be utilized to achieve CONUS coverage for the multiple scanning spot beam system. And since the multibeam and scanning beam functions are considered separately, two additional reflector systems are used for the multiple fixed spot beam service with eighteen beam city coverage.

For scanning beam operation, it is apparent that the sectorization scheme (division of CONUS into six zones) selected must be compatible with this two-antenna assumption, i.e., three sectors in the eastern half of CONUS and three in the west. Within each half-CONUS, only two possibilities exist, three vertical sectors of approximately equal size, or three horizontal sectors. Since polarization diversity is utilized to achieve maximum beam-to-beam isolation between sectors, i.e., adjacent sectors are

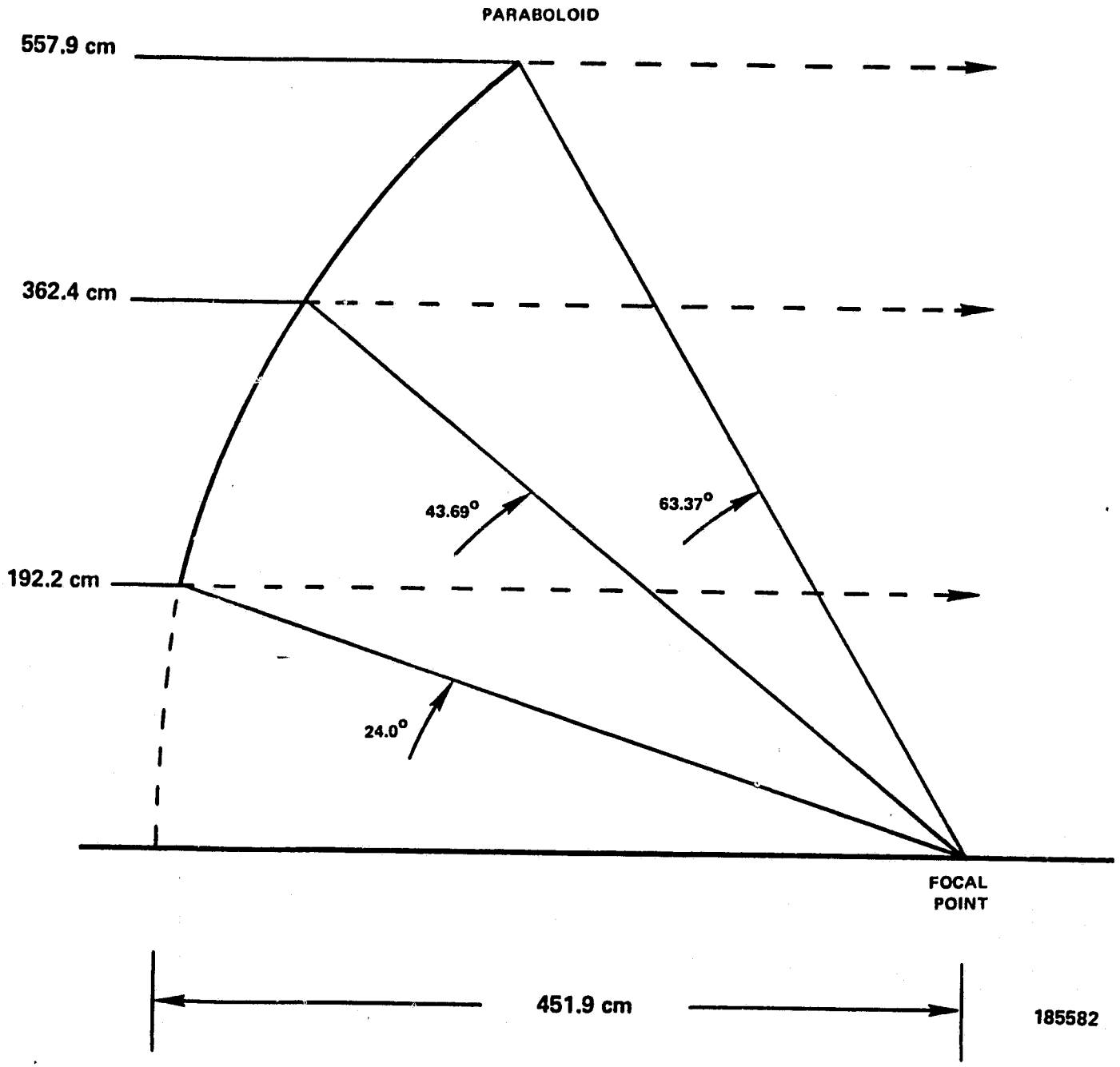

Figure 2.2a. Offset Parabolic Main Reflector Geometry

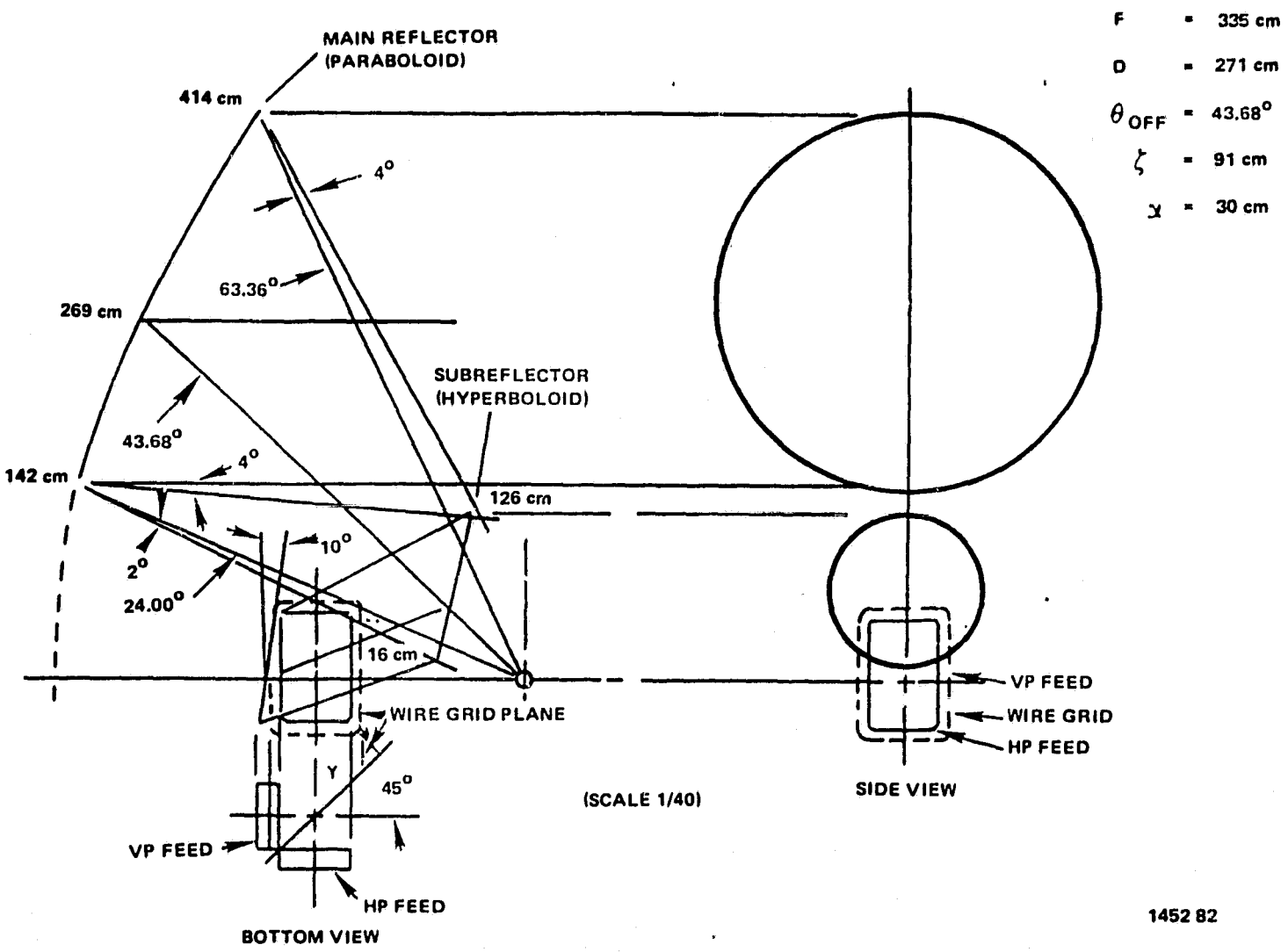

Figure 2.2b. Antenna Configuration for 30/20 GHz Multi-beam Antenna (supplied by NASA)

orthogonally polarized, a sectorization scheme is optimum in this sense when each sector is bounded by, at most, two other sectors. In the horizontal scheme, four sectors meet at one point and polarization diversity alone may not be sufficient to achieve the required isolation. Therefore, the vertical (constant longitude) sectorization scheme is employed.

Antenna boresights, selected to minimize the scan to each point within CONUS, are

38^{o} N. Lat.	110^{o} W. Long.	West Antenna
38^{o} N. Lat.	83^{o} W. Long.	East Antenna

Given these boresight locations, and the vertically-arranged sectorization scheme, CONUS can then be divided into six zones, bounded approximately by the following west longitude values;

124^{o} 114^{o} 103^{o} 94^{o} 86^{o} 78^{o} 70^{o}

where the 94^{o} west longitude line also serves as the east/west CONUS dividing line for the two multibeam trunking antennas. The eighteen cities are arranged as shown in Table 2.2. Cities in sectors 1, 2, and 3 are covered by the west multibeam antenna (7 cities), and cities in sectors 4, 5, and 6 are covered by the east multibeam antenna (11 cities).

3.0 SCANNING BEAM ANTENNA SYSTEM

3.1 Summary of Requirements

For the multiple scanning spot beam system, recall that emphasis in this study is placed on phased array-fed reflector design approaches in dual offset antennas, integrating solid state MMIC amplifier and phase modules into the feed array design. As design goals, the Advanced Communication Technology Satellite System objective requirements, shown again in Table 3.1, have been selected. In accomplishing this, it was considered best to first optimize the reflector geometry, including the overall dimensions of the feed array, and then proceed to the detailed electrical and mechanical design of the phased array.

Table 2.2. Sector/City Locations

124°	114°	103°	94°	86°	78°	70°

Sector 1	Sector 2	Sector 3	Sector 4	Sector 5	Sector 6
San Francisco	Denver	Dallas	Chicago	Atlanta	New York City
Seattle	Phoenix	Houston	Minneapolis	Detroit/ Cleveland	Washington D.C.
Los Angeles			St. Louis		Boston
			New Orleans	Miami	
				Buffalo/ Pittsburgh	

Table 3.1

Beam Configuration		Multibeam	Scanning Beam
Antenna Size		Shuttle Compatible	
Operation Frequency Range (GHz)	-Downlink -Uplink	17.7 - 20.2 27.5 - 30.0	17.7 - 20.2 27.5 - 30.0
Number of Beams	-Operational	10 - 18	6 Trans
Minimum Gain (dB)	-20 GHz -30 GHz	53 56	53 53
Bandwidth (MHz)	-20 GHz -30 GHz	500 500	500 500
Polarization		Linear	Linear
C/I Performance (dB)(1)		30	30
Pointing Accuracy (degrees)	-E & H Plane Polarization	0.02 0.4(2)	0.02 0.4
Power/Beam (EIRP) dBW		52 - 62	67 - 75

(1) Carrier to interference ratio for each beam relative to all other beams.

(2) Degrees rotation from reference (i.e., true satellite vertical or horizontal).

In conformance with this approach and the statement of work, a parametric study of possible reflector geometries was conducted, resulting in the selection of an initial point design reflector system configuration. Utilizing this geometry, two integrated feed/reflector systems are recommended for further study and detailed design. The remainder of the study focuses attention on the hardware design and implementation of these phased array feeds.

3.2 Selection of Reflector Type

Before a parametric study of reflector geometries can be accomplished, it is necessary to choose a generic type of reflector optics. Restrictng this selection, are the assumptions outlined previously, that is, an offset parabolic main reflector, 3.7M (12 feet) in diameter, no shaped reflector surfaces, and not more than one subreflector.

Close inspection of the objective requirements of Table 3.1, results in the elimination of several generic reflector candidates. Notice that the single difference between the multibeam and scanning beam far field transmit performance requirements is EIRP. Each of the six transmit scanning beams must radiate 67 to 75 dBW. This is due to the fact that many users rely on small aperture, low gain ground terminal antennas, as opposed to the high gain trunking beam city coverage antennas. Recalling that the maximum nominal output power level of the variable power amplifier (VPA) module is 500 mW, and that the gain specification of the reflector system is 53 dB, it becomes readily apparent that a very large number of radiating feed elements (one VPA per element) is needed for each beam to meet the high EIRP specification. This large number of elements implies an electrically large feed aperture. Simple calculations readily show, that for the reflector geometries considered, the subreflector is in the near-field of this electrically large phased array, and is in fact, within the Rayleigh distance, R, given by

$$R = \frac{0.5\ D^2}{\lambda}$$

Recall, that in the near-field of an antenna, and in particular, a phased array feed, the propagating phase front is best characterized as a pseudo-plane wave, diametric in character to a spherically expanding phase front in the far field. This fact suggests a deviation from traditional focused optics.

A review of reflector optics reveals two possible "unfocused", or near-field, generic types of dual offset reflector antennas. These reflector systems, shown in Figure 3.2, are known as the near-field Gregorian, and the near-field Cassegrain, offset reflector antennas. Both consist of a parabolic main reflector and a confocal parabolic subreflector, and are commonly referred to as imaging reflector systems. The Gregorian configuration suffers from the fact that the subreflector is located below the symmetric axis of the main parent paraboloidal reflector, and results in a less compact design than the Cassegrain. Also, the Gregorian requires longer transmission line runs from the feed array to the satellite, because the feed is located further from the vertex of the main reflector. Considering these facts, and possible future integration of the scanning beam and multibeam antennas, the offset near-field Cassegrain antenna is selected as the generic reflector type.

3.3 Scanning Spot Beam Design Procedure

In the design of a multiple scanning spot beam antenna utilizing an offset near-field Cassegrainian reflector system, it becomes necessary to relate the far field objective requirements of the antenna system to physical dimensions of the feed array and subreflector. A procedure is outlined here which assists the engineer in this design, assuming the use of a 3.7-m (12-foot) offset main reflector.

Recall, that a near-field Cassegrain antenna, offset or symmetric, can be thought of as an imaging reflector system, i.e., a magnified image of the feed array aperture distribution is produced in the aperture of the secondary reflector, where the magnification factor is given by the ratio of main reflector to subreflector focal lenghts. Alternatively, this system could be thought of as transforming a planar wavefront, incident on the subreflector from a direction parallel to the symmetric axis of the

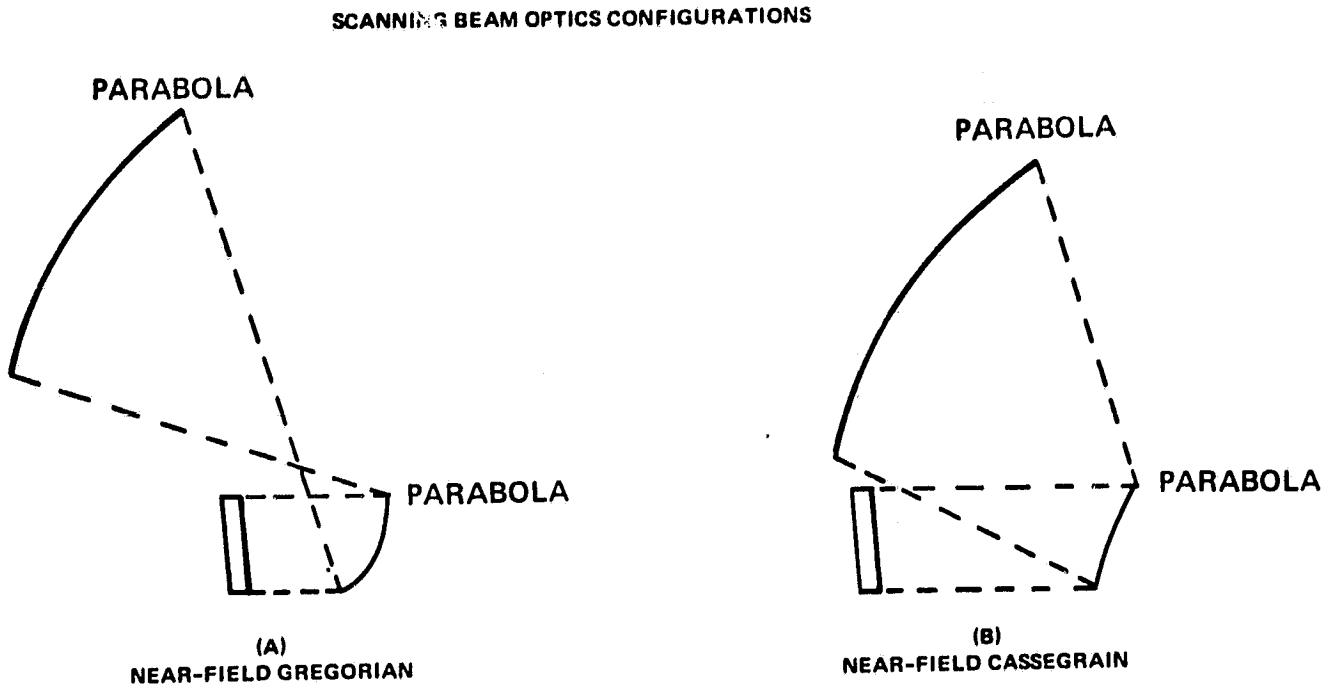

Figure 3.2. Scanning Beam Optics Configurations

paraboloids of revolution, into a plane wave in the secondary aperture. For this design procedure, it is assumed that the reflector system ideally transforms this feed aperture distribution, in both amplitude and phase, to the secondary aperture, or in other words, the antenna is considered to be a perfect imaging reflector system. Based on this assumption, it is now possible to directly relate the far field beam requirements within the coverage sector to physical dimension criteria on the aforementioned magnified image of the feed-array, henceforth referred to as the aperture array, shown in Figure 3.3.

Consider a sector coverage area of approximately 3.5^{0} in elevation and 1.25^{0} in azimuth as viewed from the satellite in geosynchronous orbit. It is desirable for each point, or ground terminal, in the sector to lie within the 3 dB beam spot area of each individual element in the aperture array. This criterion is imposed so that each element in the array will constructively contribute to all of the far field spot beams within the scan sector. It does, however, imply an inherent 3 dB loss in gain at the edge of the sector for a scanned spot beam relative to the on-focus beam. This can be readily shown by a calculation of the array pattern using pattern multiplication and the array factor. To achieve less gain loss, e.g., 1 dB gain loss imposing a 1 dB sector edge illumination requirement, would require many more elements, complicating hardware implementation and heat dissipation. This is discussed further in Section 3.6. Assuming the use of circular aperture elements, and given that the 3 dB beamwidth of a uniformly illuminated circular aperture of diameter D is

$$\theta_{BW} = 58.5 \frac{\lambda}{D} ,$$

the maximum aperture array element diameter becomes

$$D_{EL} = 16.7 \lambda$$
$$D_{AZ} = 46.8 \lambda .$$

Since circular, rather than rectangular, aperture elements are assumed, the more stringent diameter criterion dictates the aperture array element diameter. Recalling that a 3.7M (12 foot) (243 λ @ 20 GHz) diameter circular aperture array is required, and that the individual element diameter is 16.7 λ, the minimum number of elements required to achieve the far field scan coverage is found to be approximately 177.

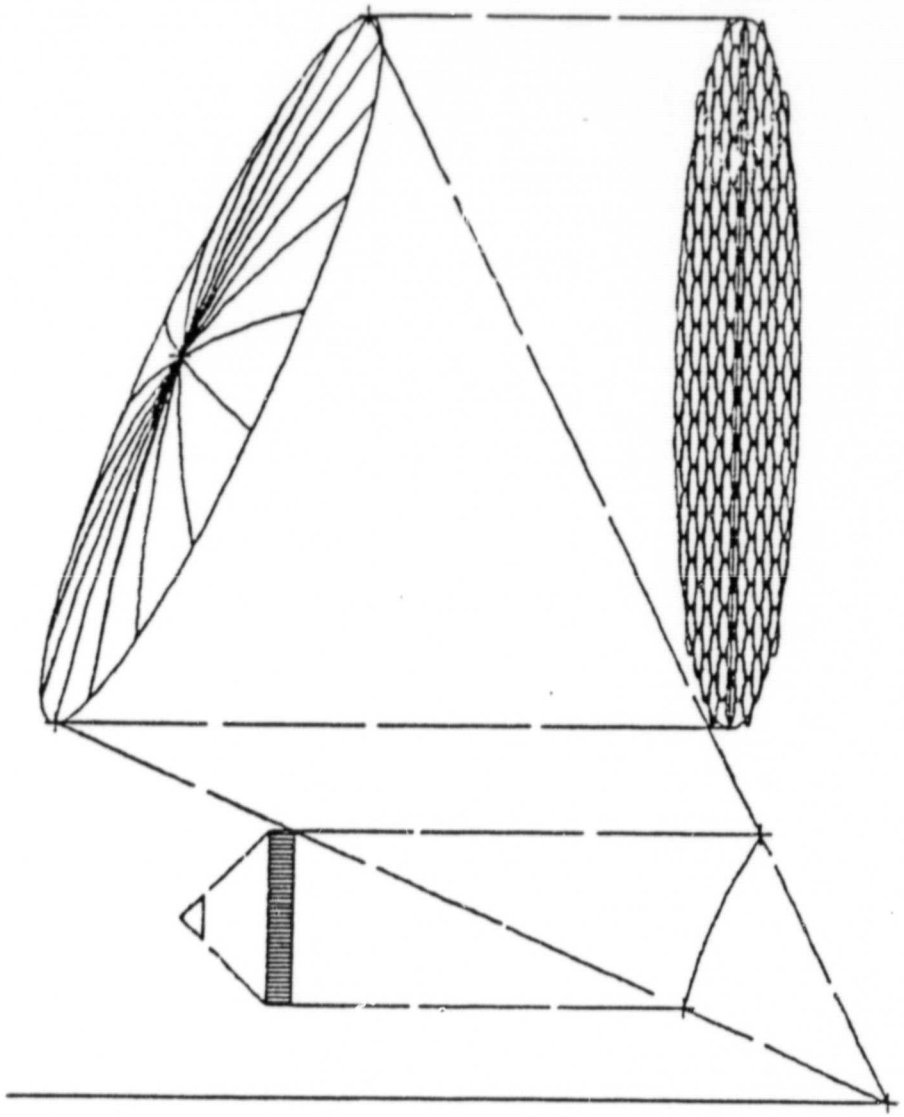

1453 82

Figure 3.3. Offset Near-Field Cassegrain Geometry Showing Aperture Array

The actual feed array size and element spacing is determined directly from the aperture array size and element spacing through the magnification factor M, where

$$M = \frac{\text{main reflector focal length}}{\text{subreflector focal length}} .$$

Since the feed array and subreflector are of approximately equal diameter, the selection of magnification factor M uniquely determines the feed array size.

3.4 Parametric Analysis

A parametric study was performed to optimize the offset near-field Cassegrain reflector geometry. Five configurations were selected, as shown in Figure 3.4, providing a sufficient data base from which to choose a geometry for further investigation, and gain insight into the trade-offs involved in the design of the scanning beam antenna system. These five antenna configurations were obtained by varying the geometric input parameters of Table 3.4-1, shown numerically in Table 3.4-2. The data base is generated through a calculation of the output parameters of Table 3.4-1 for each of the five geometries.

3.5 Analytical Approach

Offset near-field Cassegrain reflector antenna systems for spaceborne satellite applications are still in the early stages of development, and as such, very little if any attention has been devoted to them in the literature. Also, computer software for the analysis of these antenna systems was not available at the start of this study. Significant development effort was therefore put forth in this area.

Two new computer codes now exist at Harris Corporation for the far field radiation pattern prediction of offset near-field Cassegrain antennas. The first, is a very fast, efficient design tool utilizing geometrical optics raytracing techniques combined with the aperture integration (AI) method. The second, is a more sophisticated, and more accurate reflector antenna analysis code also utilizing the raytracing techniques of geometrical optics with a

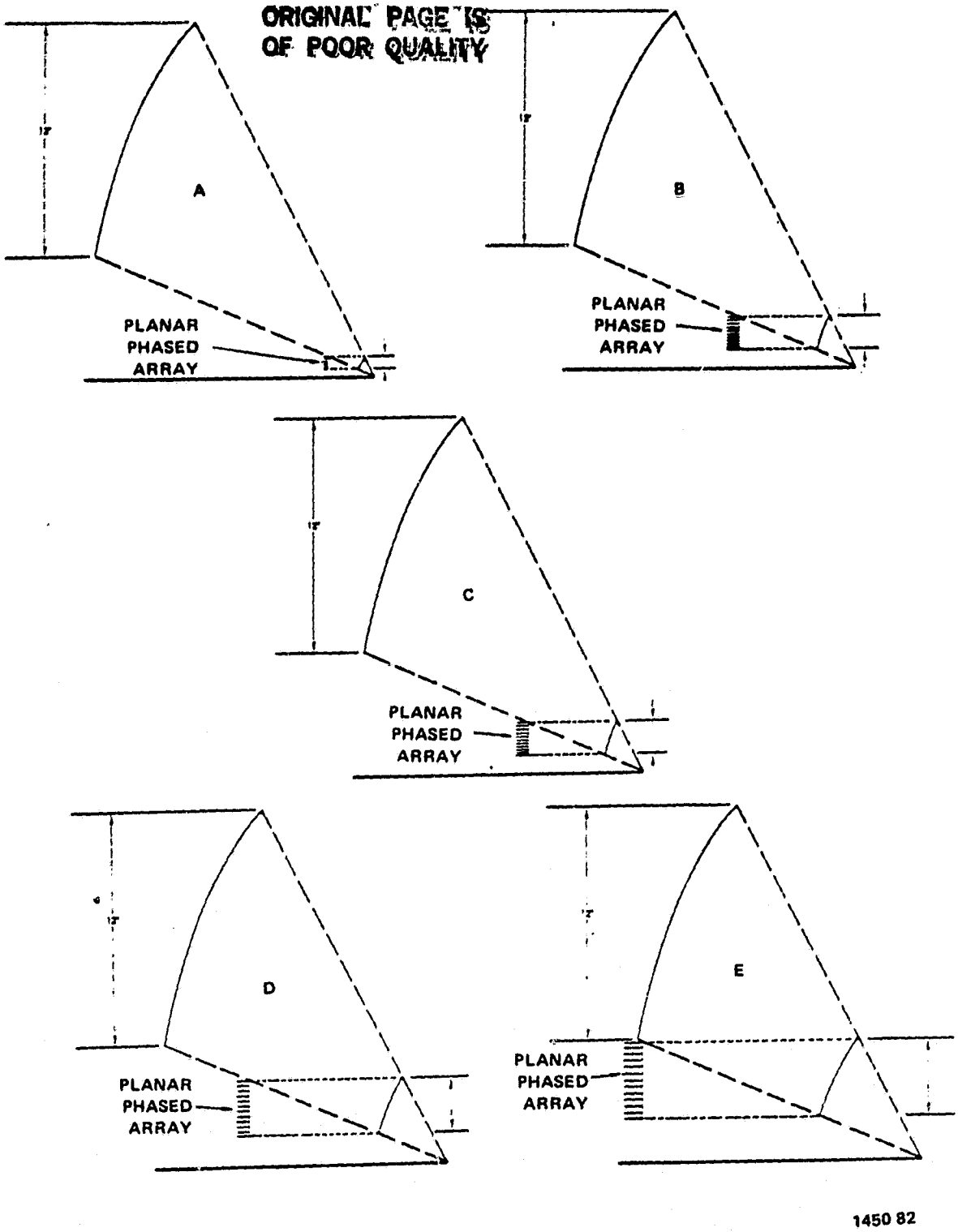

Figure 3.4. Offset Near-Field Cassegrain Configurations

Table 3.4-1. Input and Output Parameters for the Parametric Analysis

Input Parameters	Output Parameters
Main Reflector Diameter	Gain
Main Reflector F/D	Sidelobe Level
Main Reflector Offset	Bandwidth
Subreflector Diameter	Efficiency (under illumination, spillover)
Subreflector Focal Points	Crosspolarization
Subreflector Curvature	
Array Size (area)	
Array Gain (or beamwidth)	
Physical Orientation (array & reflectors)	
Phase Resolution (of monolithic module)	
Amplitude Resolution (of monolithic module)	
No. of Beams (scanning beam)	
No. of Beams (multibeam)	

Table 3.4-2. Range of Parametric Analysis Input Parameters

	Subreflector Diameter	Mag Factor	Subreflector F/D	Focal Length
A	22.86 cm (9")	16	0.405	28.2 cm (11.1")
B	45.72 cm (18")	8	0.405	56.4 cm (22.2")
C	68.58 cm (27")	5.3	0.405	84.8 cm (33.4")
D	91.44 cm (36")	4	0.405	113.0 cm (44.5")
E	114.30 cm (45")	3.2	0.405	141.2 cm (55.6")

surface current integration (SCI). Inputs to both include feed array position and orientation, linear or circular polarization sense, feed element radiation pattern, reflector geometry, frequency of operation, and far field pattern specifications.

To circumvent the need for a complete, time-consuming analysis of the near-field of the phased array feed using the well known plane wave spectrum technique, an element-by-element superposition of field is utilized in the secondary aperture for the AI code, and on the surface of the main reflector for the SCI code. Array element weightings, in amplitude and phase, can be applied to each field distribution at this time. A single far field integration is then needed to determine the radiation pattern of the array/reflector system. The superposition technique holds the unique advantage of being readily adaptable to element weighting coefficient optimization as discussed in Section 3.6.1, and has been found to produce very accurate results in the main beam region and over the first few sidelobes. Antenna gain calculated in this way includes the efficiency measures of phase error loss, illumination loss, spillover loss, and cross-polarization loss. Further discussion can be found in Appendix B.

3.6 Results of Parametric Analysis

The five geometric configurations of near-field Cassegrains that are to be analyzed, essentially represent a trade-off study of unfocused optic magnification factors, paralleling a study on the effect of equivalent f/D ratios in traditional Cassegrain reflectors. Recall that the magnification factor of this imaging reflector is defined as the ratio of main reflector diameter to subreflector diameter. Since, in the near-field of the feed array, wave propagation is nearly collimated, the phased array and subreflector are of approximately equal diameter. Knowing the array size and number of elements (found to be 177 based on the far field sector scan requirements), the individual element diameter can be determined. So, given the system magnification factor, the feed array element size is defined, and vice versa. As Figure 3.6-1 shows, for a given array diameter, the number of elements (177) determines the element size (assuming circular aperture elements to minimize coupling effects).

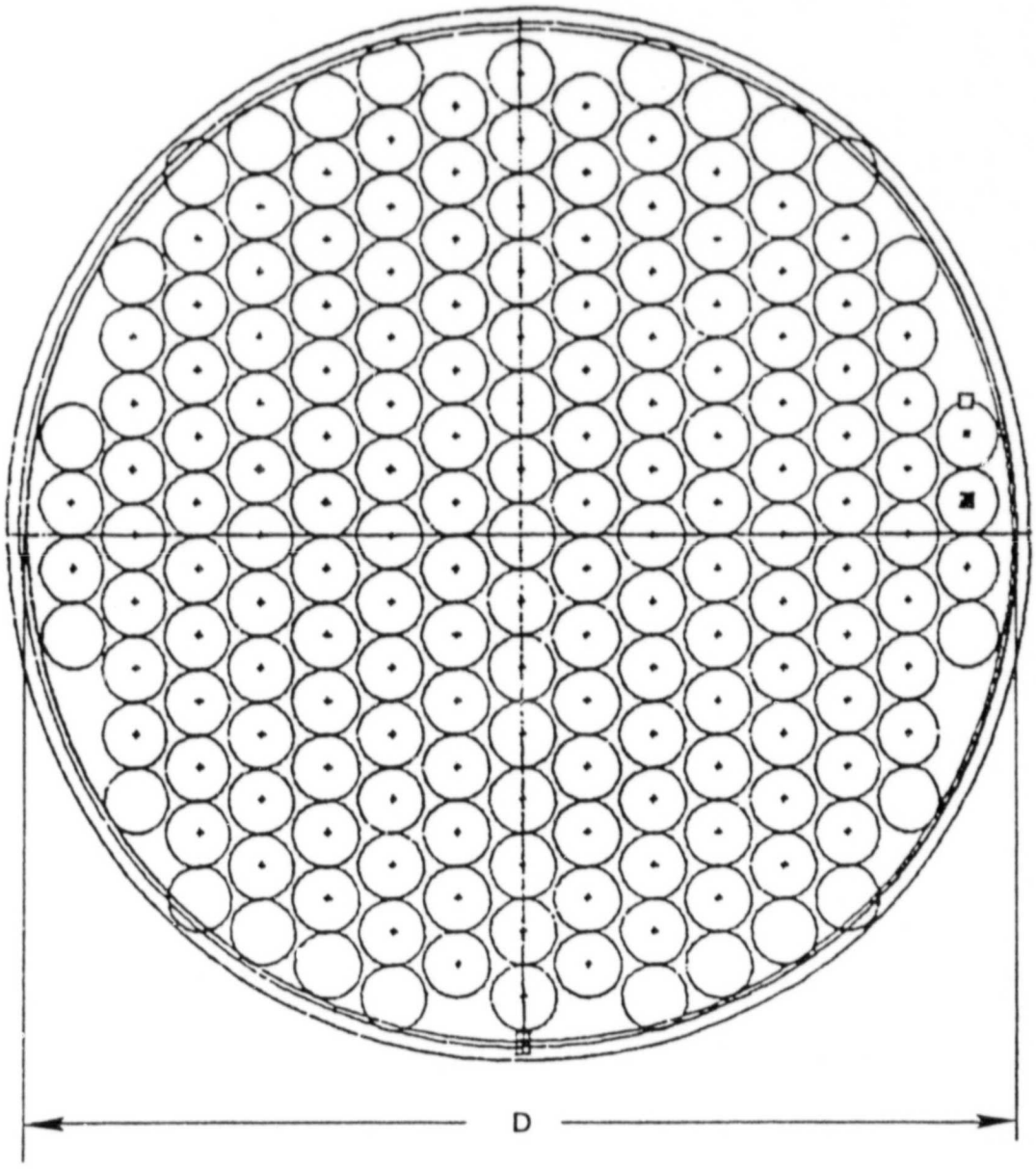

Figure 3.6-1. 177 Phased Array Feed Elements Are Required Based On The Far-Field Sector Scan Criteria

Radiation patterns were calculated on-focus for the five geometries, and are shown in Figures 3.6-2 to 3.6-11. Each element diameter corresponds to a different feed array size and magnification factor as described in Table 3.6. All calculations were made assuming dominant mode conical horns, and a field amplitude weighting distribution for each element proportional to

$$\cos(\pi\rho/D)$$

where ρ is the radial distance to each element, and D is the diameter of the feed array. All elements are assumed to radiate in phase for the calculation of the on-focus patterns, and the frequency of operation is assumed to be 20 GHz.

Gain versus element diameter is plotted in Figure 3.6-12. Notice that the gain of the reflector system decreased as element diameter, and correspondingly element spacing, increased. This is probably due to primary spillover. Cross polarization levels, shown in Figure 3.6-13, are found to be well below the specification of 30 dB, and does not appear to be a significant problem.

Table 3.6. Element Size Versus System Magnification Factors

Reflector Geometry	Feed Element Diameter	Array Diameter	System Magnification
A	1λ	22.6 cm (8.9")	16
B	2λ	45.0 cm (17.7")	8
C	3λ	67.6 cm (26.6")	5.3
D	4λ	89.9 cm (35.4")	4
E	5λ	112.5 cm (44.3")	3.2

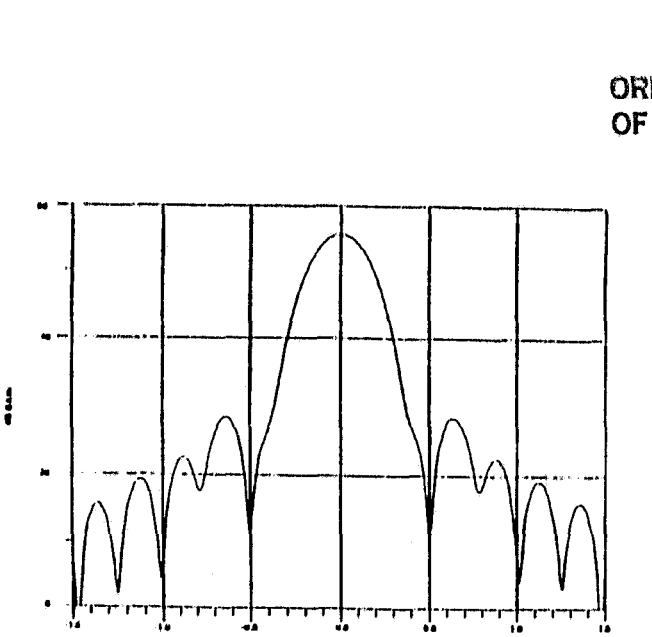

NEAR-FIELD CASSEGRAIN GEOMETRY ON FOCUS CO-POL FAR FIELD PATTERN
FOR ONE WAVELENGTH DIAMETER CIRCULAR FEED ELEMENTS

Figure 3.6-2

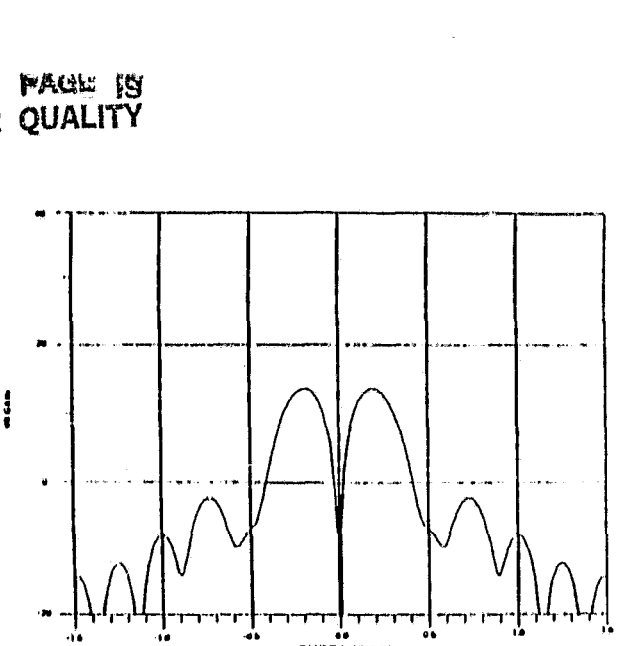

NEAR-FIELD CASSEGRAIN GEOMETRY ON FOCUS CROSS-POL FAR FIELD PATTERN
FOR ONE WAVELENGTH DIAMETER CIRCULAR FEED ELEMENTS

Figure 3.6-3

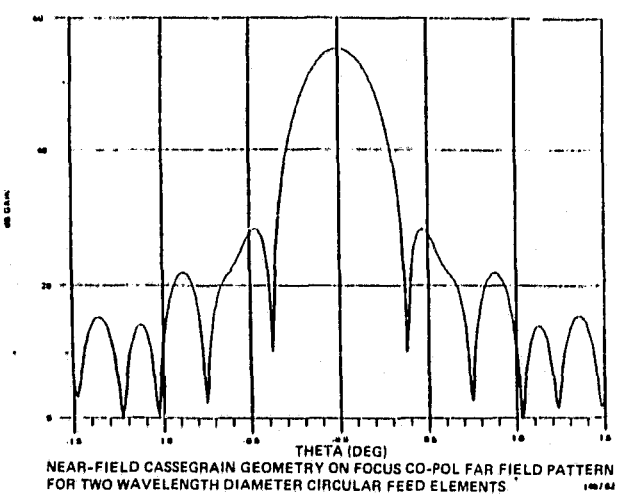

NEAR-FIELD CASSEGRAIN GEOMETRY ON FOCUS CO-POL FAR FIELD PATTERN
FOR TWO WAVELENGTH DIAMETER CIRCULAR FEED ELEMENTS

Figure 3.6-4

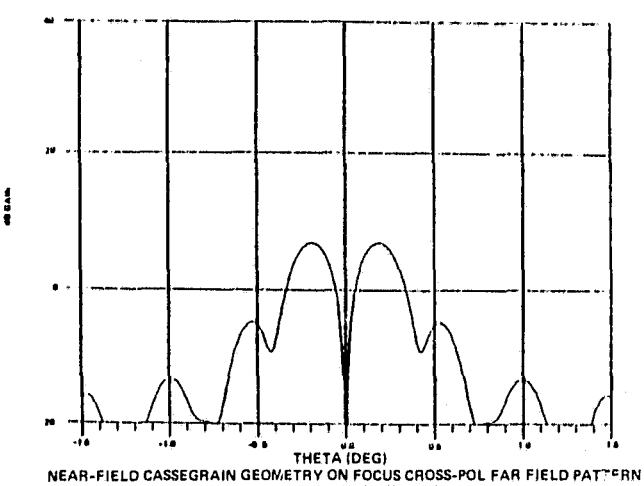

NEAR-FIELD CASSEGRAIN GEOMETRY ON FOCUS CROSS-POL FAR FIELD PATTERN
FOR TWO WAVELENGTH DIAMETER CIRCULAR FEED ELEMENTS

Figure 3.6-5

ORIGINAL PAGE IS
OF POOR QUALITY

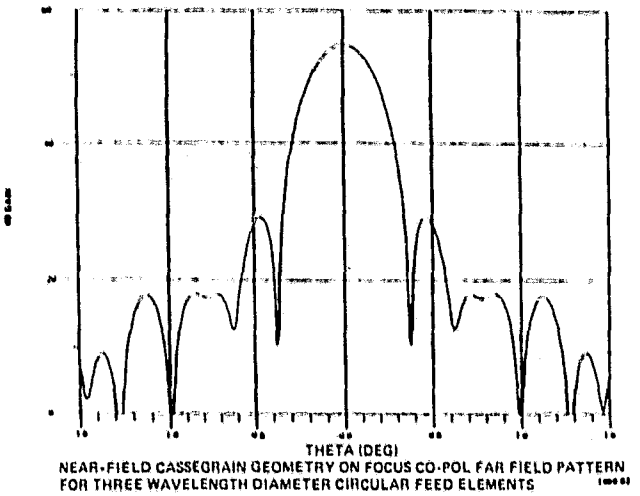

Figure 3.6-6

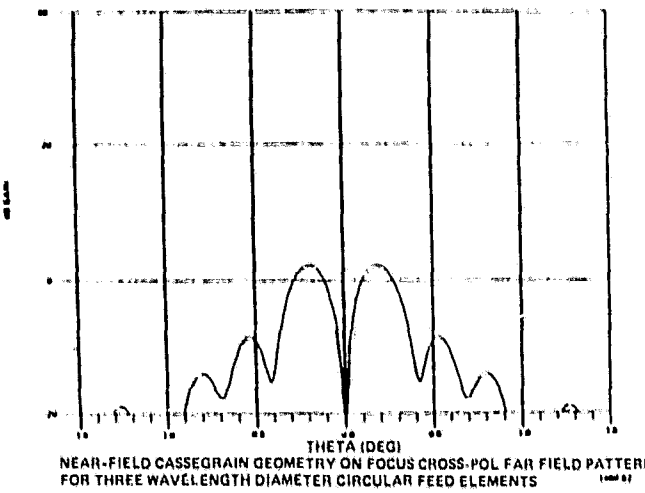

Figure 3.6-7

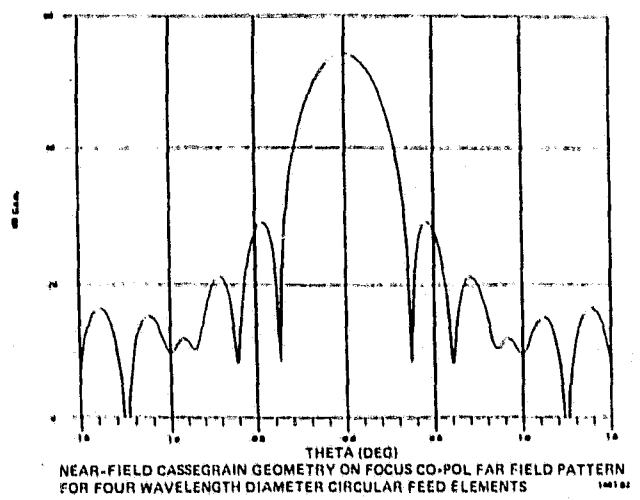

Figure 3.6-8

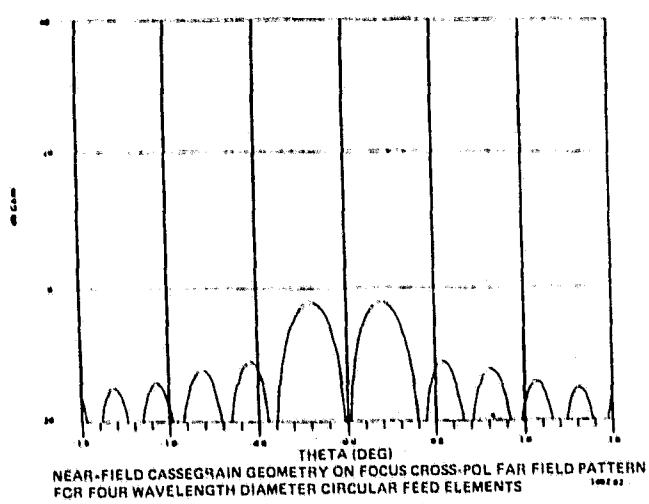

Figure 3.6-9

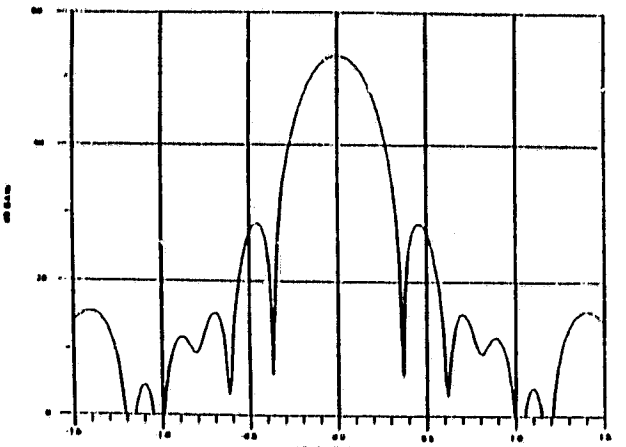

NEAR-FIELD CASSEGRAIN GEOMETRY ON FOCUS CO-POL FAR FIELD PATTERN
FOR FIVE WAVELENGTH DIAMETER CIRCULAR FEED ELEMENTS

Figure 3.6-10

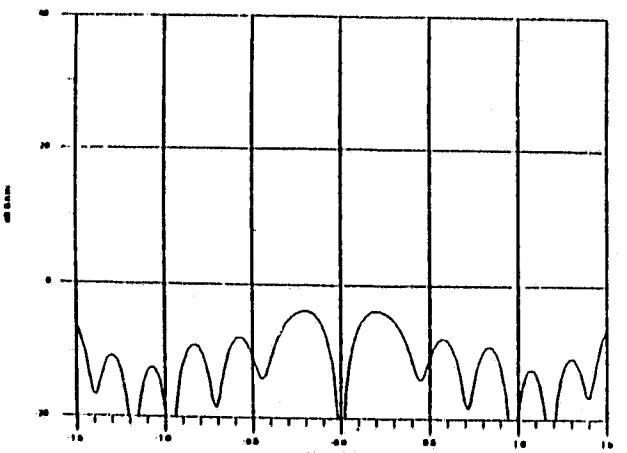

NEAR-FIELD CASSEGRAIN GEOMETRY ON FOCUS CROSS-POL FAR FIELD PATTERN
FOR FIVE WAVELENGTH DIAMETER CIRCULAR FEED ELEMENTS

Figure 3.6-11

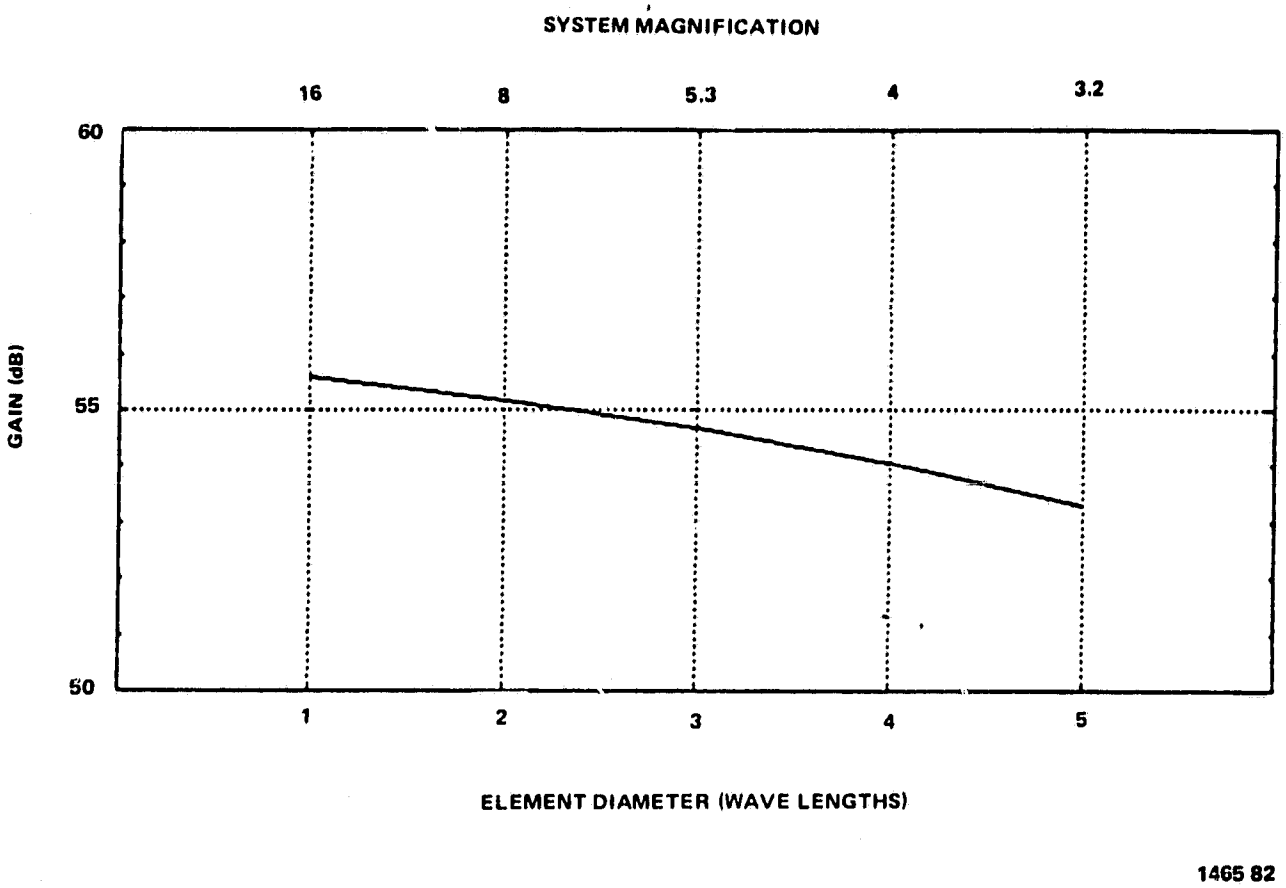

On-focus Gain Vs Element Diameter.
Feed Array Contains 177 Dominant Mode Conical Horns with an Amplitude Weighting Distribution Proportional to COS ($\pi \rho / D$)

Figure 3.6-12.

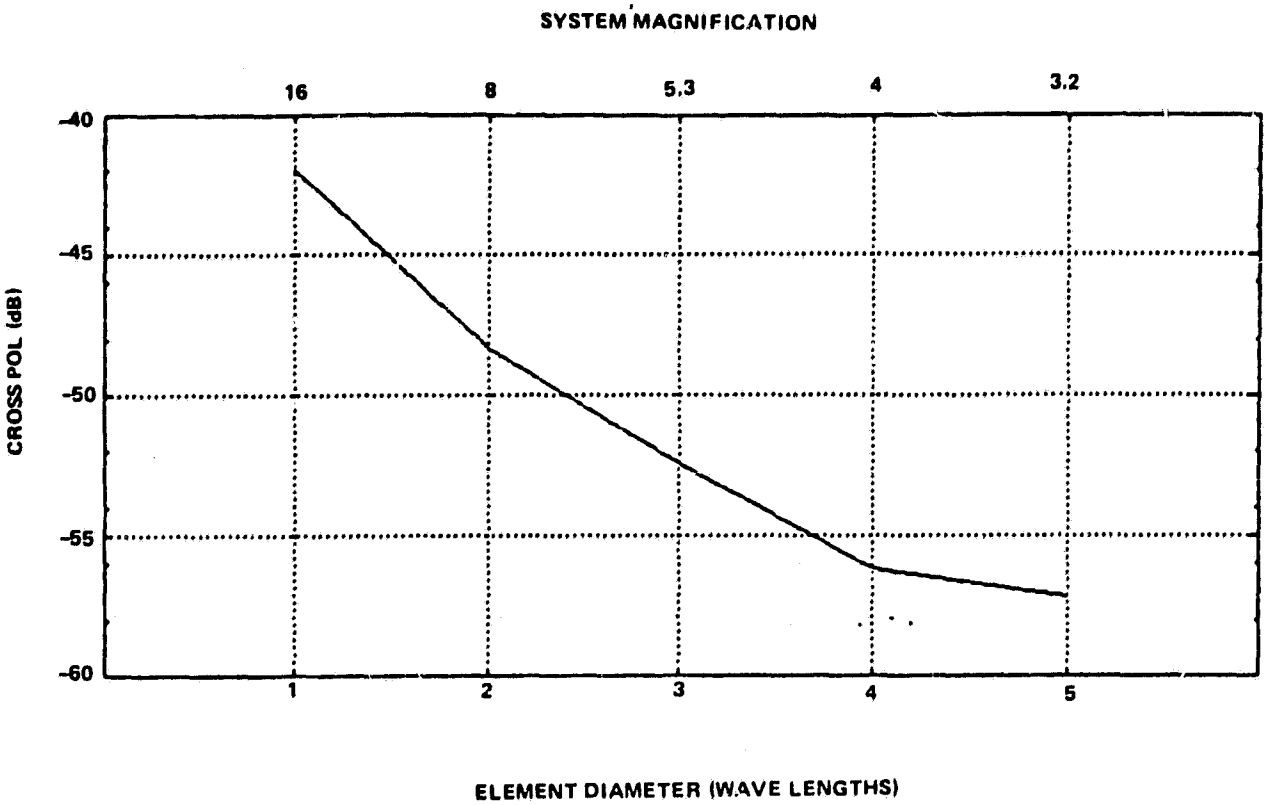

Cross Polarization Levels Vs Element Diameter For An On-focus Beam. Feed Array Contains 177 Dominant Mode Conical Horns with an Amplitude Weighting Distribution Proportional to COS ($\pi \rho / D$)

Figure 3.6-13.

Further insight is gained when radiation patterns are calculated for a typical scan case, say 2-1/2 beamwidths. These patterns are shown in Figures 3.6-14 to 3.6-23, for each of the five configurations under consideration. Loss in gain, relative to the on-focus gain calculated previously, is shown in Figure 3.6-24. Notice that scan loss is in excess of 15 dB, at only 2 1/2 beamwidths of scan, for the configuration with one wavelength elements and magnification factor of 16. In the configurations with lower system magnification, scan loss is much less. Recalling the on-focus gain calculations, it is apparent that non-scanned antenna gain must be sacrificed for superior scan performance. These calculations, it should be pointed out, were made without utilizing the inherent pattern compensation available with the MMIC modules, namely variable amplitude and variable phase element weightings. Improved beam performance can be achieved when these weights are optimized as discussed in Section 3.6.1. It appears, though, that 15 dB scan loss might be beyond the compensatory capabilities of the array modules. Therefore, it seems that lower system magnification (larger elements) is preferred for limited scan performance. However, this implies the use of a large phased array feed. In fact, as the magnification factor approaches unity, the feed array diameter approaches that of the main reflector, significantly increasing the weight of the antenna system. Therefore, in order to most effectively utilize the imaging reflector system and obtain acceptable far field beam performance, the reflector with system magnification of 4 is selected. For this geometry, the loss in gain is minimal at 2-1/2 beamwidths of scan, and the feed array size is not exceedingly large. The selected geometry is therefore, configuration D of Figure 3.4, shown in more detail in Figure 3.6-25, with a feed array and subreflector diameter of approximately 99.4 cm (36 inches).

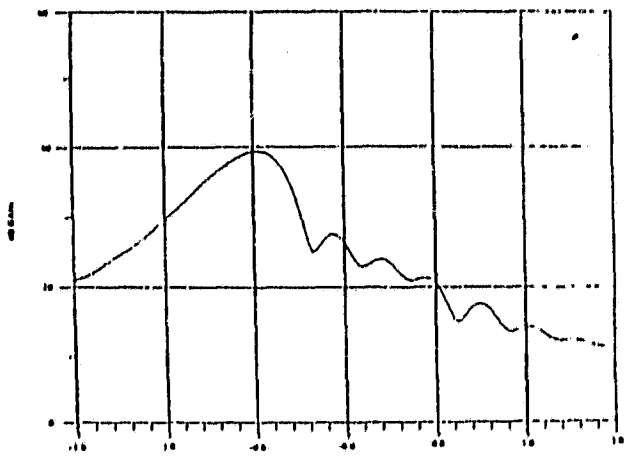

NEAR-FIELD CASSEGRAIN GEOMETRY 2.5 BW SCANNED CO-POL FAR-FIELD PATTERN FOR 1 WAVELENGTH DIAMETER CIRCULAR FEED ELEMENTS

Figure 3.6-14

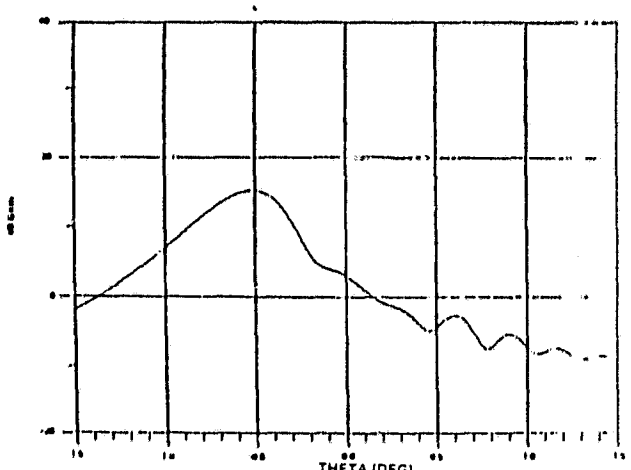

NEAR-FIELD CASSEGRAIN GEOMETRY 2.5 BW SCANNED CROSS-POL FAR FIELD PATTERN FOR 1 WAVELENGTH DIAMETER CIRCULAR FEED ELEMENTS

Figure 3.6-15

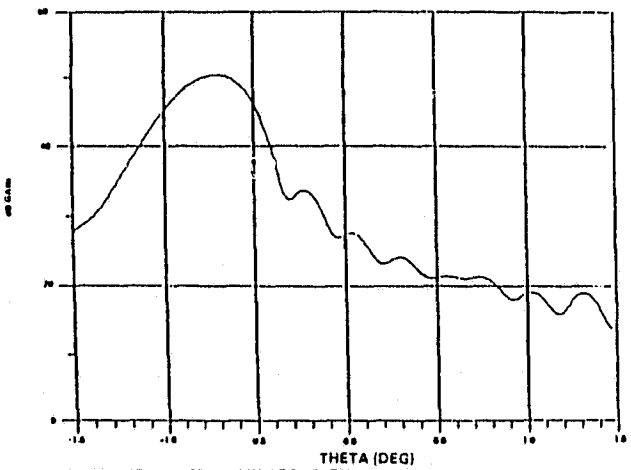

NEAR-FIELD CASSEGRAIN GEOMETRY 2.5 BW SCANNED CO-POL FAR-FIELD PATTERN FOR 2 WAVELENGTH DIAMETER CIRCULAR FEED ELEMENTS

Figure 3.6-16

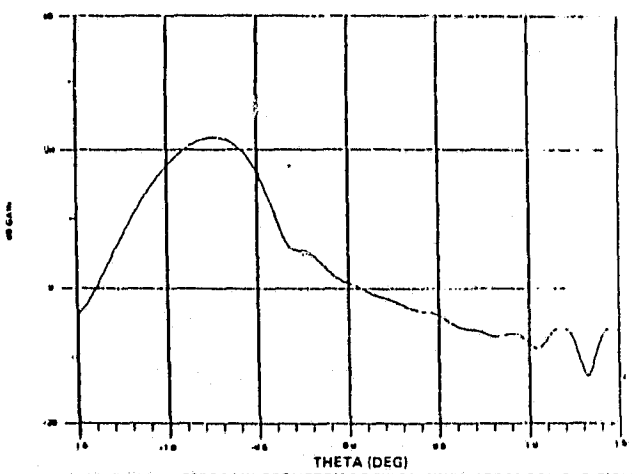

NEAR-FIELD CASSEGRAIN GEOMETRY 2.5 BW SCANNED CROSS-POL FAR FIELD PATTERN FOR 2 WAVELENGTH DIAMETER CIRCULAR FEED ELEMENTS

Figure 3.6-17

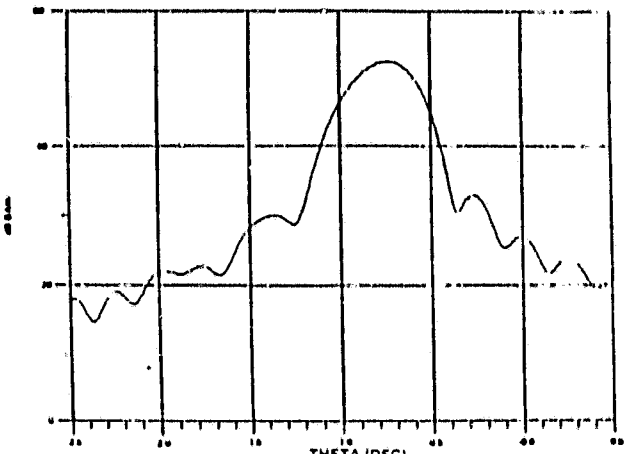

NEAR-FIELD CASSEGRAIN GEOMETRY 2.5 BW SCANNED CO-POL FAR-FIELD PATTERN FOR 3 WAVELENGTH DIAMETER CIRCULAR FEED ELEMENTS

Figure 3.6-18

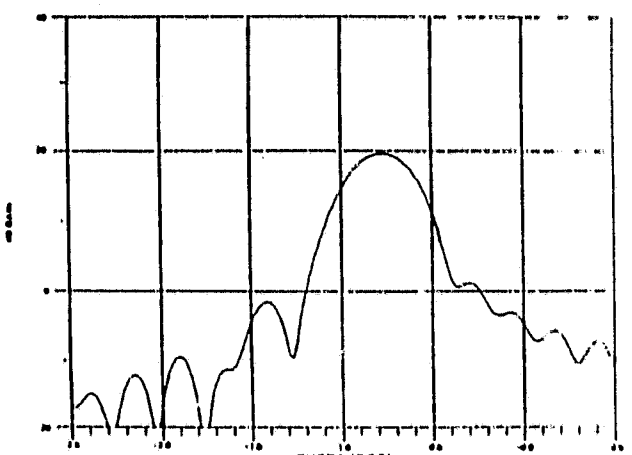

NEAR-FIELD CASSEGRAIN GEOMETRY 2.5 BW SCANNED CROSS-POL FAR FIELD PATTERN FOR 3 WAVELENGTH DIAMETER CIRCULAR FEED ELEMENTS

Figure 3.6-19

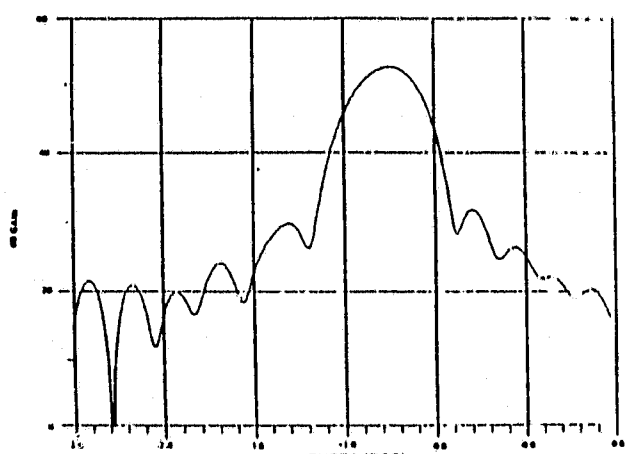

NEAR-FIELD CASSEGRAIN GEOMETRY 2.5 BW SCANNED CO-POL FAR-FIELD PATTERN FOR 4 WAVELENGTH DIAMETER CIRCULAR FEED ELEMENTS

Figure 3.6-20

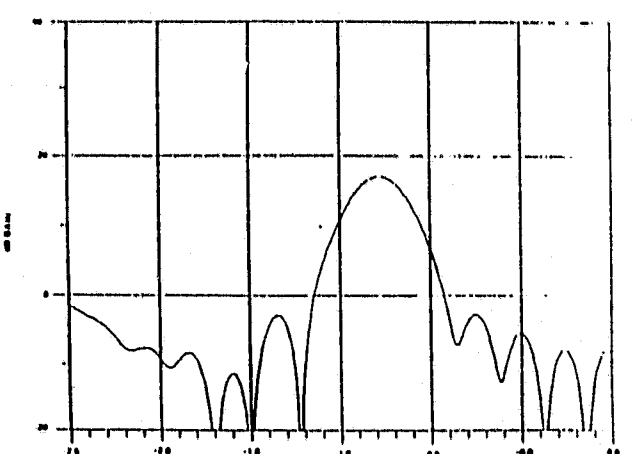

NEAR-FIELD CASSEGRAIN GEOMETRY 2.5 BW SCANNED CROSS-POL FAR FIELD PATTERN FOR 4 WAVELENGTH DIAMETER CIRCULAR FEED ELEMENTS

Figure 3.6-21

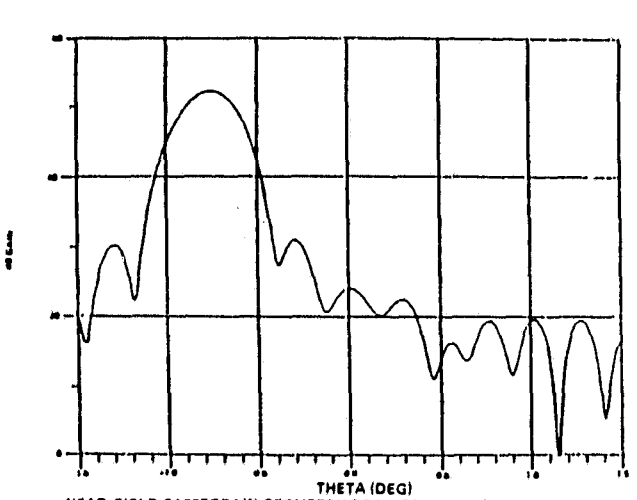

NEAR-FIELD CASSEGRAIN GEOMETRY 2.5 BW SCANNED CO-POL FAR-FIELD PATTERN FOR 5 WAVELENGTH DIAMETER CIRCULAR FEED ELEMENTS

Figure 3.6-22

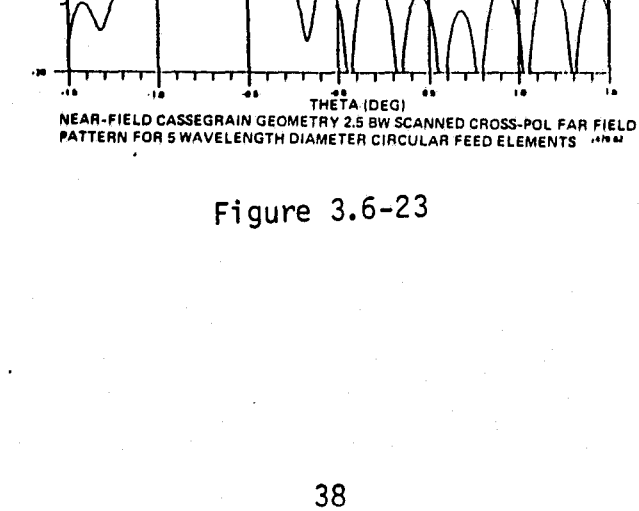

NEAR-FIELD CASSEGRAIN GEOMETRY 2.5 BW SCANNED CROSS-POL FAR FIELD PATTERN FOR 5 WAVELENGTH DIAMETER CIRCULAR FEED ELEMENTS

Figure 3.6-23

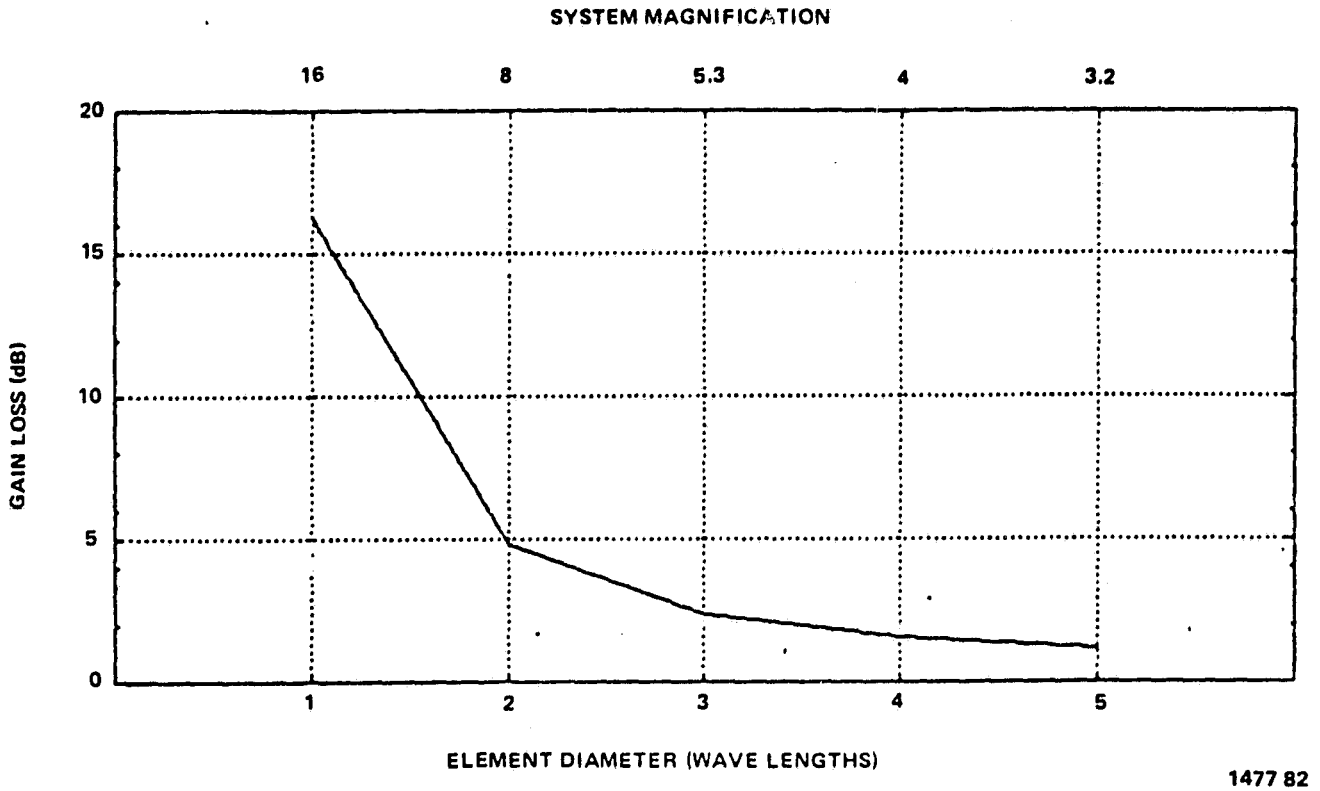

Gain Loss Vs Element Diameter for 2 1/2 Beamwidths Scan.
Feed Array Contains 177 Dominant Mode Conical Horns With An Amplitude Weighting Distribution Proportional to COS ($\pi \rho / D$).

Figure 3.6-24.

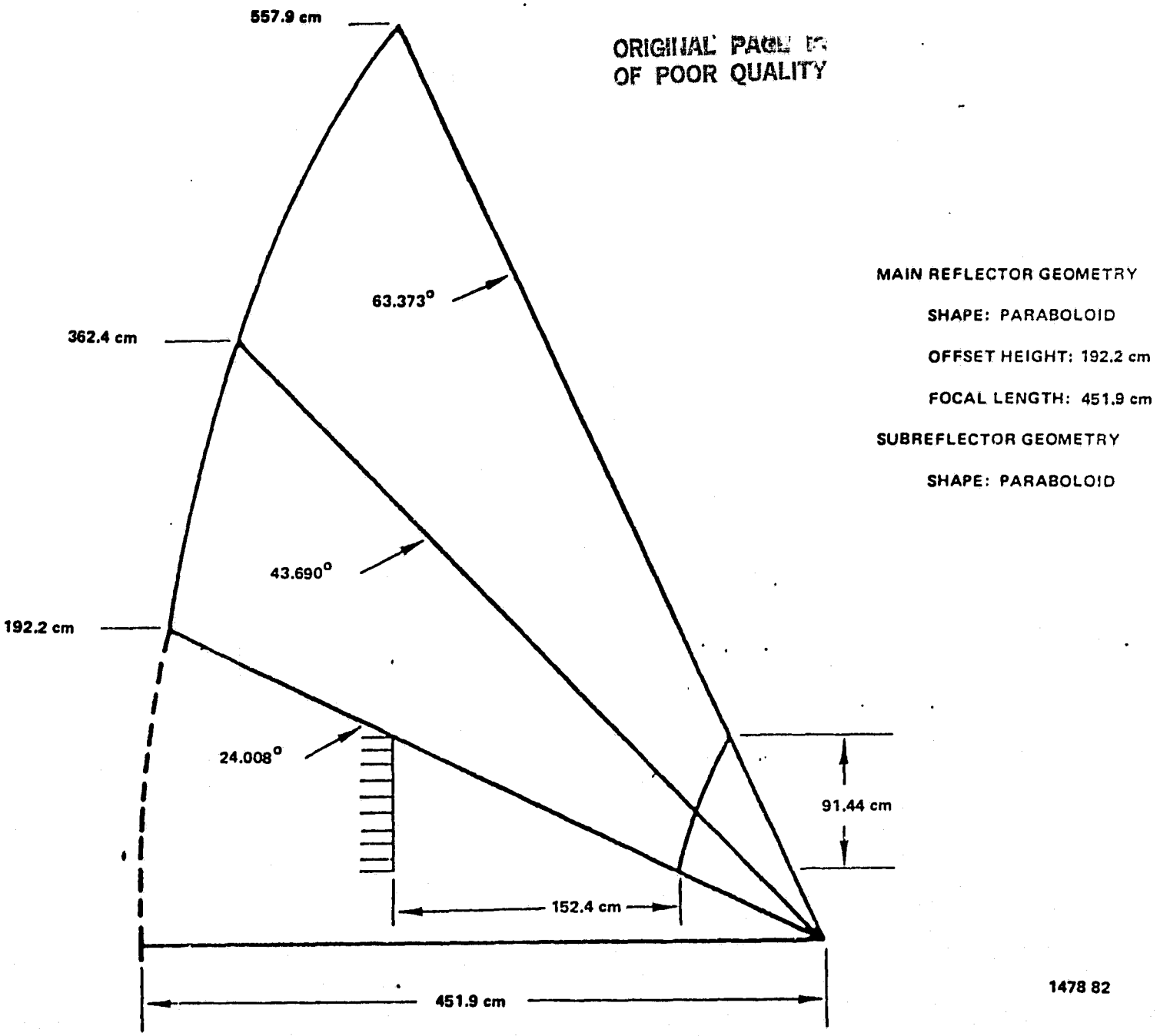

Figure 3.6-25. Initial Point Design Scanning Beam Configurations

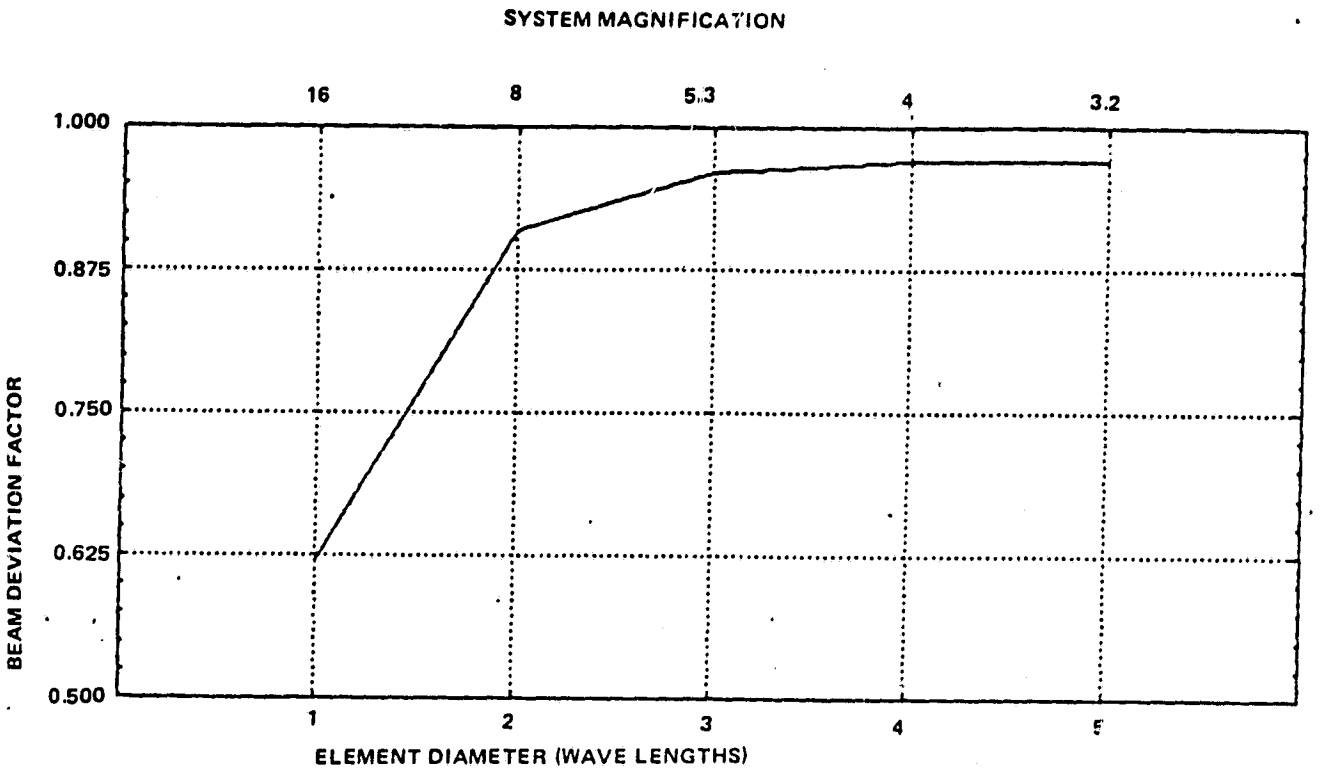

Beam Deviation Factor Vs Element Diameter for 2-1/2 Beamwidths Scan. Feed Array Contains 177 Dominant Mode Conical Horns With An Amplitude Weighting Distribution Proportional to COS ($\pi \rho / D$).

Figure 3.6-26.

This choice is further supported by Figure 3.6-26, showing the beam deviation factor (BDF) of each reflector configuration. The BDF, as calcualated here, is a measure of the reflector system's effectiveness in transferring a phase front from the feed array aperture to the main reflector aperture. In other words, a phase tilt in the feed aperture perfectly imaged to the secondary aperture would correspond to a BDF of one. All five feed arrays were weighted so as to ideally produce 0.75^{o} of scan (2-1/2 beamwidths @ 0.3^{o} beamwidth). As Figures 3.6-14 to 3.6-23 clearly show, far field scan is significantly less than 0.75^{o} for configurations with high system magnification. This again suggests the use of lower magnification reflector systems. Figure 3.6-26 is, in many ways, analagous to the traditional beam deviation factor for focused reflectors, e.g., parabolic reflectors, Cassegrains, etc.

Additional calculations were made for the selected geometry, showing far field radiation patterns from one to four beamwidths of scan. These patterns appear in Figures 3.6-27 to 3.6-36. A field amplitude weighting distribution of the form

$$(1 - (2\rho/D)^2)^2,$$

where ρ is the radial distance to each element, and D is the feed array diameter, was used in order to obtain the required low level sidelobes. Figure 3.6-37 shows the scan loss at four beamwidths is about 3.5 dB. Recall that the design procedure of Section 3.3 called for an aperture array element diameter of 16 λ, yielding an inherent 3 dB loss in gain at 1.75^{o} from boresight. We note, therefore, that the scan loss of 3.5 dB can actually be considered as the sum of two smaller losses. First, the inherent element pattern loss at four beamwidths ($\sim 1.2^{o}$) of approximately 2 dB for the selected feed array geometry. The additional 1.5 dB is attributable to reflector effects such as primary spillover, phase error loss,

cross-polarization loss, etc. Furthermore, the 2 dB element pattern loss can readily be decreased by the addition of more elements in the feed array, while the loss in gain due to reflector effects can be significantly reduced with the optimal utilization of the MMIC variable amplitude and variable phase modules as discussed in Section 3.6.1. Therefore, the resultant scan loss can approach that of the element pattern level at the sector's edge, and with additional elements, say 541 per feed array, this loss can be reduced to about 1 dB. Cross polarization levels, shown in Figure 3.6-38, are again seen to be well below the required -30 dB level.

One final point concerning the scanning performance of the near-field Cassegrain should be mentioned. Some part of the 3.5 dB scan loss, calculated above, is attributable to primary spillover. This can be recovered in part by oversizing either the subreflector or the feed array. A simple extension of the parabolic subreflector contour, however, may not be sufficient to properly collimate the scanned beams, so some reflector surface shaping may be necessary. By oversizing the feed array, on the other hand, it is possible to recover the lost energy. The amount of oversizing necessary can be approximated graphically as shown in Figure 3.6-39 and 3.6-40. These plots were generated by tracing an incoming plane wave through the near-field Cassegrain reflector system for elevation scans of $\pm 1.75^{o}$. For a particular scan direction, only a portion of the feed array would be illuminated, thereby requiring more than the proposed 177 feed elements to cover an entire sector, but the scan performance of the system will be significantly improved.

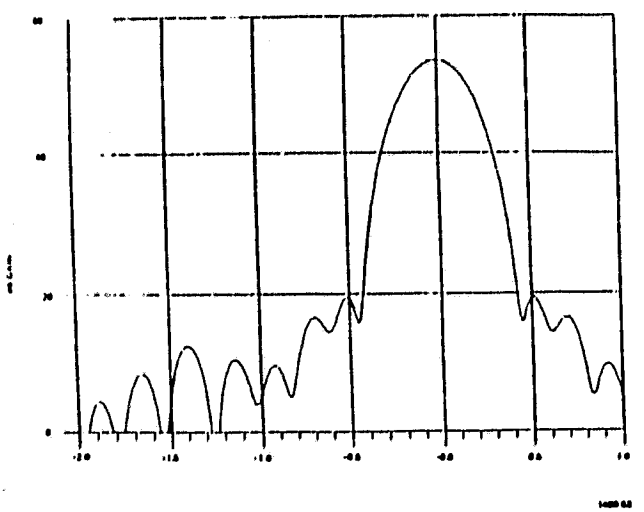

THETA (DEG)
FAR-FIELD CO-POL RADIATION PATTERN FOR 177-4 λ ELEMENTS WITH AMPLITUDE WEIGHTING DISTRIBUTION PROPORTIONAL TO $(1-(2\rho/D)^2)^2$; ON-FOCUS

Figure 3.6-27

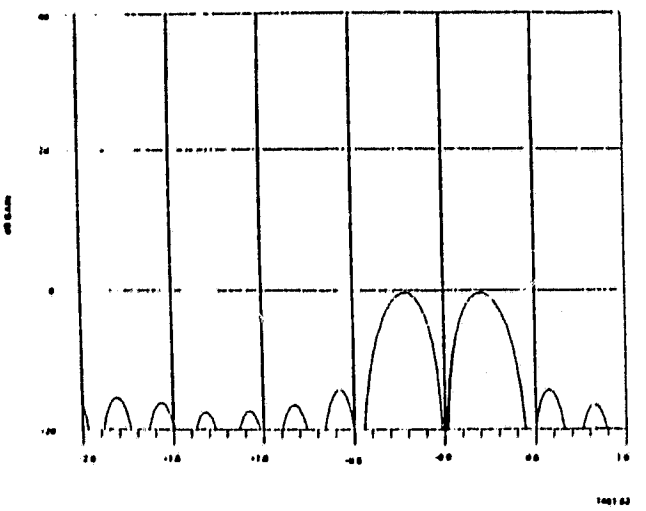

THETA (DEG)
FAR-FIELD CROSS-POL RADIATION PATTERN FOR 177-4 λ ELEMENTS WITH AMPLITUDE WEIGHTING DISTRIBUTION PROPORTIONAL TO $(1-(2\rho D)^2)^2$ ON-FOCUS

Figure 3.6-28

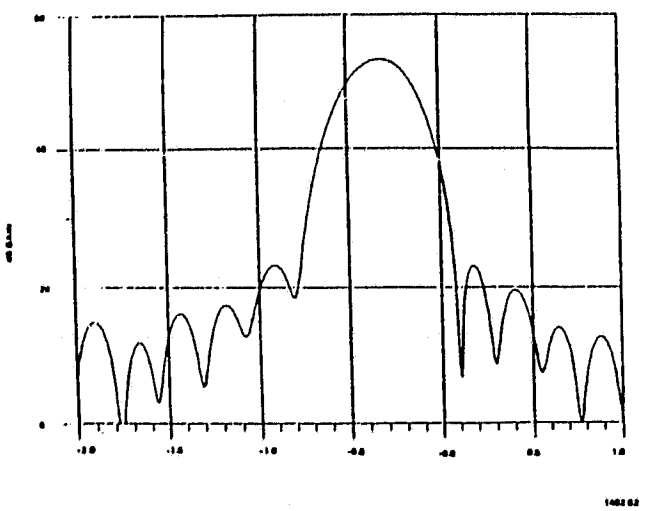

THETA (DEG)
FAR-FIELD CO-POL RADIATION PATTERN FOR 177-4 λ ELEMENTS WITH AMPLITUDE WEIGHTING DISTRIBUTION PROPORTIONAL TO $(1-(2\rho/D)^2)^2$; ONE BEAMWIDTH SCAN

Figure 3.6-29

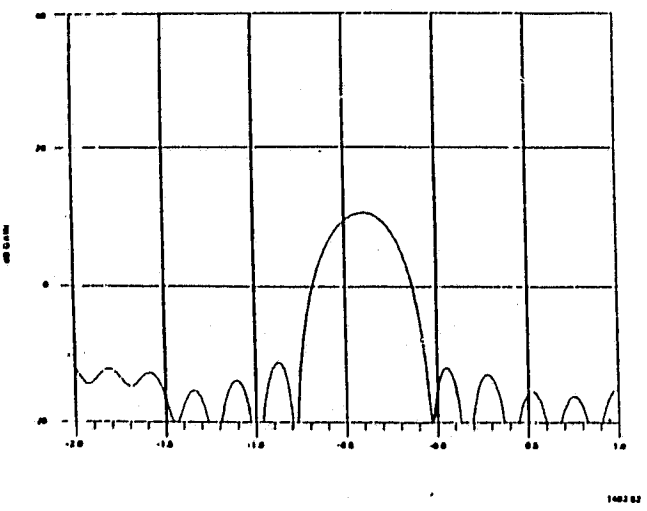

THETA (DEG)
FAR-FIELD CROSS-POL RADIATION PATTERN FOR 177-4 λ ELEMENTS WITH AMPLITUDE WEIGHTING DISTRIBUTION PROPORTIONAL TO $(1-(2\rho/D)^2)^2$; ONE BEAMWIDTH SCAN

Figure 3.6-30

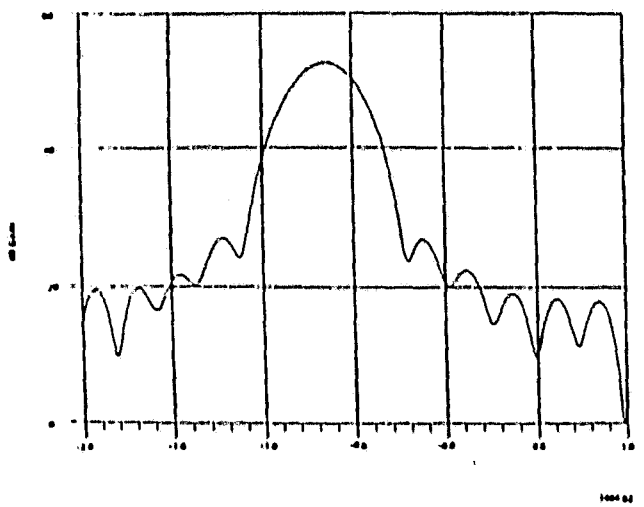

THETA (DEG)
FAR-FIELD CO-POL RADIATION PATTERN FOR 177-4 λ ELEMENTS WITH AMPLITUDE WEIGHTING DISTRIBUTION PROPORTIONAL TO $[1-(2\rho/D)^2]^2$, TWO BEAMWIDTH SCAN

Figure 3.6-31

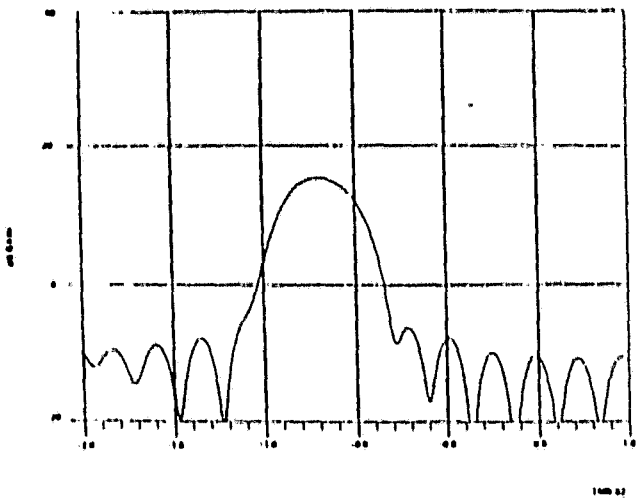

THETA (DEG)
FAR-FIELD CROSS-POL RADIATION PATTERN FOR 177-4 λ ELEMENTS WITH AMPLITUDE WEIGHTING DISTRIBUTION PROPORTIONAL TO $[1-(2\rho/D)^2]^2$ TWO BEAMWIDTH SCAN

Figure 3.6-32

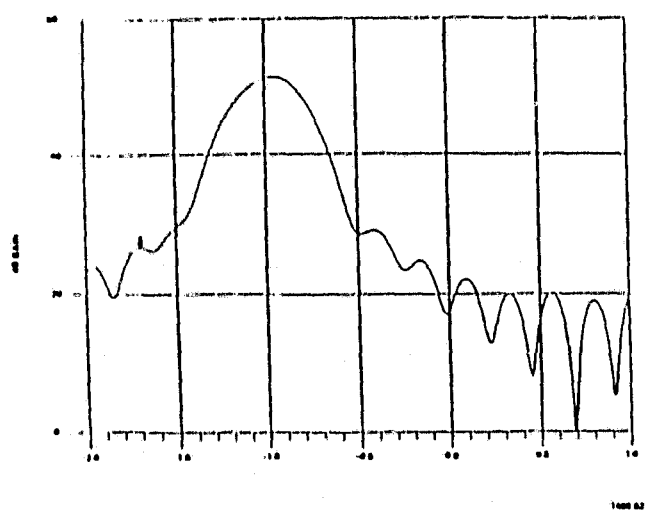

THETA (DEG)
FAR-FIELD CO-POL RADIATION PATTERN FOR 177-4 λ ELEMENTS WITH AMPLITUDE WEIGHTING DISTRIBUTION PROPORTIONAL TO $[1-(2\rho/D)^2]^2$, THREE BEAMWIDTH SCAN

Figure 3.6-33

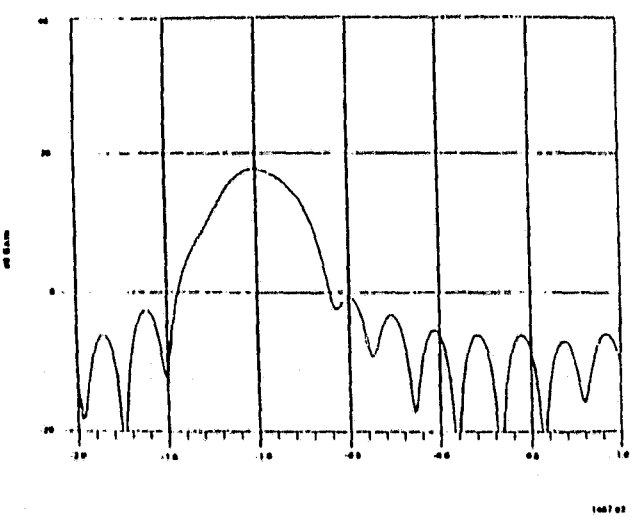

THETA (DEG)
FAR-FIELD CROSS-POL RADIATION PATTERN FOR 177-4 λ ELEMENTS WITH AMPLITUDE WEIGHTING DISTRIBUTION PROPORTIONAL TO $[1-(2\rho/D)^2]^2$, THREE BEAMWIDTH SCAN

Figure 3.6-34

ORIGINAL PAGE IS
OF POOR QUALITY

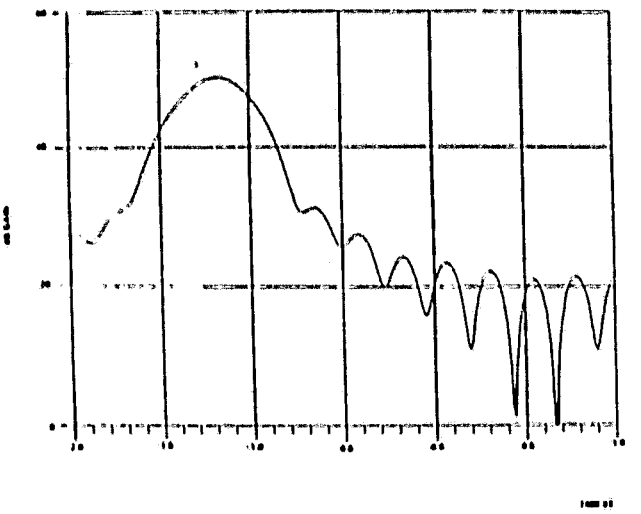

THETA (DEG)
FAR-FIELD CO-POL RADIATION PATTERN FOR 177.4 λ ELEMENTS WITH AMPLITUDE WEIGHTING DISTRIBUTION PROPORTIONAL TO $(1-(2\rho/D)^2)^2$, FOUR BEAMWIDTH SCAN

Figure 3.6-35

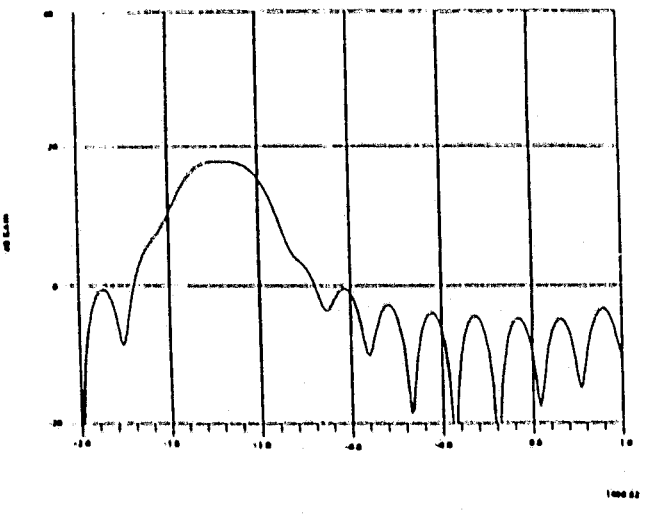

THETA (DEG)
FAR-FIELD CROSS-POL RADIATION PATTERN FOR 177.4 λ ELEMENTS WITH AMPLITUDE WEIGHTING DISTRIBUTION PROPORTIONAL TO $(1-(2\rho/D)^2)^2$, FOUR BEAMWIDTH SCAN

Figure 3.6-36

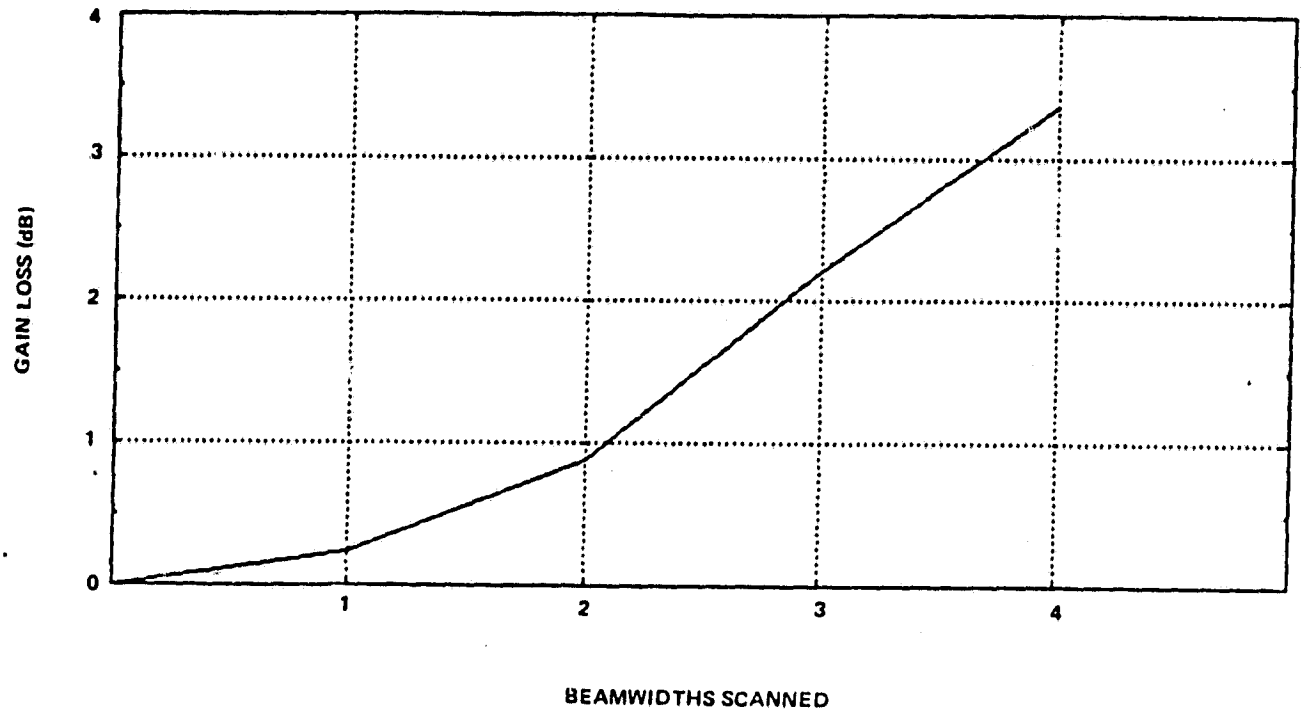

Gain Loss Vs Scan For 177 Element Feed Array With Amplitude Weighting Distribution Proportional to $(1-(2\rho/D)^2)^2$.

Figure 3.6-37.

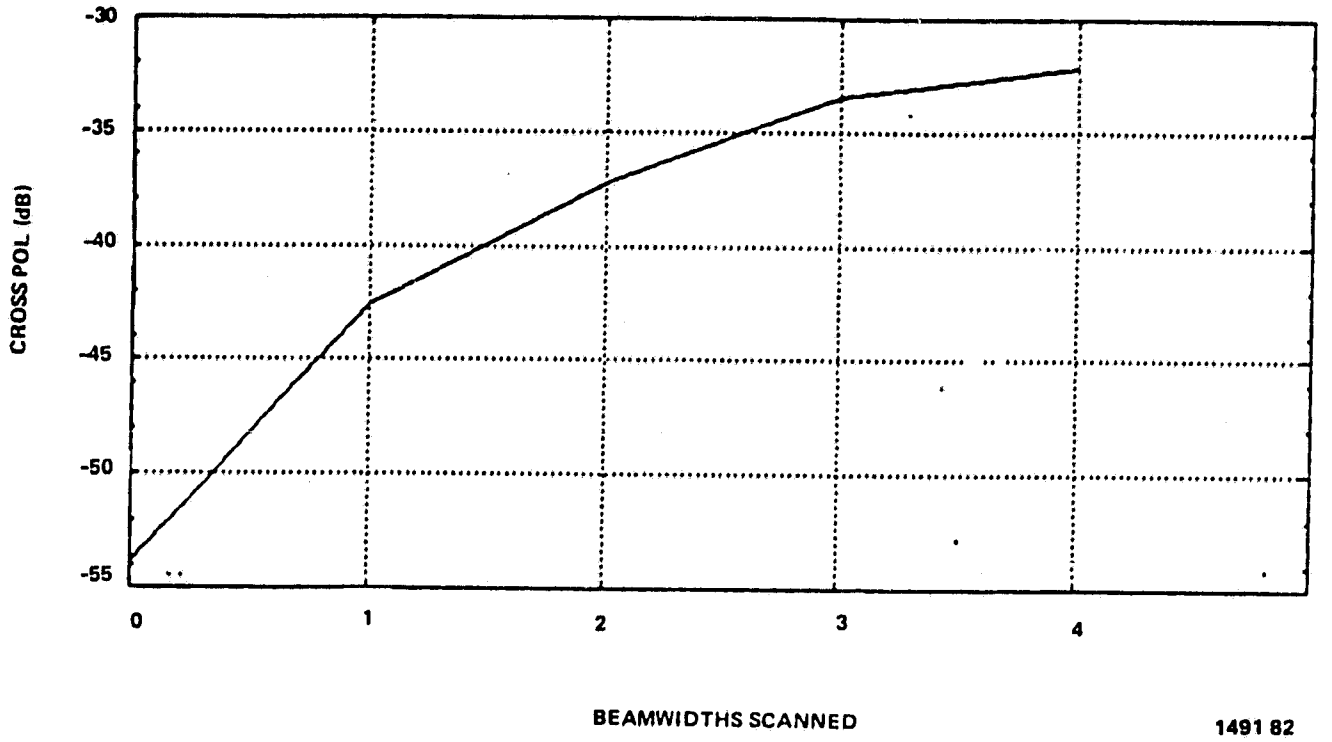

Cross Polarization Levels Vs. Scan For 177 Element Feed Array With Amplitude Weighting Distribution Proportional to $(1-(2\rho/D)^2)^2$.

Figure 3.6-38.

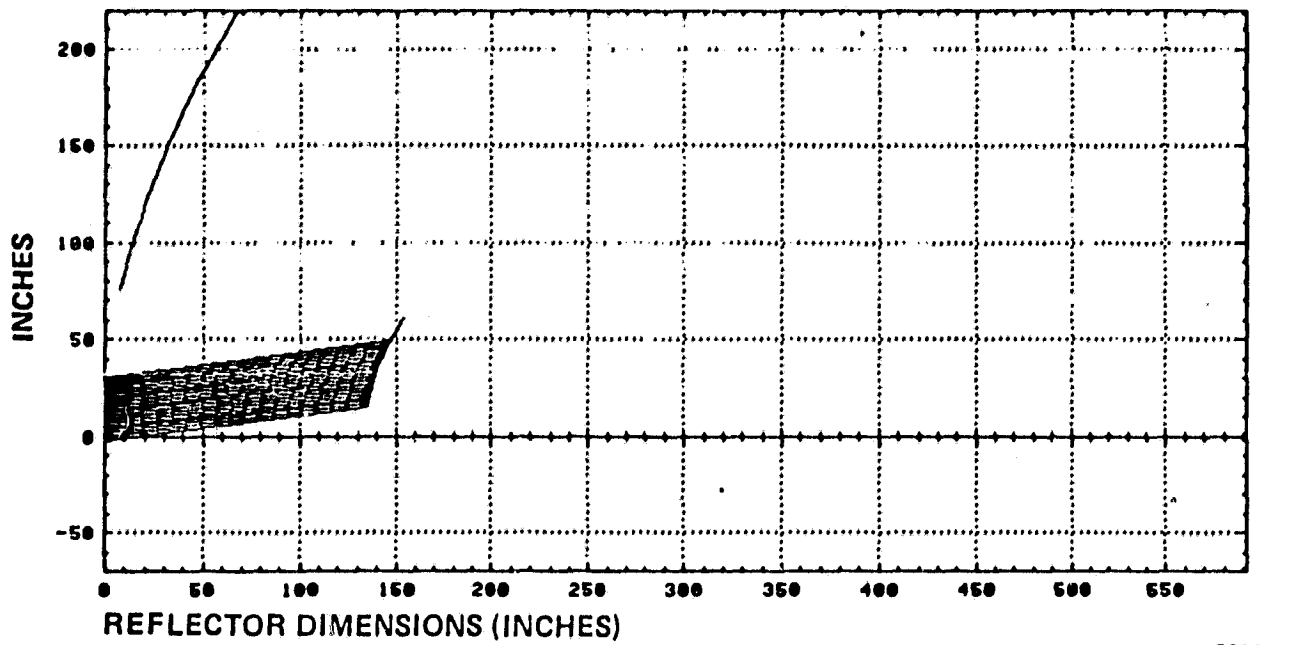

Figure 3.6-39. Reflected Rays for 1.75° Elevation Scan

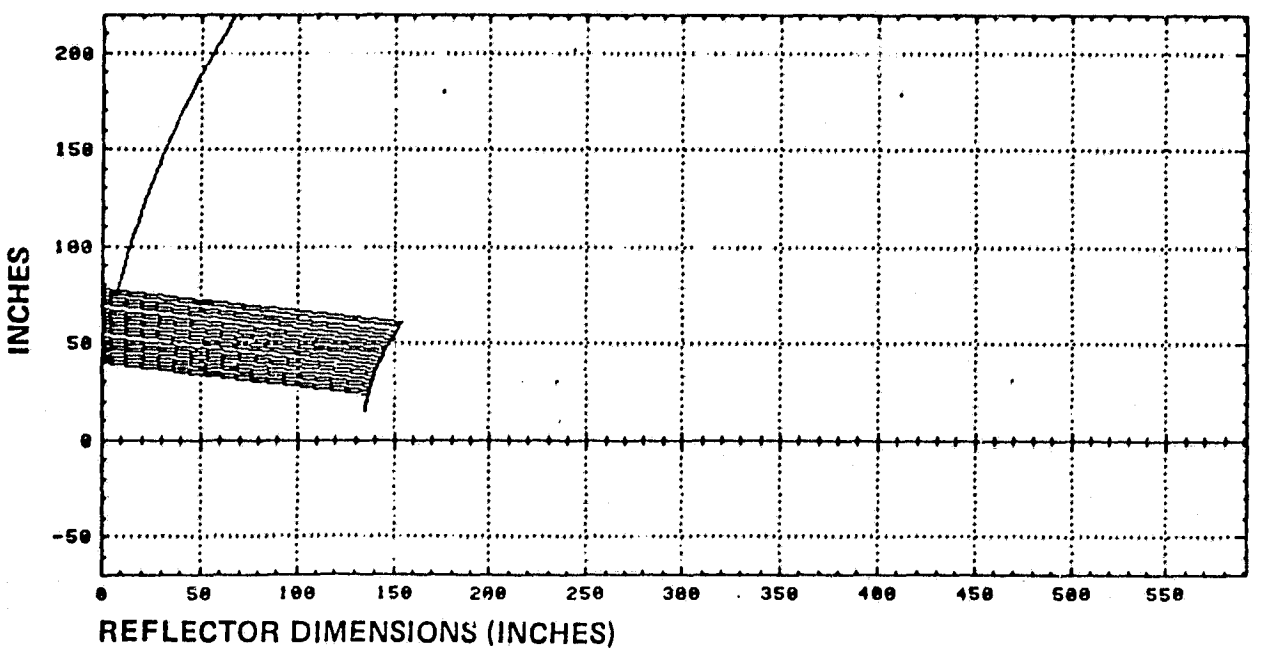

Figure 3.6-40. Reflected Rays for -1.75° Elevation Scan

3.6.1 Element Weighting Coefficient Synthesis From Reflector Secondary Characteristics

The far field radiation characteristics of the array/reflector system can be greatly improved by optimum selection of the feed element excitation coefficients, in both amplitude and phase. These can be dynamically incremented to any of a number of preselected levels to provide beam movement and optimum pattern shape at each position. This is one of the unique advantages gained through effective utilization of the MMIC transmit modules. Two methods of determining these weighting coefficients are outlined below which are applicable to reflector systems in general, and the offset near-field Cassegrain in particular.

The first of these methods, utilizes a system transformation matrix R, relating the complex excitation coefficients of N feed elements to N corresponding complex secondary aperture field points. This can be written as:

$$\begin{bmatrix} AF_1 \\ AF_2 \\ \vdots \\ AF_n \end{bmatrix} = \begin{bmatrix} \text{SYSTEM} \\ \text{TRANSFORMATION} \\ \text{MATRIX} \\ R \end{bmatrix} \begin{bmatrix} W_1 \\ W_2 \\ \vdots \\ W_n \end{bmatrix},$$

where AF_n is the complex principal component of the electric field vector in the aperture of the secondary reflector (or on the main reflector surface itself), and W_n is the complex relative excitation coefficient of the n^{th} feed element. Based on a particular set of far field beam requirements, a set of desired aperture fields can be determined, and the required weighting coefficients are found as:

$$\begin{bmatrix} W_1 \\ W_2 \\ \vdots \\ W_n \end{bmatrix} = \begin{bmatrix} & \text{SYSTEM} & \\ & \text{TRANSFORMATION} & \\ & \text{MATRIX} & \\ & R & \end{bmatrix}^{-1} \begin{bmatrix} AF_1 \\ AF_2 \\ \vdots \\ AF_n \end{bmatrix} ,$$

This technique has been found to calculate weighting coefficients which do indeed produce the required aperture distributions, and therefore, the desired far-field radiation patterns, but are not optimized with respect to power. (See Appendix D.)

To resolve this power problem, a second, more sophisticated, optimization procedure is suggested. Referred to as the method of steepest descent, or gradient method, it provides a way of finding the minimum of a system function with many unknowns. It is an iterative process well suited to implementation on digital computers, and, while it usually does not exhibit tremendously fast convergence properties, is fairly simple to understand and easy to program.

The first step in using the method of steepest descent is the determination of the function to be minimized. This can be referred to as the "error function" and should depend on all N complex weights, as shown below:

$$E = f(W_1, W_2, W_3, \ldots, W_N)$$

Incidentally, since each weight consists of an amplitude and a phase, this function actually depends on 2N parameters. The error function should somehow relate the pattern produced by the present weights to the desired pattern. This relation should be such that the value of E becomes smaller and smaller as the actual pattern approaches the desired pattern.

The choice of the error function depends on the criteria which must be met by the system. For the scanning beams, the system specifications require that peak gain be at, or above, a particular level, and that gain in the sidelobe regions be below some lower relative level. This selection of error function should be made judiciously so that the solution will converge to the proper point. But once it is selected, the process becomes straightforward.

At each step of the iterative process, the 2N parameters are adjusted in such a way as to decrease the value of E. The rule for adjusting each parameter W_i is:

$$W_i^{k+1} = W_i^k - \alpha \left(\frac{\partial E}{\partial W_i} \Big/ \frac{\partial^2 E}{\partial W_i^2} \right)$$

where k is the iteration number and α is a step size. The value for α is important in determining the success of the algorithm, but its best value can only be found by trial and error. For this reason α is sometimes known as the "magic factor". Note that at each stage of the algorithm, 2N first partial derivatives and 2N second partial derivatives must be calculated. The necessity of finding closed forms for these expressions should encourage the designer to keep the definition of E as simple as possible.

After each parameter has been adjusted, a convergence test is made. Several conditions for convergence are possible, such as the new value of E falling at or below some threshold, the sum of all the first partial derivatives falling below a cutoff point, or a maximum number of iterations being reached. If convergence is reached, the process is terminated and the latest values of the parameters are considered optimum. If the conditions for convergence are not met, the parameters are readjusted, and so on. A flow graph for the entire process is shown in Figure 3.6.1.

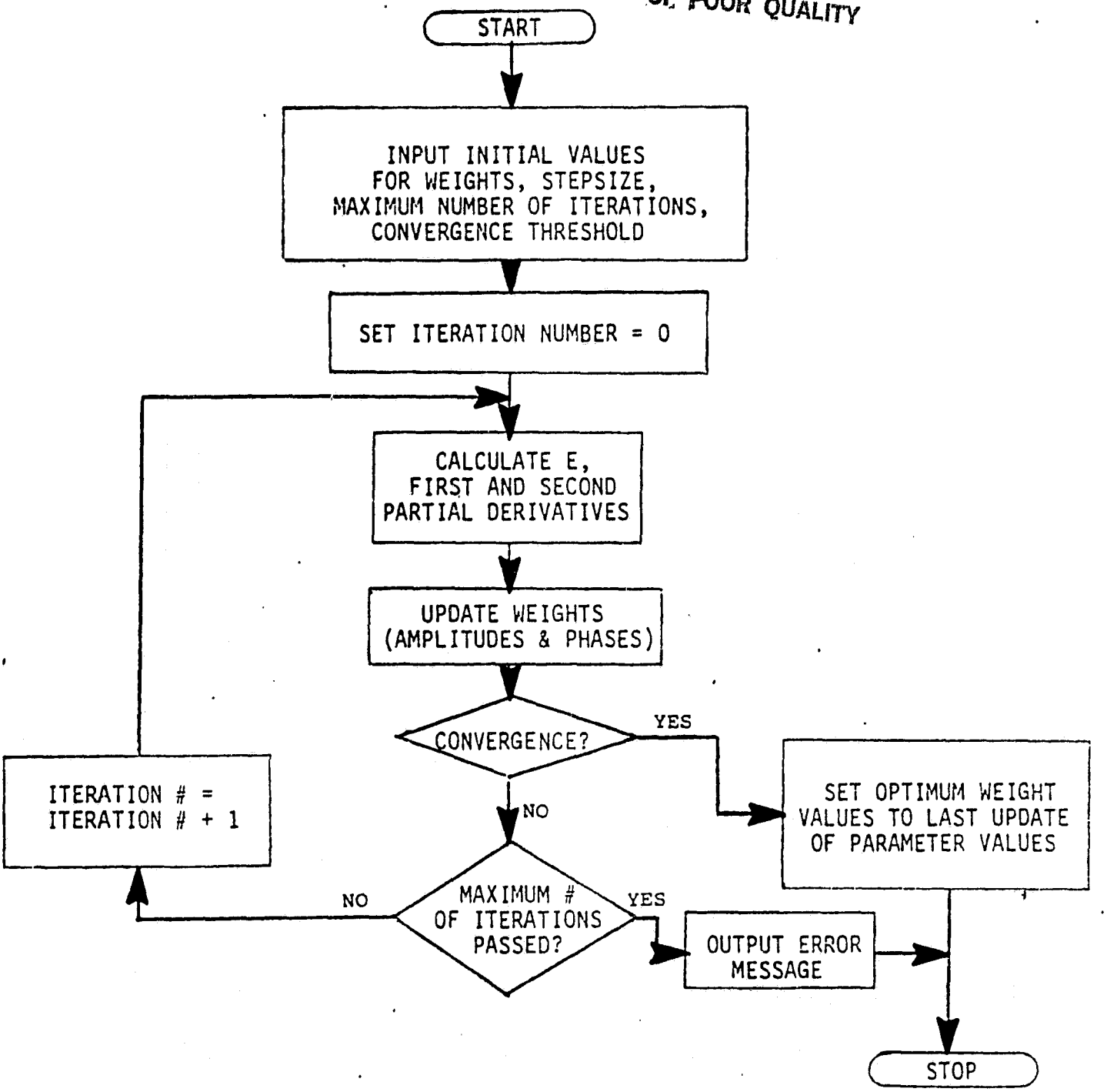

Figure 3.6.1. Flow Graph of Steepest Descent Procedure

3.7 Recommended Configurations

Based on the results of the parametric study, it is now possible to recommend configurations for hardware design. These two scanning spot beam configurations are outlined in Table 3.7. Notice that they differ only in MMIC module combinations utilized to achieve beam performance. It was determined during the parametric analysis (see Appendix D) that variable amplitude and phase control would be required in order to meet the performance specifications. This is reflected by configuration A. It may be possible, though, to "thin" the array (discussed in Section 3.12.1) as indicated by configuration B. This module thinning can be implemented only after all weights are determined by the optimization procedure outlined in Section 3.6.1 for each beam position.

3.8 Scanning Beam Phased Array Design

Design of the scanning beam phased array presents some unique problems, most important of which is integration of the monolithic modules into the array. The phased array design can be broken down into three independent parts which correspond to the basic parts of the array: radiating element selection, monolithic module integration, and feed system design.

Radiating element selection involves selection of element size and type to satisfy sector coverage requirements. Integration of monolithic modules into the phased array requires design of a configuration for mounting the modules, and design of transistions for RF signals to and from the modules. Additionally, some provisions must be made for bias and control input signals and for conduction of heat from the modules. The goal of feed system design is to provide an RF distribution network that will divide the power from one source and distribute it at appropriately proportioned levels to each of the elements. The relative advantages of the two general types of feed systems will be discussed before demonstrating the most advantageous for this application.

Table 3.7. Two Recommended Scanning Spot Beam Configurations

CONFIGURATION A - SCANNING SPOT BEAM	
Main Reflector:	3.7M (12 foot) diameter paraboloid
Subreflector:	91.44 cm (36 inch) diameter paraboloid
Feed:	Spacefed lens with active elements
Elements:	177 circular waveguide with MMIC modules
MMIC Modules:	Variable Phase Shift (VPS), Constant Gain Amplifier (CGA), Variable Power Amplifier (VPA)
Module Gain:	VPS, -3 dB; CGA, 19 dB; VPA, programmed to produce weighted amplitude, 20 dB max
Module Phase:	Phase programmed to produce weighted phase for low sidelobes and beam pointing
EIRP:	Approximately 70 dBW
Output Power:	15 dBW (31.6 Watts)

CONFIGURATION B - SCANNING SPOT BEAM
Same as Configuration A except that a thinning technique will be used wherein the radiating elements of the array (lens) can have the following combinations of modules: 1) Variable Phase Shift module only 2) Variable Phase Shift and Constant Gain Amplifier modules 3) Variable Phase Shift and Variable Power Amplifier modules 4) Variable Phase Shift, Constant Gain Amplifier, and Variable Power Amplifier modules

3.9 Radiating Element Selection

3.9.1 Element Size and Type

Selection of the size of the radiating element for the scanning beam phased array was based on analysis of sector coverage requirements imaged through the reflector system. The analysis showed that an array of 177 elements of 4 wavelengths in diameter was required to achieve scan performance over the entire sector. Circular elements are preferred for large arrays because of their equal E and H-plane beamwidths, reduced coupling, and multimode capability.

3.9.2 Element Design

The initial design was a four wavelength dominant mode conical horn, although a multi-mode horn could be used if required. The horn is shown below in Figure 3.9.2.

The 7^{o} flare angle produces a maximum aperture phase error of 36^{o}, well within the acceptable limits. A 3-wavelength circular-to-rectangular transition is included based on design criteria developed by Reich. Its total length, including the transition, is 24.5 cm (9.64 inches).

3.10 Monolithic Module Integration

3.10.1 Requirements

Integration of monolithic modules into the phased array requires design of a configuration for mounting the modules, and design of transitions for RF signals to and from the modules. Additionally, some provision must be made for bias and control input signals and for conduction of heat away from the modules.

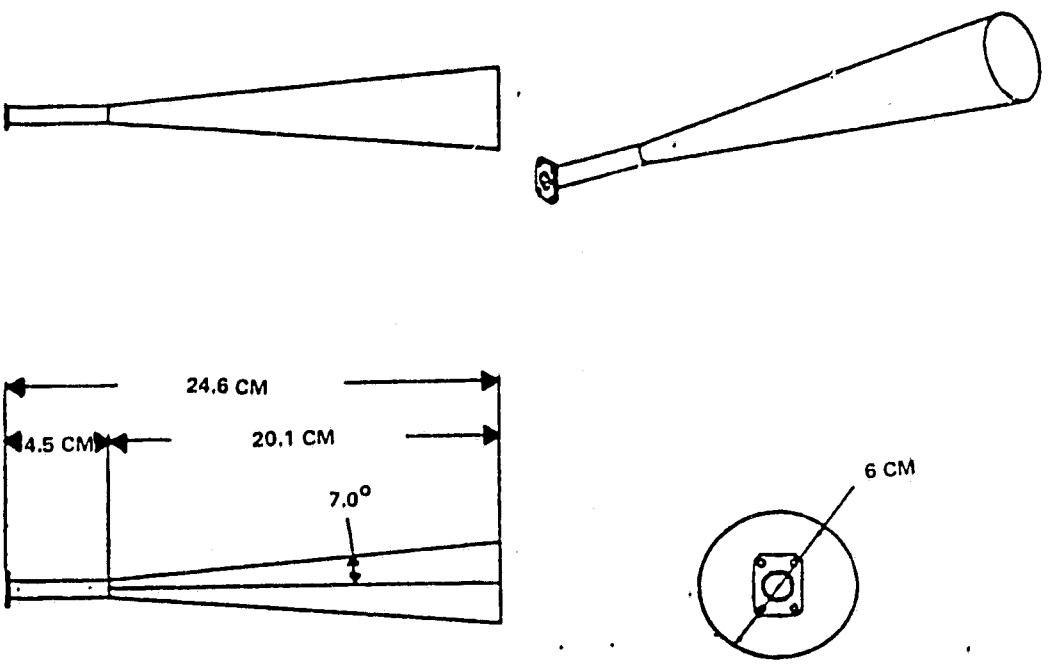

Figure 3.9.2. Four Wavelength Horn

3.10.2 Monolithic Module Mounting Configuration

Table 3.10.2 lists some important factors in the design of microelectronic packaging for spacecraft. In addition to those factors, there are several unique system constraints which must be considered in design of the mounting configuration. The size of the completed package must be compatible with waveguide dimensions to fit in the space behind the radiating element. Also, the package must be compatible with the transition used between waveguide and the monolithic modules. Finally, provision must be made for routing control and bias lines to the modules.

Table 3.10.2. Important Factors in Microelectronic Packaging for Spacecraft

Factor	Characteristics
Reliability	Number of Connections Structural Integrity
Physical Characteristics	Size Weight Thermal Properties
Environmental Protection	Shock and Vibration RF Interference Humdity

A mounting configuration has been devised which appears to meet the requirements of Table 3.10.2 and is compatible with the system constraints. The configuration, shown in Figure 3.10.2, uses microwave leadless chip carriers for mounting the monolithic modules, then integrates the chip carriers onto a single substrate for routing of RF, bias and control signals. The MMIC's would be bonded into the chip carriers using an epoxy adhesive, then a ceramic cover would be attached to provide a hermetically sealed chip carrier. The chip carrier would in turn be attached to the substrate using

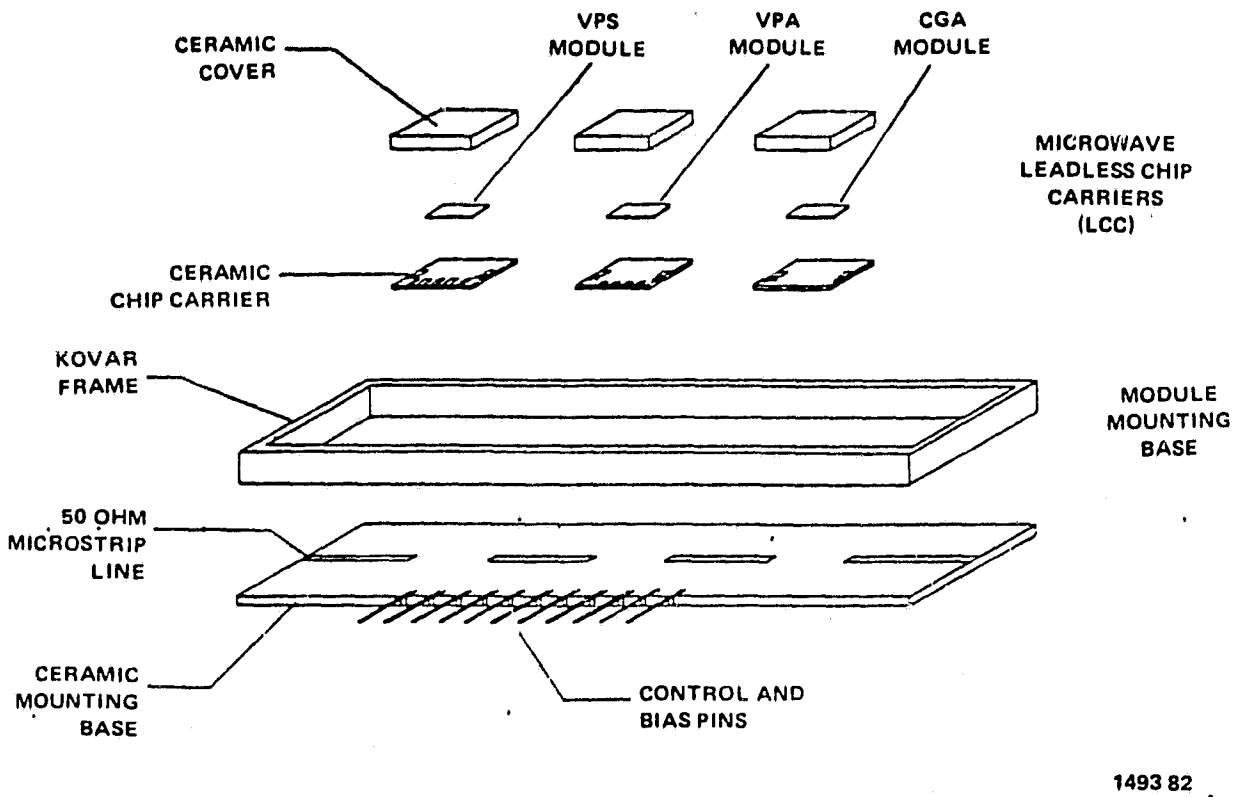

Figure 3.10.2. Monolithic Transmit Module Mounting Configuration

conventional soldering techniques. Conductors for carrying RF, bias and control signals would he etched on the surface of the substrate. Finally, a frame could be attached as shown to provide some strength and rigidity to the structure. Conventional alumina ceramics would he used unless thermal problems required use of Berylium Oxide.

3.10.3 Transition

3.10.3.1 Design Alternatives[5]

Since microstrip offers the most attractive interface to the monolitnic transmit modules, a transition is needed between waveguide in the feed system and radiating elements, and microstrip which connects to the modules. The technology assessment in Appendix A outlines several common methods of accomplishing this transition. Some desirable features for a waveguide to microstrip transition are listed below.[6]

1. High return loss to reduce reflection in the feed system and improve EIRP
2. Low transmission loss
3. Easily attached to microstrip with reproducible results
4. Mechanically easy to reproduce

3.10.3.2 Design Approach

The design approach chosen is to transform impedance from waveguide to microstrip using a broadband stepped ridgeline transformer mechanically connected to the microstrip using a tab. For a given bandwidth and return loss, the desired impedance at each step can be computed by the method outlined by Cohn[7]. The mechanical dimensions required to achieve desired impedances can be computed from ridgeline data given by Hopfer[8]. A reproducible microstrip ridgeline junction is made by setting the height of the last step so that the substrate will hit and stop against the ridgeline.

The reactance at the microstrip-ridgeline junction can be reduced by tapering the edge of the transformer at the junction. The transformer is easily machined out of aluminum or similar material and bonded or screwed to the inside of the waveguide. The completed transition and transformer are shown below in Figures 3.10.3.2 a and b.

3.10.3.3 Performance of Transition[7]

Schneider[6] built a transition for the 27.5-31.3 GHz band. Return loss measurements, plotted below in Figure 3.10.3.3, show the transition has more than 30 dB return loss over a 17 percent bandwidth. Insertion loss is less than 0.1 dB.

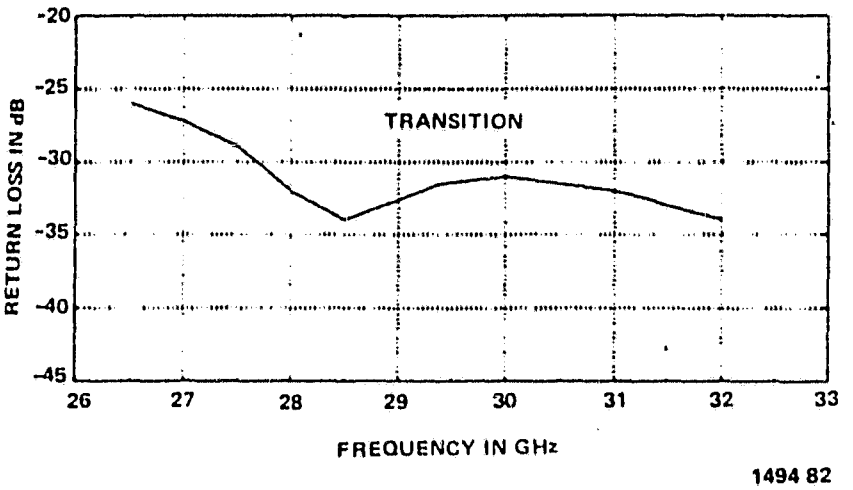

Figure 3.10.3.3. Return Loss of Microstrip-to-Waveguide Transistion From 26.5 to 32 GHz

3.10.4 Integration of Transitions and Modules

To enable integration of transitions and modules, the monolithic transmit module assembly (Figure 3.10.2) is bonded inside an open waveguide section as shown in Figure 3:10.4-1. An opening in the wall of the module section allows access to module control and bias pins.

The resulting section has interfaces compatible with the transition sections, enabling quick and accurate integration of the modules and transitions. Details of the connection are shown in Figure 4.10.4-2. After the flanges are aligned and bolted together, the electrical connection is made using laser

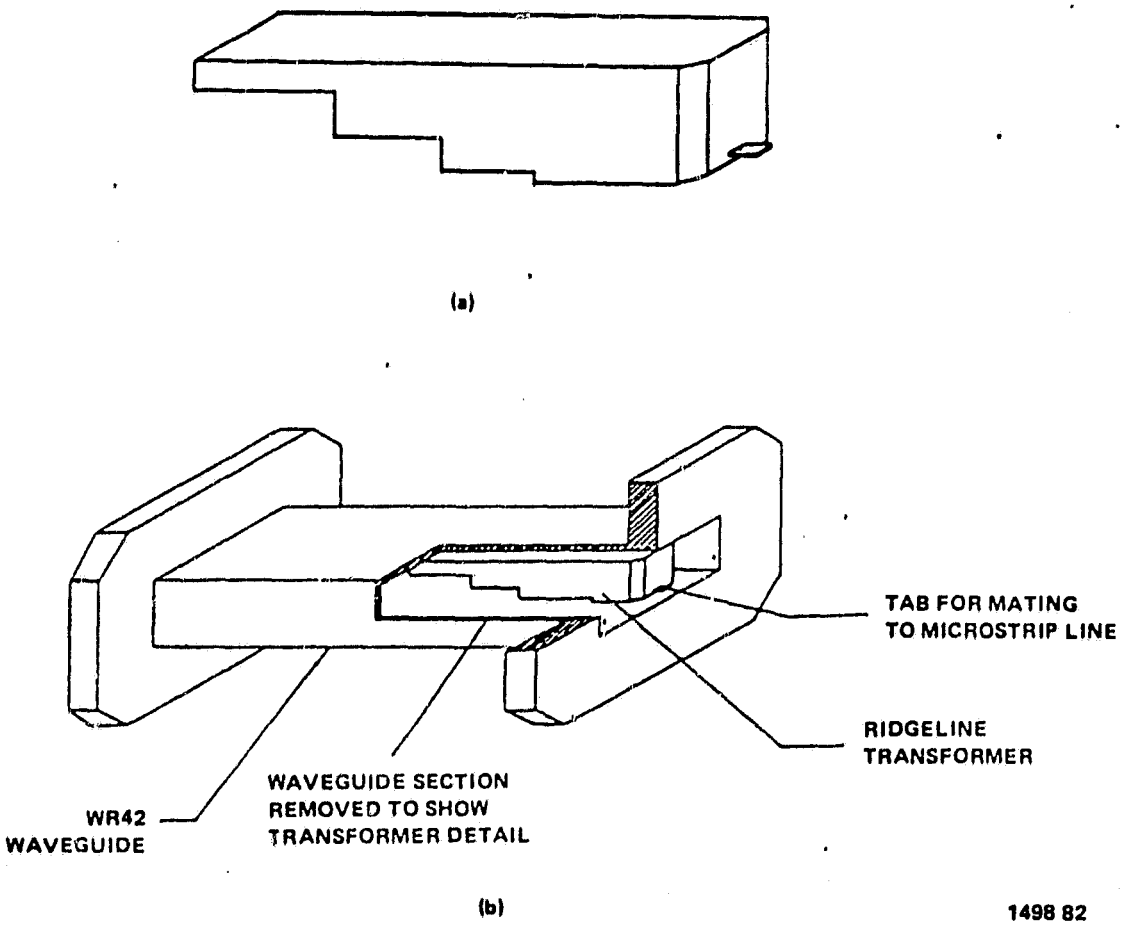

Figure 3.10.3.2. Waveguide to Microstrip Transition:
(a) Ridgeline Transformer, (b) completed transition
- wall sectioned to show detail

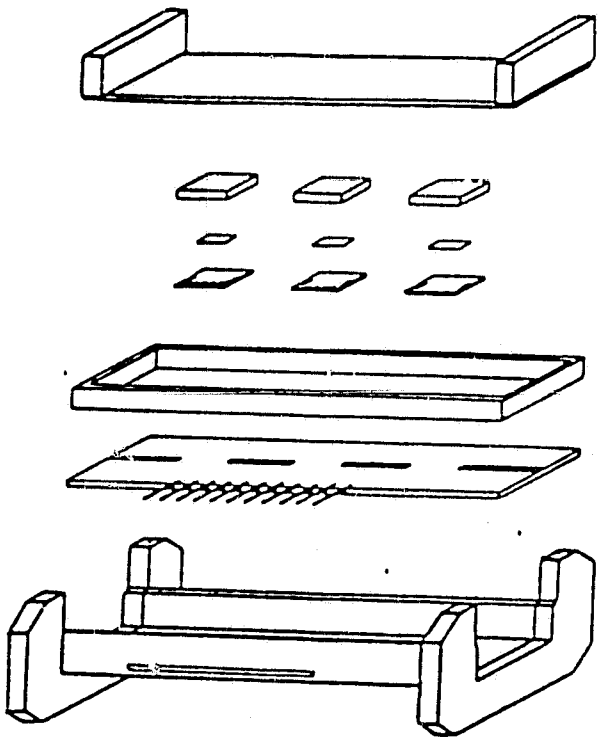

1495 82

Figure 3.10.4-1. Mounting Monolithic Transmit Module Assembly in Waveguide Section

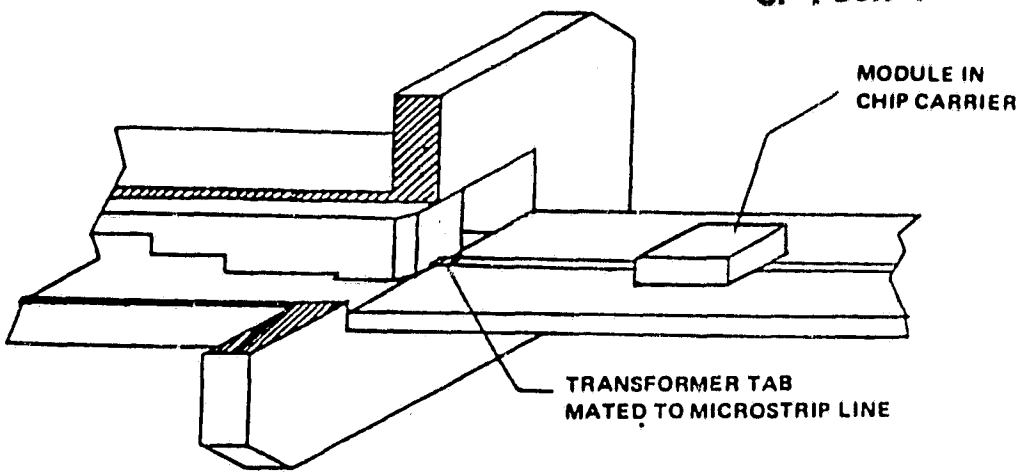

Figure 3.10.4-2. Detail of Transformer - Microstrip Connection

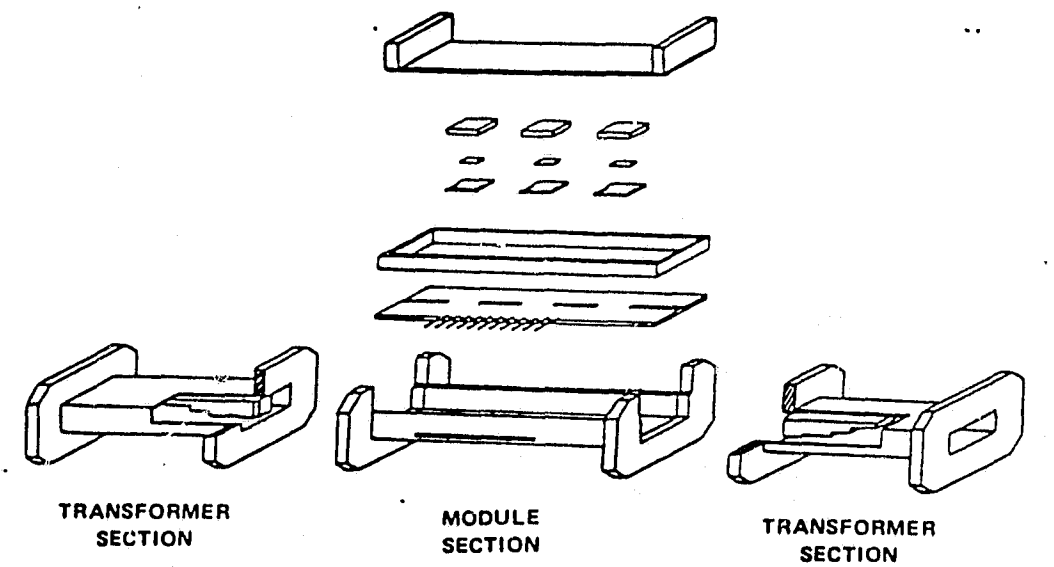

Figure 3.10.4-3. Monolithic Module Transition and Mounting Configuration

reflow soldering or IR spot heater techniques. Finally, the protective cover is placed on the module section. The resulting assembly provides a highly rigid base for the module-transition combination and affords environmental protection for the monolithic transmit modules. An exploded view of the module-transition assembly is shown in Figure 3.10.4-3.

3.10.5 Thermal Analysis of Heat Flow From Modules

An analysis of heat flow from the modules can be conducted to verify that the conductive cooling provided by the mounting configuration is sufficient to allow the modules to operate at full power.

3.10.5.1 Model for Analysis

The analysis models the thermal conducting path as a series of slabs of different thermal conductivities. Heat flow is calculated using

$$q = -KA \frac{dT}{dx}$$

where q = heat in watts

T = temperature

A = area of the conducting slab

K = thermal conductive of slab

x = distance in the direction of heat flow

By treating each slab separately and allowing the area to become a function of x, the analysis can accurately model the tendency for heat to spread out over a progressively larger area as it moves away from the module. A quick calculation reveals that the separation distance between adjacent modules is sufficient that their thermal conducting paths can be considered independent. Thus, analysis of the worst case module (largest heat dissipation) is adequate to verify the conductive cooling of the mounting configuration.

3.10.5.2 Worst Case Module

The VPA module in full power operation represents the highest heat dissipator among the modules. As shown in Figure 3.10.5.2, with 500 mW RF output, the module requires 5 mW RF input and 3.3 W DC input (15% efficiency).

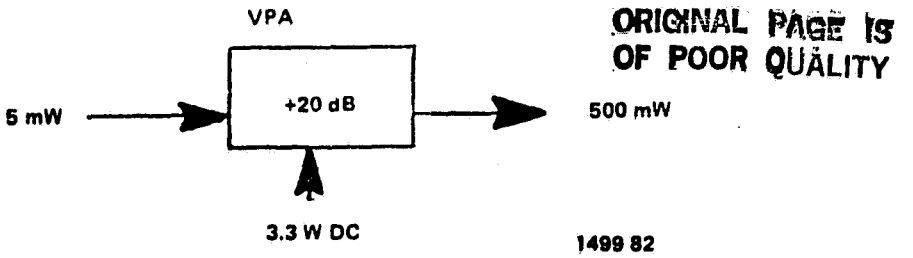

Figure 3.10.5.2. VPA Module in Full Power Operation

Assuming that power is conserved, 2.80 W of heat is generated in the module.

3.10.5.3 Results

The output of the analysis is the thermal resistance of each slab in ^{o}C/watt. This represents the temperature gradient generated across the slab per watt of heat flow. A summary of thermal resistances for each layer is given in Table 3.10.5.3.

The total thermal resistance through the bottom of the waveguide is 10.77^{o}C/watt. Thus, for a heat dissipation of 2.80 watts, a 30.2^{o}C temperature gradient exists between the module and the bottom of the waveguide.

Table 3.10.5.3. Thermal Resistance Summary

Layer #	Material	Function	K	$\Delta T/q$ (^{o}c/watt)
0	GaAs	MMIC	1.26	0.2525
1	36-2 epoxy	adhesive	0.017	3.12
2	Alumina 94%	chip carrier	0.24	2.34
3	Sn 60-63 solder	connection	0.47	0.169
4	Alumina 99.5%	substrate	0.32	1.52
5	518 epoxy	adhesive	0.01	3.28
6	aluminum	waveguide	2.0	0.086

3.10.5.4 System Thermal Design

A thermal analysis of heat conduction from the monolithic modules was treated in Section 3.10.5.3. That analysis assumed existence of a heat sink in the area under the waveguide containing the modules. Figure 3.10.4-4 shows a cooling concept utilizing a honeycomb heat pipe plate. Individual waveguides pass through the plate and are mechanically attached at their center section, the region of heat dissipation. Heat is conducted into the plate and evaporates a working fluid such as methanol. By capillary action, vapor is radially transported through wicks to the plate edge where condensation takes place. Heat is then rejected to space via the plate edge region which acts as a space radiator. Since heat is transferred using evaporization and condensation of a working fluid, there is very little temperature built-up from the plate center to edge which is ideal for this application.

Results of thermal analysis indicate that the plate condenser area should be 1 foot wide which produces a 5 foot diameter plate. The maximum waveguide mounting temperature with full sun stabilization temperature is $66^{o}C$..

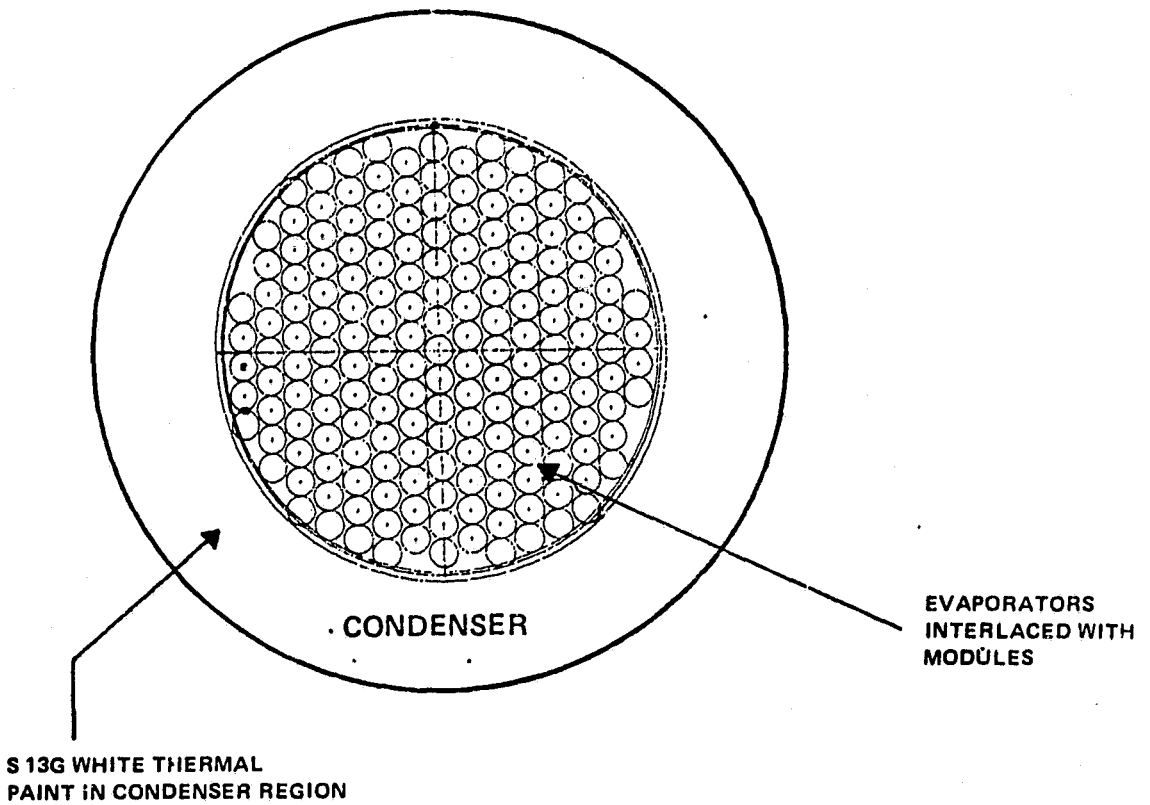

Figure 3.10.4-4

3.11 Feed System Design

3.11.1 Types of Feed Systems

The role of the feed system is to provide an RF distribution network that will divide the power from one source and distribute it at appropriately proportioned levels to each of the elements. The numerous methods for achieving this distribution can be classified into two general types. The first employs transmission line techniques for routing signals from the feed point to the array elements. Since all transmission takes place over closed paths, this type is termed a constrained, or corporate feed. The second method uses free space propagation to spread the signal out from the feed point to the array elements, and hence is called a space feed.

3.11.2 Corporate Feed

The corporate feed employs various types of power dividers in conjunction with lengths of transmission line to divide a single input signal into multiple outputs. Very precise amplitude control is possible at each output; however, large amplitude errors can be generated due to the cumulative effects of mismatch. A typical corporate feed is shown in Figure 3.11.2.1. This feed uses branch-guide couplers as power dividers and various waveguide bends and twists to form 9 outputs.

3.11.2.1 Losses

Losses in the corporate feed arise from power losses in feed components: power dividers, bends, twists, and straight sections. A loss budget for a typical 177 element corporate feed is shown in Table 3.11.2.2.

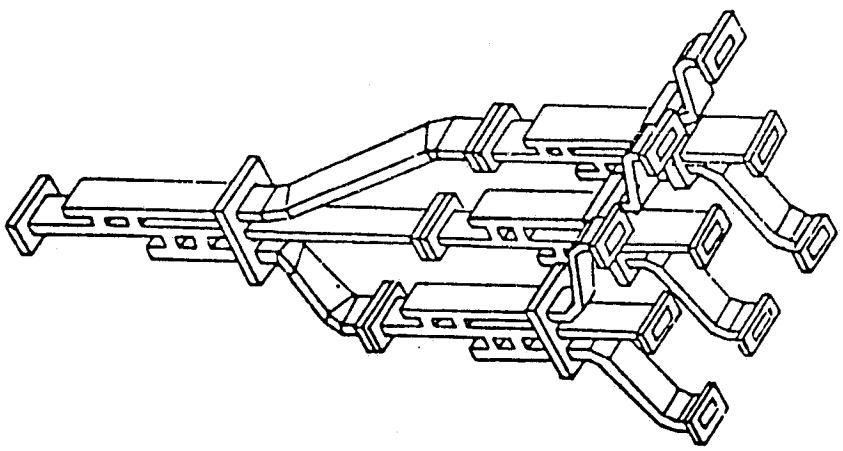

Figure 3.11.2.1. Corporate Feed Configuration

Table 3.11.2.2. Losses for 177 Element Corporate Feed

Component	Loss
Power dividers (5 levels)	1.5 dB
Bends (12)	1.2 dB
Waveguide length (1.2 m)	0.5 dB
Total	3.2 dB

3.11.2.2 Input Power Requirements

Required RF input power to a corporate feed can be calculated by adding losses to the total input power required by the radiating elements. For the feed in Table 3.11.2.2, 1.85 watts RF input would be required if each radiating element required 5 mW input.

3.11.3 Space Feed

Since the space feed uses free-space propagation to divide the signal among the radiating elements, it is ideal for arrays of large numbers of elements where cost and space considerations would make corporate feeding impossible. While amplitude control over each individual element is not normally possible, the presence of monolithic amplifiers in this application removes that disadvantage. Although transmission line losses are low, the space feed is subject to spillover loss due to the illumination not being confined to the angle subtended by the array.

Figure 3.11.3.1 shows a typical space feed configuration. The phased array becomes a feed thru array with a receiving aperture and a transmitting aperture. Active elements such as phase shifters and amplifiers are located between these apertures. One or more horns are located some

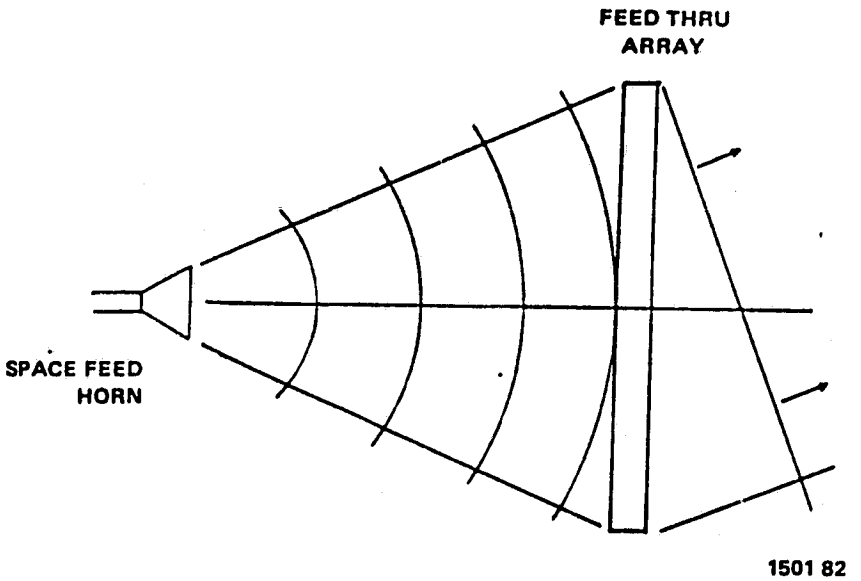

Figure 3.11.3.1. Space Feed Configuration

distance behind the array to provide primary illumination for the space feed. Use of a space feed requires design of additional radiating elements: the space feed horn for primary illumination and radiating elements for the receive aperture of the feed thru array. For the purposes of computations, it is assumed that radiating elements on each aperture of the feed thru array are identical, although this is not true in general.

3.11.3.1 Losses

Losses in the space feed arise from space losses in propagation of the signal from the space feed horn to the receive aperture and from spillover loss due to the illumination not being confined to the angle subtended by the array. Additional loss will occur as a function of the packing density of the array. However, the spillover loss can be minimized by use of a corrugated horn with low side and back lobes. Extending the aperture of the horn to the array by the use of an absorbing type shroud can reduce space loss and undesired radiation.

3.11.3.2 Input Power Requirements

Required RF input power for a space feed can be calculated by considering element size at the receive aperture and calculating the power density at the receive aperture to supply the required element input power. Multiplying that power density by the area of the array and adding in spillover losses gives the total RF input power.

For a 177 element space feed with four wavelength elements on the receive aperture, a power density of 0.176 mW/cm^2 is required to provide 5 mW per element. Assuming an array diameter of 91 cm and 3 dB spillover loss, the total RF input power required is 2.3 watts.

3.11.4 Space Vs Corporate Feed

To provide additional input for a decision on feed type, trade-off calculations can be made to quantify differences in power requirements for each type. For easy comparison, equal output power can be assumed and required input power can be calculated. Feed systems can then be compared solely on the basis of input power, or the array power-added-efficiency (PAE) can be calculated. Besides feed system choice, an additional trade-off factor in this application is amplifier configuration. Single or cascaded configurations can be considered, where the trade-off is an additional amplifier stage for lower RF input power. To provide the most complete data, trade-off calculations will be made for each configuration and both feed types.

3.11.4.1 Relevant Assumptions

Assumptions used in making these calculations include:

1. Reflector gain is 53 dB
2. Corporate feed loss is 3.2 dB
3. Space feed spillover loss is 3 dB
4. VPS-VPA configuration has 10 mW in, 185 mW out, 12.5% efficiency on VPA. (185 mW represents the average RF output per element)
5. VPS-CGA-VPA configuration has 0.125 mW in, 185 mW out, 15% efficiency on CGA, 12.5% efficiency on VPA
6. The 177 element array has 4λ (6 cm) element apertures. Array diameter is 91 cm

3.11.4.2 Results of Trade-Off Calculations

Results of amplifier and feed configuration trade-off calculations are shown in Table 3.11.4.1. RF output power (and EIRP) is equal in all cases. The effect of changing amplifier configurations is clearly seen, as a slightly higher DC input power is required but RF input power is dramatically less. The effect of changing from corporate to space feed is an increase in required RF input power of about 20%. From PAE calculations, the space-fed single amplifier configuration is least efficient, while the corporate-fed cascaded amplifier configuration is most efficient. Note, however, that the difference in efficiency between space and corporate-fed cascaded configurations is only 0.004%. This suggests that only a negligible price is paid for the substantial cost and weight savings provided by the space-feed. As an alternative, a corrugated feed horn with absorber cone can be used to decrease spillover to less than 2 dB, resulted in a space feed advantage. The use of microstrip for the corporate feed configuration would reduce the number of transitions required to feed the MMIC modules and, consequently, a reduction of weight and complexity. However, the loss of microstrip (1.2 dB/ft) compared to waveguide (0.14 dB/ft) would impose a severe penalty on the RF input requirements.

3.11.5 Feed System Summary

Both feed types have been reviewed and their uses in this application explored. The corporate feed offers advantages of near exact power division between elements and no extra radiation of RF signals. Considering the number of elements involved here, a corporate feed would be costly and bulky. The space feed, on the other hand, uses no heavy power division network. It offers lower cost and weight, and no power balance uncertainty. Trade-off calculations show that losses in both feed types are about equal. Therefore, it appears that the space feed is preferred for this application for the cost and weight savings it offers. Additional investigations should be made concerning the use of microstrip for the corporate feed and the RF input requirements.

Table 3.11.4.1. Space Vs Corporate Feed

Feed Type	Module Type	RF Input Power Per Element	Number of Elements	Total RF Input Power*	DC Input Power Required	Total RF Output Power	EIRP **	Array Efficiency
Corporate	VPS-VPA	10 mW	177	3.7 W	254.9 W	32.75 W	68.15 dB	11.397%
Space	VPS-VPA	10 mW	177	4.5 W	254.9 W	32.75 W	68.15 dB	11.083%
Corporate	VPS-CGA-VPA	0.125 mW	177	46.2 MW	260.7 W	32.75 W	68.15 dB	12.545%
Space	VPS-CGA-VPA	0.125 mW	177	56.0 MW	260.7 W	32.75 W	68.15 dB	12.541%

* Includes feed losses

** Including 53 dB reflector gain

$$\text{ARRAY EFFICIENCY} = \frac{\text{RF Output} - \text{RF Input}}{\text{DC Input}}$$

An additional conclusion reached from the trade-off calculations is that the cascaded amplifier configuration is preferred because it provides a 1.5% higher efficiency. This is because each amplifier is operating in a more efficient mode.

3.12 Module Thinning

From the space vs corporate feed calculations (Table 3.11.4.1), it is evident that the high EIRP requirements coupled with transmit module efficiencies make for a severe DC input power requirement. One of the selected scanning beam configurations calls for a module thinning scheme to reduce this requirement. Basically, module thinning implies removing some modules from some elements in an attempt to improve overall efficiency of the system. The sections below outline the development of two module thinning configurations and show how the modules can be thinned according to a typical weighting scheme. These results are then applied to the 177 element array and compared with a non-thinned array.

3.12.1 Method Used

The method used to arrive at a module-thinned phased array is:

- Consider all possible combinations of 1, 2, and 3 modules
- Choose several cases of RF input power which allow use of full module capability without saturation
- Thin modules according to a weighting scheme, considering quantization levels
- Calculate EIRP and DC INPUT POWER
- Compare thinned with non-thinned case

3.12.2 Module Combinations

Assuming that a variable phase shift (VPS) module is required for each element, the three available modules provide five useful module combinations as listed in Table 3.12.2.

Table 3.12.2. Module Combinations

VPS only	VPS - CGA	VPS - CGA - VPA
	VPS - VPA	VPS - VPA - VPA

The VPS-VPA-VPA cascade represents a special case which provides additional output quantization levels at the cost of doubling the number of control lines. Use of this combination would be considered separately if required.

3.12.3 Module Thinning Configurations

Two module thinning configurations have been devised using the module combinations from Table 3.12.2. Thinning type A uses both single and double amplifier combinations, while thinning type B uses only single amplifiers. Module thinning type A uses four module combinations as shown in Figure 3.12.3.1 to provide 10 output quantization levels.

Module thinning type B uses three module combinations as shown in Figure 3.12.3.2 to provide 6 output quantization levels.

Summaries of efficiency states and DC input power for each quantization level for both thinning types are included in Appendix B.

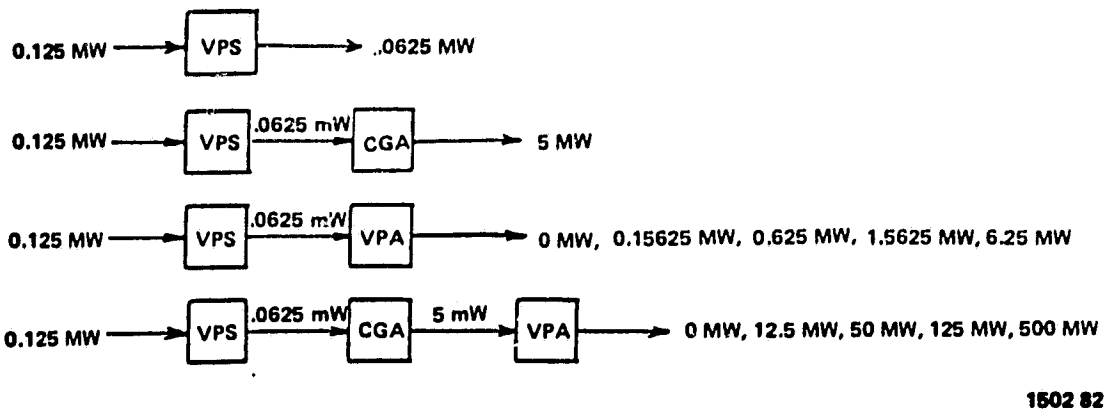

Figure 3.12.3.1. Module Thinning Type A

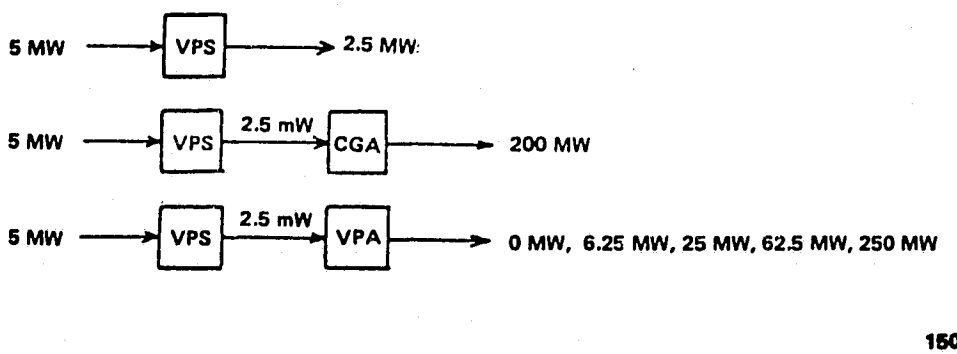

Figure 3.12.3.2. Module Thinning Type B

3.12.4 Weighting Scheme

A weighting scheme has been devised for making module thinning calculations which closely approaches the expected array amplitude distribution. The actual weighting coefficients for any scan angle would be determined by the optimization procedure outlined in Section 3.6.1.

The weighting scheme assumed here is a cosine squared power amplitude taper across the face of the array. The weighting of an element at a distance R from the center of the array is given by:

$$A = A_{max} \cos^2 (\pi R/2R_{max})$$

where A_{max} = maximum amplitude allowed.

The output quantization levels for each thinning type can be substituted in the equations above to calculate the radius at which each quantization level falls. Through this process, a series of concentric rings is created on the face of the array - each ring corresponding to a particular quantization level. The ratio of the area of a particular ring to the total area of the array gives the percentage of the total number of array elements excited at that quantization level. The results of these calculations for both thinning types are given in Appendix B. A 91 cm array diameter was assumed.

3.12.5 Application To A Specific Case

To demonstrate the benefits of module thinning, the weighting scheme was applied to the 177 element array. Details of the numbers of elements at each quantization level along with input and output powers are given in Appendix B. A summary of the results is given in Table 3.12.5.

Table 3.12.5. Summary of Module Thinning Results

Number Of Elements	Thinning Type	Number Of Modules	Total RF Input Power*	Total RF Output Power	Total DC Input Power	Array Efficiency	EIRP**
177	None	531	46.2 mW	32.75 W	260.7 W	12.545%	68.15 dBm
177	A	503	46.2 mW	44.87 W	312.7 W	14.33%	69.52 dBm
177	B	332	4.5 W	19.56 W	134.3 W	13.76%	65.92 dBm

*Includes feed losses
**Assumes 53 dB reflector gain

3.12.6 Summary

Two module thinning configurations have been devised and applied, using a weighting scheme, to the 177 element array. After completing calculations and comparing results, three benefits of module thinning become clear. The number of output quantization levels was increased from four for the non-thinned case to 11 for thinning type A. The array efficiency increased by 1.7% due to the more efficient operating state of the remaining modules. Finally, a reduction of 20% in the number of modules required was achieved (after adjusting for equal EIRP). It is important to note, however, that module thinning cannot change the fundamental limit on array efficiency imposed by the module efficiencies. DC power savings result only because the remaining VPA modules are operating at more efficient power levels.

3.12.7 Receive Aperture Horn Sizing

The introduction of module thinning into the phased array increased the number of output quantization levels from 4 to 11. If additional output levels are required to meet critical scan requirements, a method of varying horn sizes in the receive aperture of the phased array can be used to "tailor" the output power of an individual element to almost any level. Additionally this method can be used to enhance or diminish the effects of the built-in amplitude taper from the space feed.

3.12.8 Achievable Range

The power density method outlined in Section 4.11.3.3 can be used to calculate the range of output power achievable by varying horn size. Assuming horn diameters can be varied from 1 cm to 6 cm (0.7λ to 4λ), a 15 dB range of output variation is possible. Using this range in addition to the 11 available quantization levels, any single required amplitude distribution can be produced on the array.

3.13 System Considerations

A conception of the 177 element space feed scanning beam phased array is shown in Figure 3.13.1. Dimensions are included to show the overall sizes involved. Figure 3.13.1.1 shows a conceptual view of the complete scanning beam phased array as envisioned on a satellite. The three boxes on the bottom of the support arm contain the RF exciter, power supply, and logic control network. The space feed horn aperture has been extended toward the array by an absorbing type shroud to reduce loss and undesired radiation.

3.13.1 Bias and Control Network

The distribution of bias and control lines to the MMIC modules appears trivial when compared to the overall problem of designing a 20 GHz monolithic antenna system. However, considering that 177 elements will appear on each of six scanning beam feeds with each element requiring up to 13 control lines for its modules, the task becomes more complex. Effects of propagation delays on the lines must be considered, with short runs to reduce these delays. Of prime importance is maintaining equal path lengths to all the modules to equalize delays. Additionally, coupling between lines, weight and physical size must be reduced.

One approach to the problem which avoids numerous long wire runs is the use of a multiplexing technique or the use of fiber optics. Optical lines could be run to the core of the array, followed by a corporate distribution to all of the modules. Use of optical fibers would reduce system size and weight while maintaining fast response.

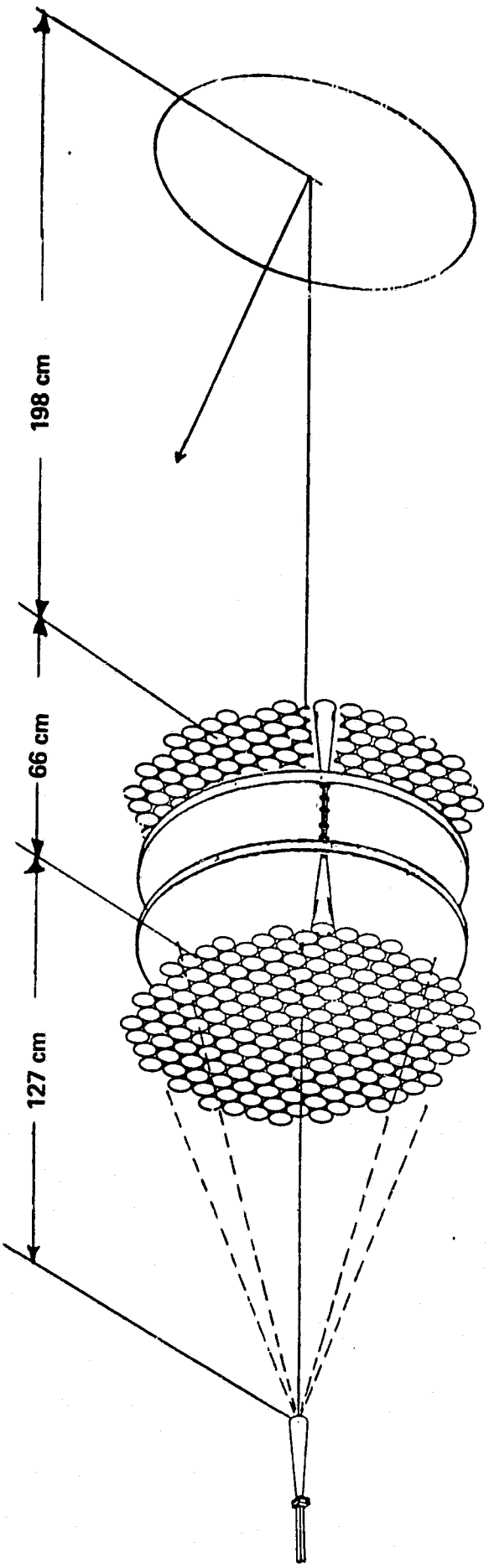

Figure 3.13.1. Scanning Beam Space Fed Phased Array

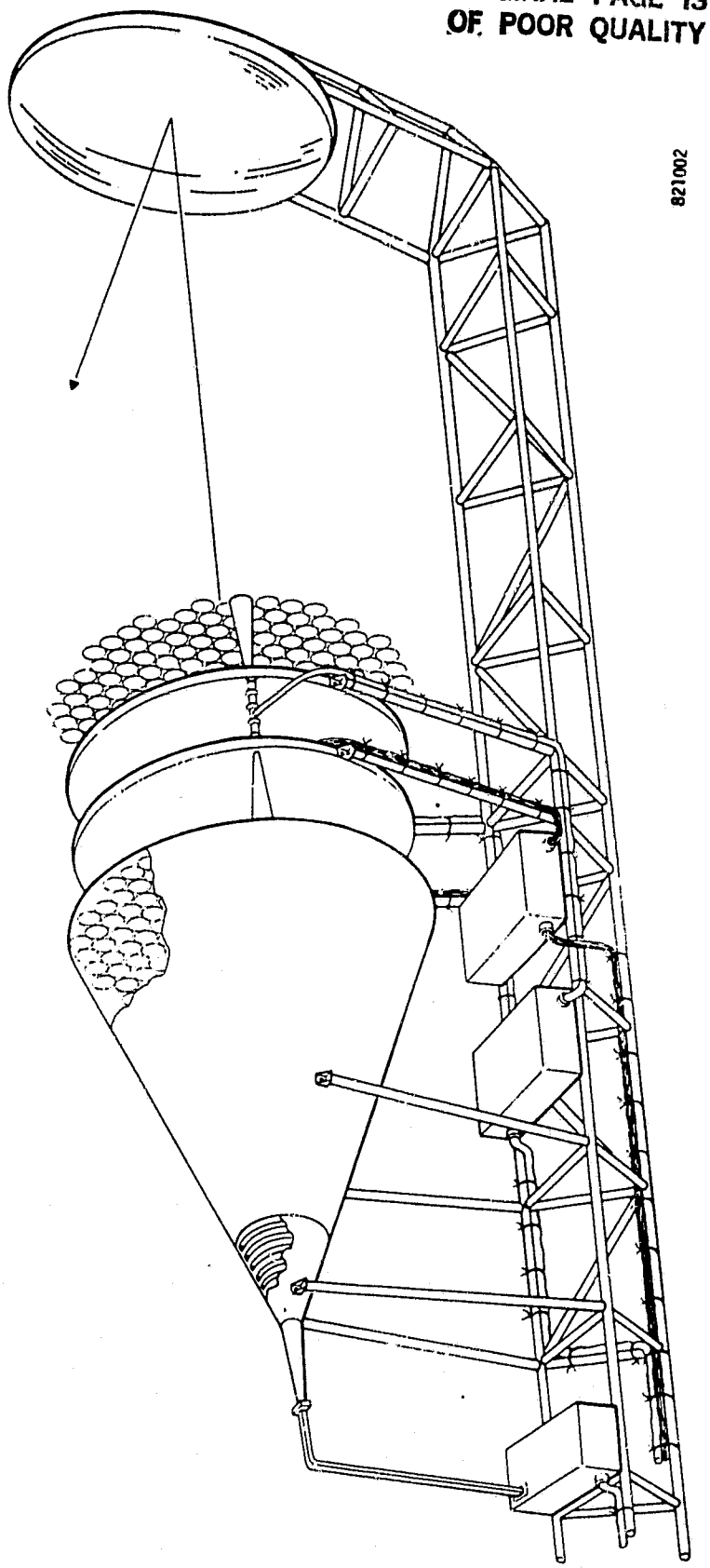

Figure 3.13.1.1. Scanning Beam Space Fed Phased Array

3.13.2 Impact of Extending Technology to 30 GHz

Extension of the technology developed from the 20 GHz phased array study to 30 GHz requires consideration of several important problems. These problems consist of radiating element selection, feed system design, and integration of the monolithic modules.

The near field nonfocused optics developed for the 20 GHz transmit scanning beam array has an advantage over focused systems when there is a transmit EIRP requirement above the available antenna gain. However, for receiving scanning beam arrays (30 GHz), this advantage is not required and there will be interference problems from sector-to-sector for multiple near field feeds operating at the same frequency. This suggests a more careful investigation into the offset dual reflector systems with the subreflector optics in the far field of the feed cluster. The use of the MMIC modules with individual element control will simplify the dual shaped optics presently proposed in the 20 GHz study.

The problems associated with the monolithic module integration include the distribution of local oscillator signals, mounting configuration, bias and control line distribution, and conduction of heat from the modules.

The distribution of the 30 GHz LO signals is analogous to the distribution of the exciter signals for the 20 GHz transmit scanning beam array. Both the space feed and corporate feed techniques can be utilized at 30 GHz with the space feed having less loss due to the increased waveguide losses at 30 GHz utilizing the corporate feed.

The MMIC module configuration can utilize the same mounting technique suggested for the 20 GHz transmit array, except scaled in size to accommodate the smaller waveguide. Present stripline techniques are capable of operating at frequencies up to 40 GHz.

The distribution of bias and control lines have the same requirements for both 30 GHz and 20 GHz and no problems are anticipated in extending the technique to 30 GHz.

The conduction of heat from the MMIC modules will be less severe at 30 GHz because the modules will be operating in a more efficient mode for the receiving applications. Additionally, there is no EIRP requirement for the 30 GHz receiving array and power levels will be lower. The technique developed for the 20 GHz transmit scanning array should provide adequate cooling for the MMIC modules.

3.13.3 Measurements Using 9-Foot Reflector

This section addresses the measurement of the scanning beam antenna system at 20 GHz using a 274.32 cm (9 foot) main reflector. In order to maitain consistent beam performance with that predicted in Section 3.6, the system magnification factor of the near field Cassegrain antenna must be held constant at 4. This implies that the subreflector diameter should be scaled to approximately 68.6 cm (27 inches) and that 177-3λ feed elements be used. On-focus gain would be lower (due to a smaller main reflector aperture) and the expected beamwidth is now about 0.4^{o}, but measured scan performance would be as computed in the parametric trade study.

3.14 Extension to Six Sector Coverage

The previous discussions of the scanning beam array has been limited to a single sector coverage. Extension of the single sector coverage to the required six sector coverage posses several major problems. The problems include location of the six space fed lens to produce the required scan angle without a major penalty in gain, isolation between beams. subreflector shape, conduction of heat from the MMIC modules, bias and control line distribution, and the available physical space.

A major break thru was obtained when the preliminary thermal and packaging analysis indicated that up to two scanning beam arrays could be packaged into one array lens. The use of OMTs (Figure 3.14.1) would permit two sector coverage with polarization isolation between the two beams thus reducing the total number of space feed lens to three. In order to obtain the required scan angle for each sector without a major penalty in gain requires the use of a shaped TRI focal subreflector shown in Figure 3.14.2. The shaped subreflector not only reduces the scan versus gain loss but decreases the dynamic range of weighting coefficients required to correct the array elements because of displacement of the array from the subreflector.

The use of OMTs requires more space due to the increase in the physical size of the OMT, additional waveguide components, and dual MMIC modules for each element of the array. The thermal analysis contained in Section 3.10.5.4 required a 1.5M (5 foot) diameter plate to conduct the heat array from the MMIC modules. The additional 60.96 cm (2 feet) should be adequate to provide space for the dual MMIC modules and the OMTs.

The distribution of bias and control lines would become less difficult since the fiber optics technique for distribution of control lines can be utilized more effectively where a large cluster of modules are in close proximity to each other.

It should be pointed out at this that the results of the preliminary thermal and packing analysis are a very critical item and that the success of the design of the SBA system is heavily dependent upon the adequate heat removal from the MMIC modules.

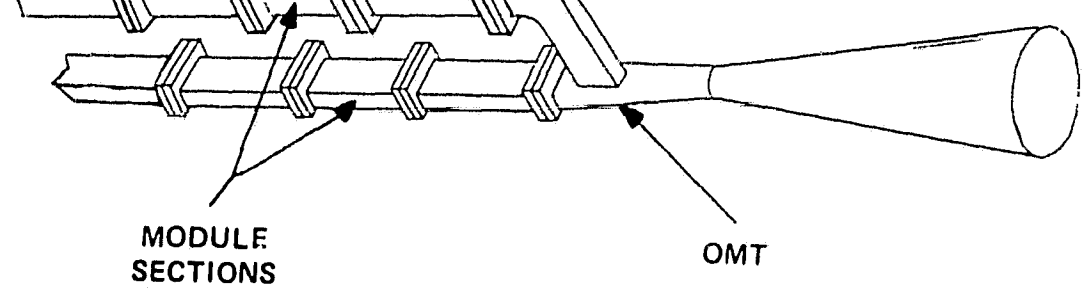

Figure 3.14.1. Feed Horn with OMT

THREE SECTOR FEED ARRAY LAYOUT

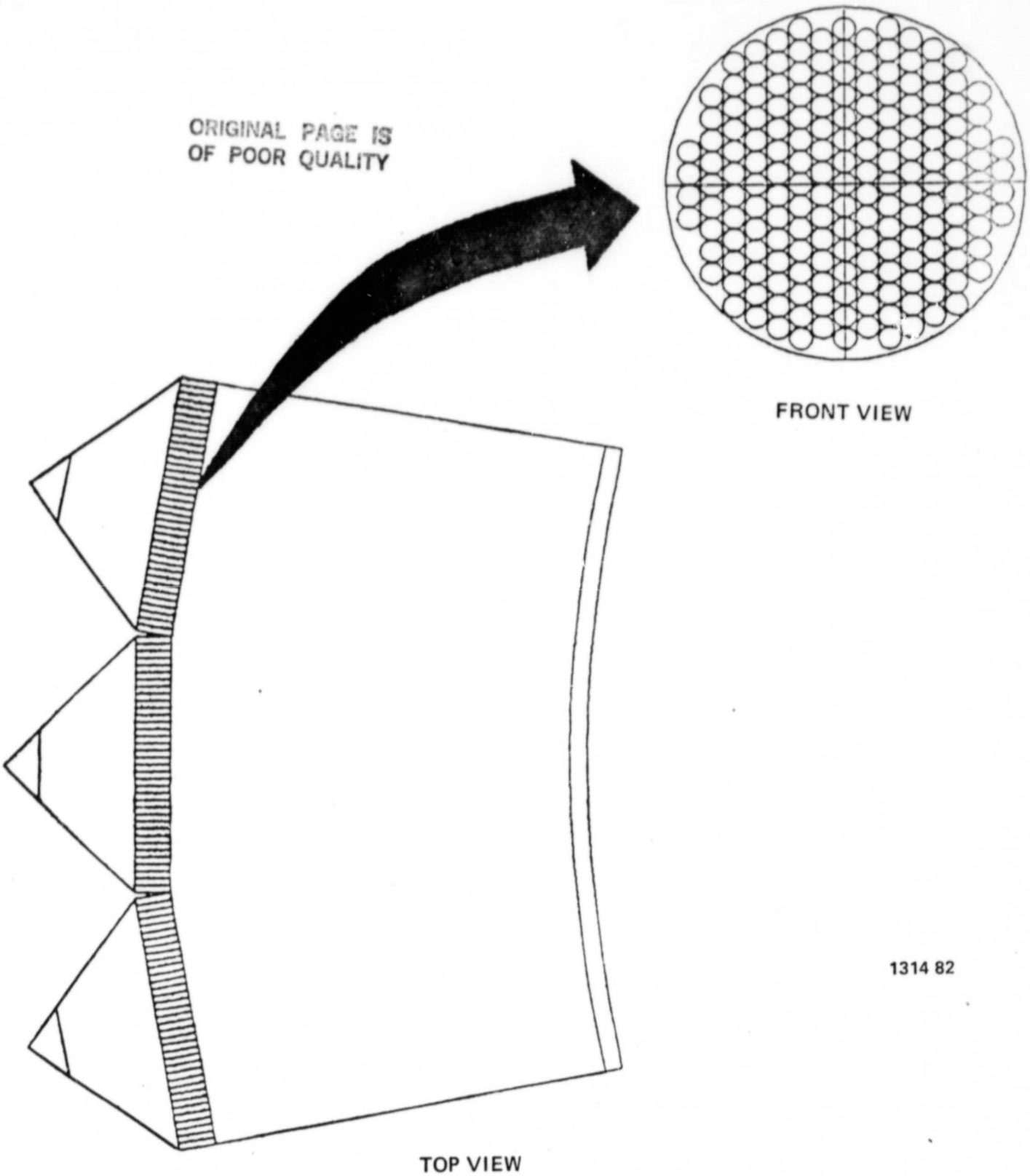

Figure 3.14.2. TRI-Focal Subreflector

3.15 Scanning Beam Antenna Summary and Conclusions

1. It has been found that near field optics is necessary to obtain the required EIRP over the specified scan angle with a minimum loss of antenna gain. Shaped tri-focal optics is required to produce the specified scan angle and maintain isolation for the 6 sector scanning beam coverage.

2. The space lens offers a substantial cost and weight saving advantage over a corporate fed in the distribution of exciter signals to the MMIC modules. Further development of light weight absorbing materials for space use is required to improve the efficiency of the space fed lens.

3. Preliminary thermal and packing analysis indicates that up to two scanning sectors can be accommodated in one array lens with the use of OMTs. The major problem of adequate cooling of the MMIC modules appears to be within the state of the art of advanced cooler designs. However, it is recommended that additional studies should be initiated of advanced cooler designs to adequately handle the heat dissipation of second generation MMIC modules with greater output power levels and increased heat dissipation requirements.

4. The present MMIC modules have sufficient phase quantization levels but finer control of amplitude is highly desirable to provide adequate beam trimming and improve C/I performance. It is recommended that additional studies be initiated to determine the hardware tradeoffs versus finer amplitude quantization levels.

5. The distribution of bias and control lines to individual MMIC modules is still a major problem due to the large number of modules required for the SBA system. A more integrated approach should be taken to this problem in which the logic control network should be considered together with the distribution of the control lines to the individual MMIC modules.

C-2

4.0 MULTIBEAM ANTENNA SYSTEM

4.1 Summary of Requirements

An approach, closely paralleling that used for the design of the scanning beam feed/reflector system, is utilized in the design of the multibeam antenna system for fixed beam service. Design goals, differing primarily in EIRP requirement, are shown in Table 4.1.1. Once again, the approach will be to first optimize reflector geometry via a parametric study, recommend two integrated feed/reflector systems, and then proceed to the electrical and mechanical design of the feed clusters.

4.2 Selection of Reflector Type

The lower EIRP requirement, combined with a gain specification of 53 dB, results in fewer elements (one VPA module per element) being needed per city beam. This implies an electrically small feed, with the reflector surfaces in the far field defined by the value R as

$$R > \frac{2D^2}{\lambda} \quad ,$$

where D is the diameter of the feed cluster and λ is the operating wavelength. The overall diameter of the feed cluster D is, incidently, essentially independent of the number of elements within the cluster, e.g., a 19-element cluster is approximately of the same diameter as a 7-element cluster, but its individual elements are smaller. Therefore, traditional focused optics reflector systems can be utilized. Gain degradation considerations, for off-axis beams, suggest the use of offset dual reflector antennas demonstrating low scan losses. Possibilities include the offset Cassegrain and dual offset shaped, or Schwartzchild, reflectors, shown in Figure 4.2.1. Since shaping is not considered in this phase of the study, the offset Cassegrain is selected.

Table 4.1.1. Advanced Communication Technology Satellite Multibeam Objective Requirements

Beam Configuration		Multibeam
Antenna Size		Shuttle Compatible
Operation Frequency Range (GHz)	-Downlink -Uplink	17.7 - 20.2 27.5 - 30.0
Number of Beams	-Operational	10 - 18
Minimum Gain (dB)	-20 GHz -30 GHz	53 56
Bandwidth (MHz)	-20 GHz -30 GHz	500 500
Polarization		Linear
C/I Performance (dB)(1)		30
Pointing Accuracy (degrees)	-E & H Plane Polarization	0.02 0.4(2)
Power/Beam (EIRP) dBW		52 - 62

(1) Carrier to interference ratio for each beam relative to all other beams.

(2) Degrees rotation from reference (i.e., true satellite vertical or horizontal).

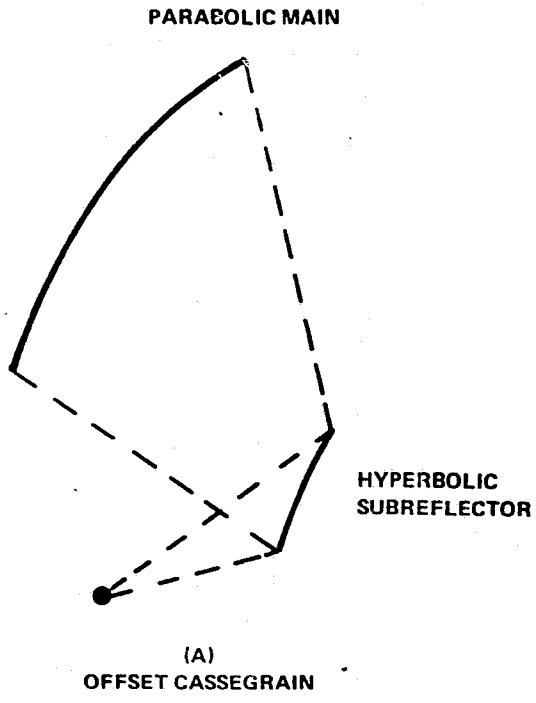

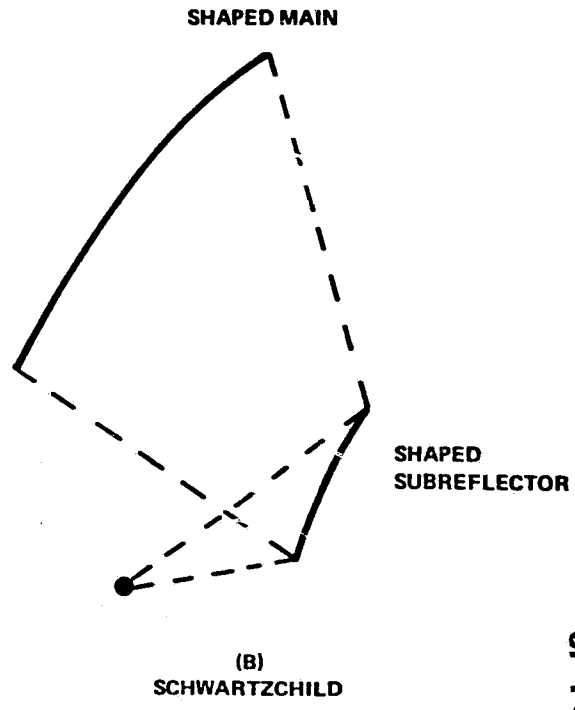

1506 82

Figure 4.2.1. Multiple Beam Optics Configurations

4.3 Parametric Analysis

The optimization of offset Cassegrain geometry, after the initial assumption of a 3.7M (12 foot) main reflector as described in Section 2.2, essentially becomes a selection of the hyperboloidal subreflector shape. In order to sample the entire range of possibilities, and provide a sufficient data base from which to choose this shape, four carefully selected configurations were analyzed. These are shown graphically in Figure 4.3-1, with corresponding parameters listed in Table 4.3.

The shape of each subreflector is best described by an eccentricity e, and each shape corresponds to a different reflector system focal point and magnification factor M, defined as

$$M = \frac{e+1}{e-1}.$$

These four real foci are labeled A through D in Figure 4.3.1, and respectively correspond to equivalent focal length to diameter ratios[9] (F/D) of 0.65, 1.0, 1.35, and 1.71, as shown in Table 4.3. Also shown is a real focus-to-virtual focus (FTF) length representing the distance between the two foci of the hyperboloid. As this distance increases, with a corresponding increase in the magnification factor M, the angle subtended by the subreflector decreases, making it more difficult to efficiently illuminate the reflectors as desired and increasing feed mispointing and spillover losses. Also, recall that a primary advantage of high magnification focused optic reflectors, i.e., large equivalent F/D ratios, is that off-axis gain degredation due to beam scanning is substantially reduced. Therefore, a subreflector shape must be selected which maximizes the subtended angle of the subreflector, substantially reducing feed design complexity and weight, while minimizing off-axis pattern degradation.

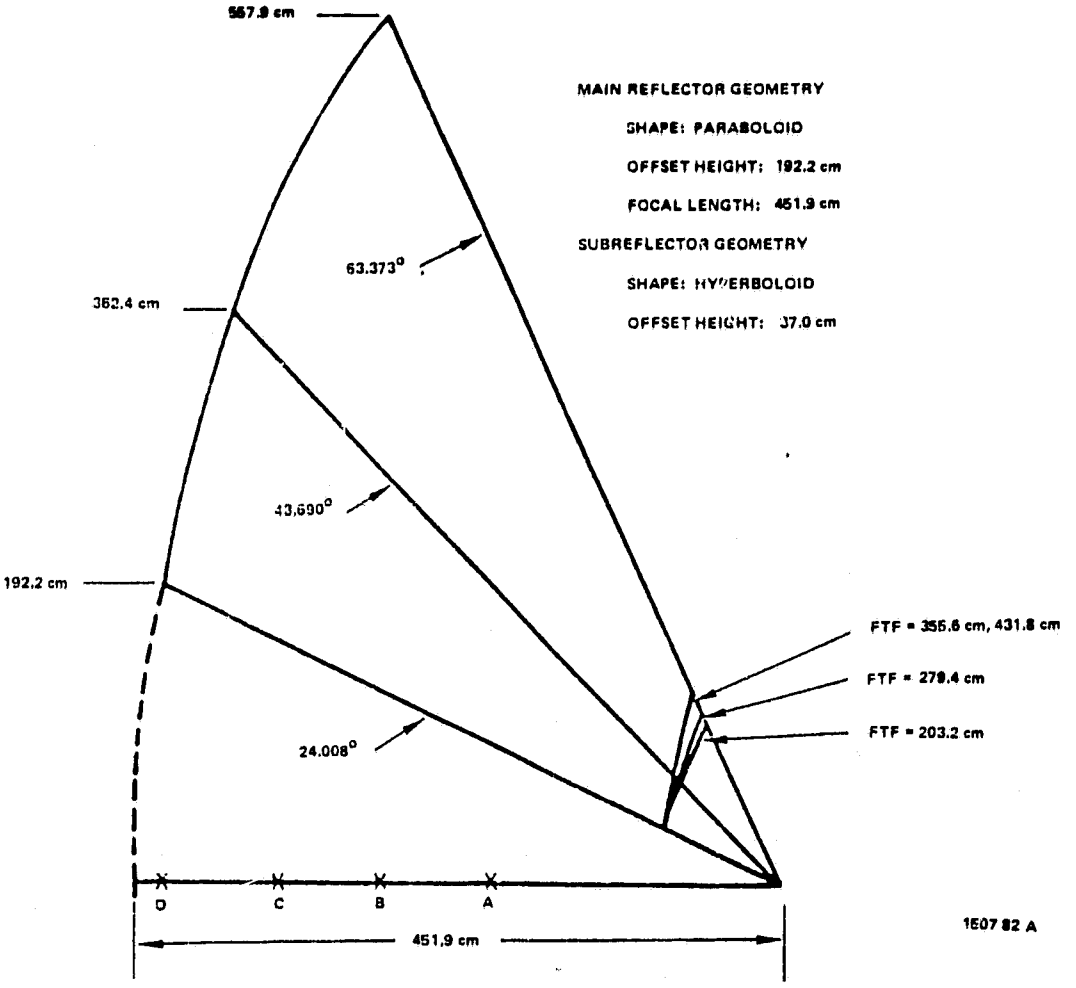

Figure 4.3-1. Initial Point Design Multi-beam Configurations

Table 4.3. Initial Point Design Geometric Parameters
Hyperboloidal Subreflector

	Equivalent F/D	Magnification Factor	Appx Subdish Diameter	Subtended Angle Of Sub	Distance Between Sub Foci "FTF"
A	0.65	1.61	114.3 cm (45")	26.89°	203.2 cm (80")
B	1.00	2.47	114.3 cm (45")	18.17°	279.4 cm (110")
C	1.35	3.34	114.3 cm (45")	13.62°	355.6 cm (140")
D	1.71	4.22	114.3 cm (45")	10.86°	431.8 cm (170")

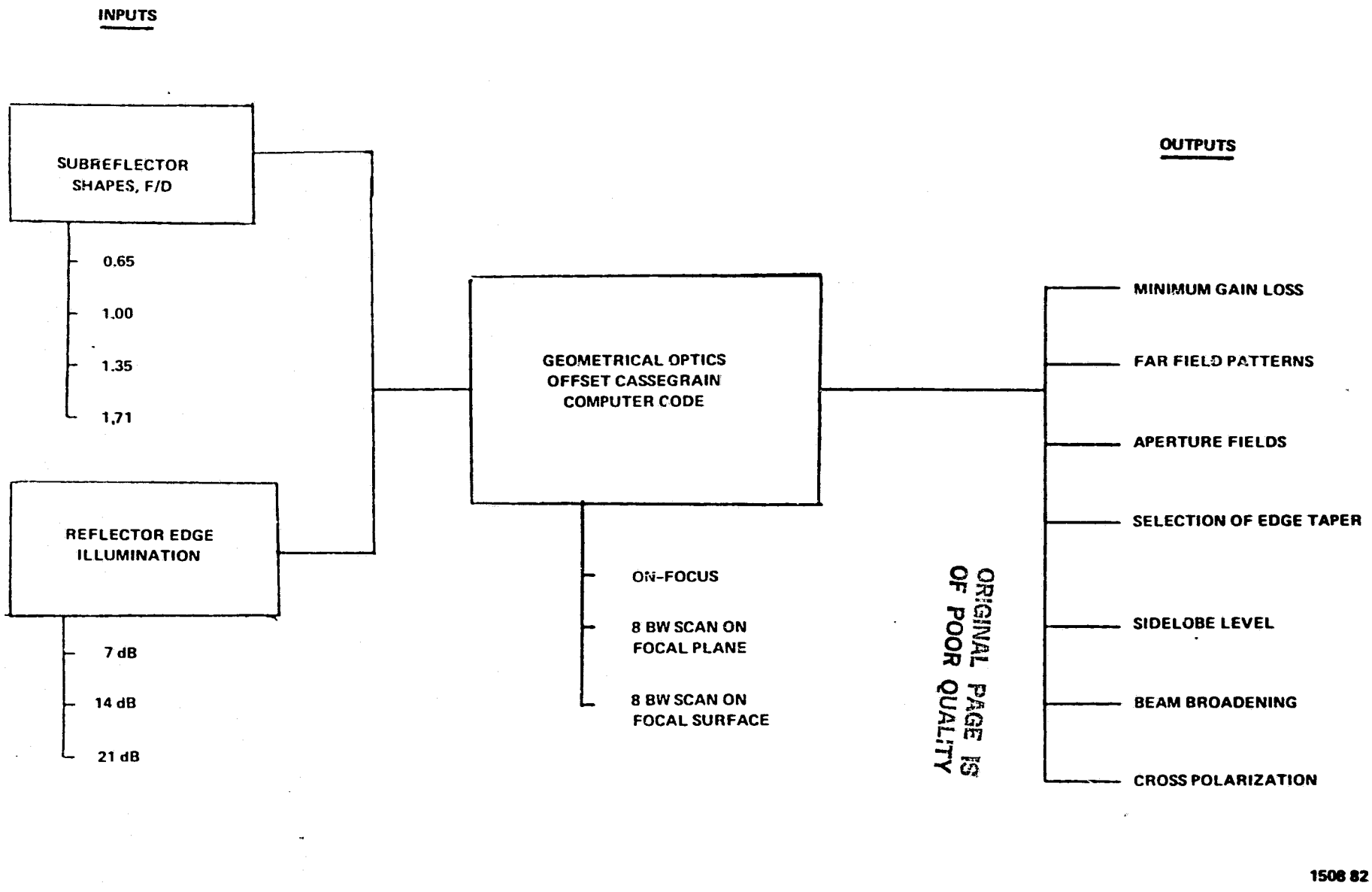

Figure 4.3-2. Multibeam Parametric Analysis Flow

An outline of the analysis flow appears in Figure 4.3-2. To study the effect of reflector edge illumination, all calculations were made using three feed radiation patterns, providing -7 dB, -14 dB, and -21 dB subreflector edge tapers, respectively. Feed patterns are assumed to be linearly polarized, circularly symmetric, and of the form

$$E(\theta) = \cos^{n}\theta,$$

where θ is measured from the boresight of the feed. Far field reflector patterns were calculated for feeds located on-focus, on the focal plane providing for 8 beamwidths of scan, and on the optimal focal surface, also providing for a scan of 8 beamwidths. All calculations were made at a frequency of 20 GHz.

4.4 Analytical Approach

To carry out the calculations just described, two computer codes were utilized. The first of these employs geometrical optics raytracing techniques together with the aperture integration (AI) method. This code has two principle advantages. First, it is a very fast and efficient offset Cassegrain design tool providing reasonably accurate radiation patterns in a very short turn-around time. Second, the AI method provides a means of readily inspecting the fields in the aperture of the main reflector, revealing valuable information to the antenna designer about the electromagnetic mechanisms controlling the far field radiation pattern before a lengthy integration is performed. Full advantage is taken of the latter, in the parametric study of the four reflector configurations.

The second computer code also employs raytracing, but calculates the radiated fields by an integration of equivalent currents[10] over the surface of the main reflector, generally referred to as the surface current integration (SCI) method. This technique has been found to provide very accurate pattern prediction for large spaceborne dual reflector antenna systems in general, and offset Cassegrain reflector antennas in particular. Computer run time is significantly increased, however, so this SCI code is used only for detailed pattern prediction once design information has been obtained from the AI computer code. Verification of both codes can be found in Appendix C.

4.5 Results of Parametric Analysis

Radiation patterns were calculated for all cases described in Figure 4.3-2, but only typical patterns and final results will be shown here. For the case of -14 dB edge illumination and an F/D ratio of 1.0, the on-focus pattern is shown in Figure 4.5-1. Antenna gain is calculated to be 56.6 dB, with the maximum sidelobe radiation greater than 28.5 dB below the beam peak. Cross polarization radiation is greater than 42 dB down. The amplitude and phase of the principal component of the electric field vector across a diameter of the secondary aperture is shown in Figures 4.5-2 and 4.5-3. Note the constant phase and the relative electric vector amplitude of approximately -14 dB at the edge of the aperture.

For the same geometry and feed illumination function, the reflector pattern was calculated at 8 beamwidths of azimuth scan, shown in Figure 4.5-4. The feed phase center is located on the "focal plane", defined as the plane perpendicular to the principal ray, or alternatively, perpendicular to the on-focus feed boresight direction. Gain loss, relative to the on-focus gain, is 3.1 dB. Aperture fields are shown in Figures 4.5-5 and 4.5-6. After moving the feed's phase center to an optimum "focal surface", significant improvement is obtained, as seen in Figure 4.5-7. Gain loss is now only 0.52 dB, relative to the on-focus gain, and sidelobe levels are reduced substantially. Corresponding aperture fields appear in Figure 4.5-8 and 4.5-9.

Complete results are summarized in Figures 4.5-10 and 4.5-11. Surprising as it may seem, gain loss actually increases with increasing F/D ratio for a constant far field beam scan when the feed phase center is confined to lie on the "focal plane." However, once the feed is moved to the optimum "focal surface", gain loss is significantly reduced, and in fact, decreases with increasing F/D. Sidelobe levels behave in a very similar manner, as evidenced by Figure 4.5-11.

The question naturally arises as to why the gain loss curves diverge for increasing F/D, as seen in Figure 4.5-10. Consider the feed to be "in-focus" for a position along the optimum focal surface and badly "out-of-focus" for a position along the focal plane. Figure 4.5-12 shows that

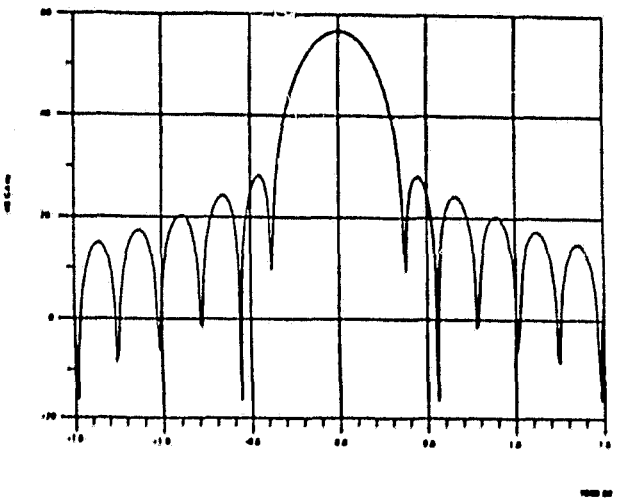

THETA (DEG)
OFFSET CASSEGRAIN GEOMETRY, F/D = 1.00, -14 dB EDGE ILLUMINATION
CO-POL FAR-FIELD PATTERN FOR AN ON-FOCUS FEED

Figure 4.5-1

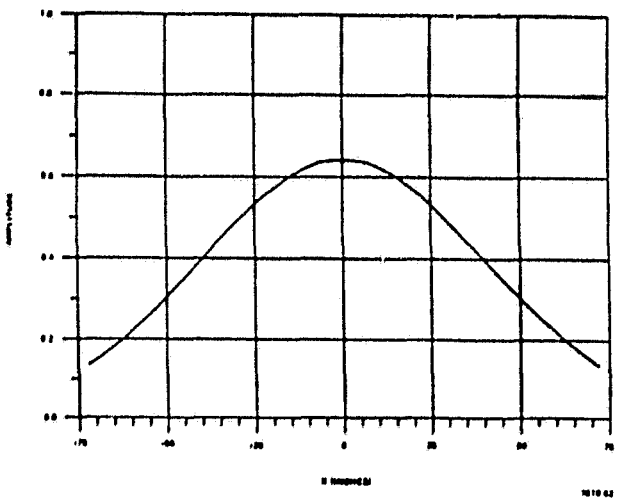

OFFSET CASSEGRAIN GEOMETRY: F/D = 1.00, -14 dB EDGE ILLUMINATION
APERTURE AMPLITUDE DISTRIBUTION FOR AN ON-FOCUS FEED

Figure 4.5-2

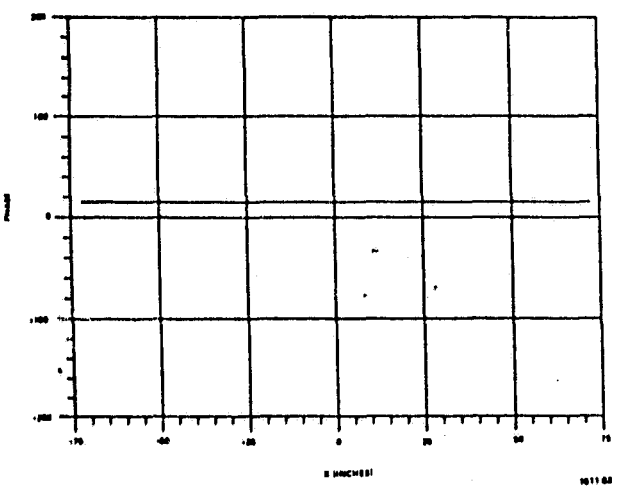

OFFSET CASSEGRAIN GEOMETRY, F/D = 1.00; -14 dB EDGE ILLUMINATION
APERTURE PHASE DISTRIBUTION FOR AN ON-FOCUS FEED

Figure 4.5-3

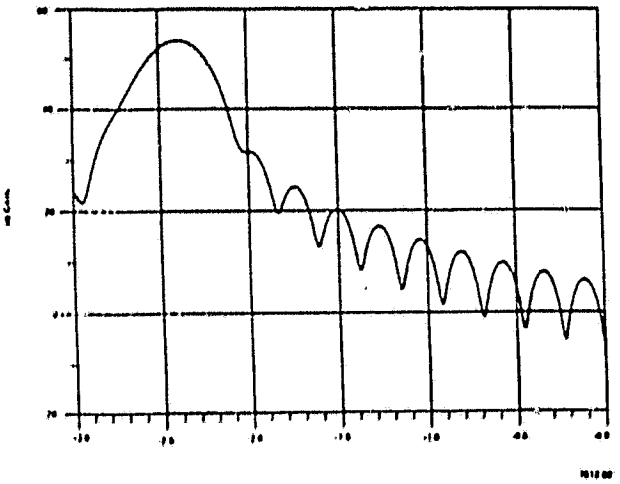

THETA (DEG)
OFFSET CASSEGRAIN GEOMETRY, F/D = 1.00, -14 dB EDGE ILLUMINATION
CO-POL FAR-FIELD PATTERN FOR 8 BEAMWIDTHS SCAN WITH FEED LOCATED
ON THE " FOCAL PLANE"

Figure 4.5-4

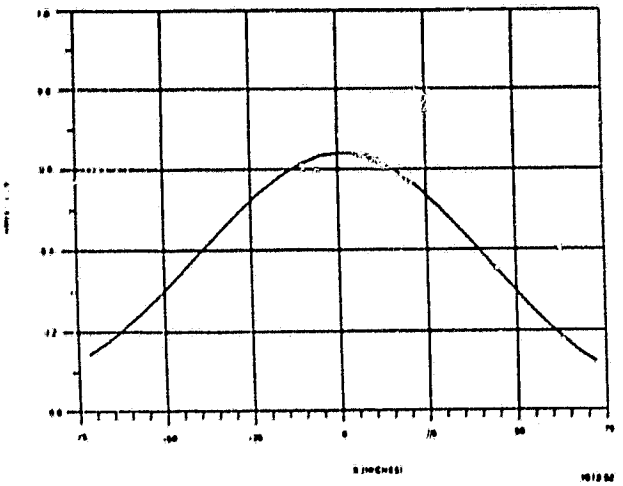

OFFSET CASSEGRAIN GEOMETRY, F/D = 1.00 -14 dB EDGE ILLUMINATION
APERTURE AMPLITUDE DISTRIBUTION FOR 8 BEAMWIDTHS SCAN WITH
FEED LOCATED ON THE "FOCAL PLANE"

Figure 4.5-5

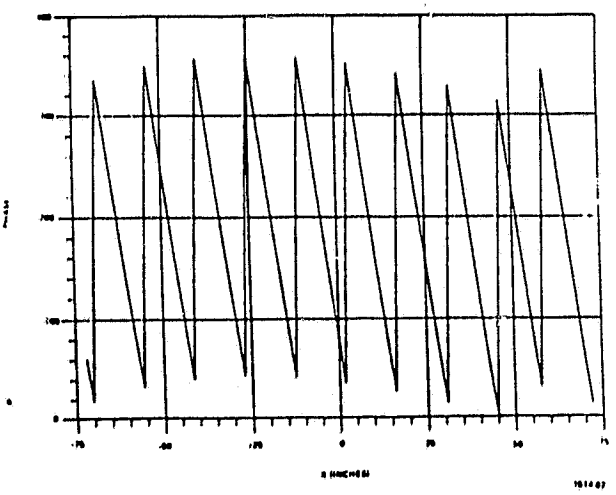

OFFSET CASSEGRAIN GEOMETRY; F/D = 1.00; -14 dB EDGE ILLUMINATION
APERTURE PHASE DISTRIBUTION FOR 8 BEAMWIDTHS SCAN WITH THE FEED
LOCATED ON THE "FOCAL PLANE"

Figure 4.5-6

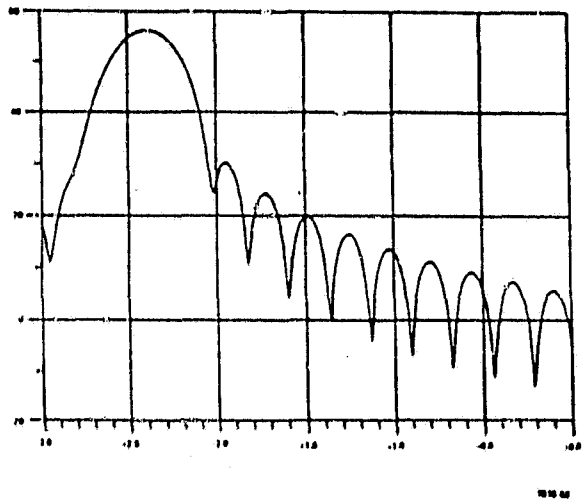

THETA (DEG)
OFFSET CASSEGRAIN GEOMETRY, F/D = 1.00, -14 dB EDGE ILLUMINATION
CO-POL FAR-FIELD PATTERN FOR 8 BEAMWIDTHS SCAN WITH FEED LOCATED
ON THE OPTIMUM "FOCAL SURFACE"

Figure 4.5-7

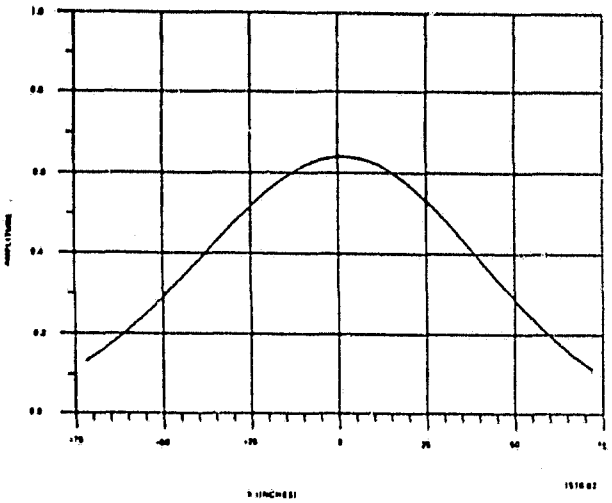

OFFSET CASSEGRAIN GEOMETRY, F/D = 1.00; -14 dB EDGE ILLUMINATION
APERTURE AMPLITUDE DISTRIBUTION FOR 8 BEAMWIDTHS SCAN WITH FEED
LOCATION ON THE OPTIMUM "FOCAL SURFACE"

Figure 4.5-8

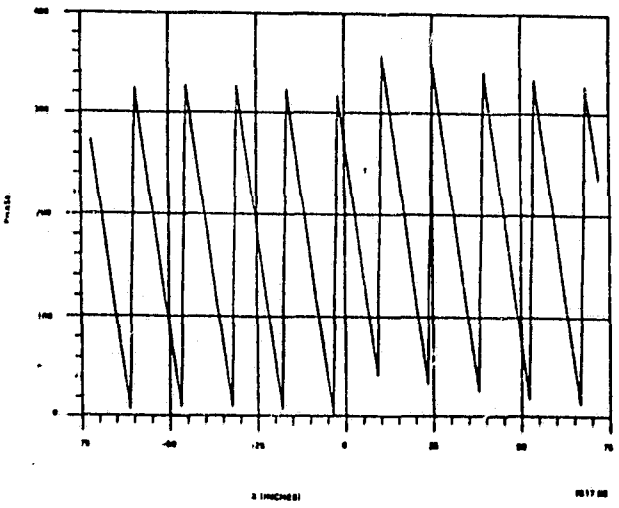

OFFSET CASSEGRAIN GEOMETRY, F/D = 1.00; -14 dB EDGE ILLUMINATION
APERTURE PHASE DISTRIBUTION FOR 8 BEAMWIDTHS SCAN WITH FEED
LOCATED ON THE OPTIMUM "FOCAL SURFACE"

Figure 4.5-9

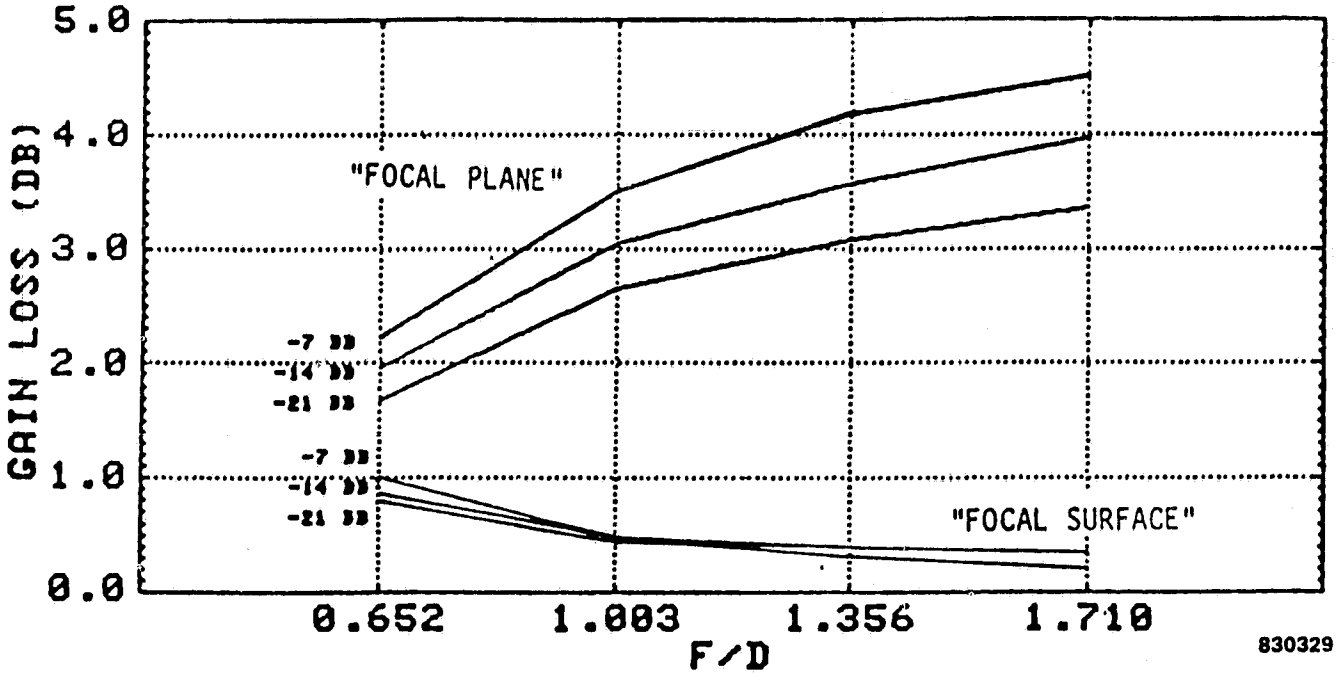

Gain Loss vs F/D Ratio in an Offset Cassegrain Antenna for Feeds Offset Along both the "Focal Plane" and Optimum "Focal Surface" Corresponding to Eight Beamwidths Scan.

Figure 4.5-10

Maximum Sidelobes Level Vs F/D Ratio in an offset Cassegrain antenna. Feed offset along the "Focal Plane" corresponding to 8 beamwidths scan.

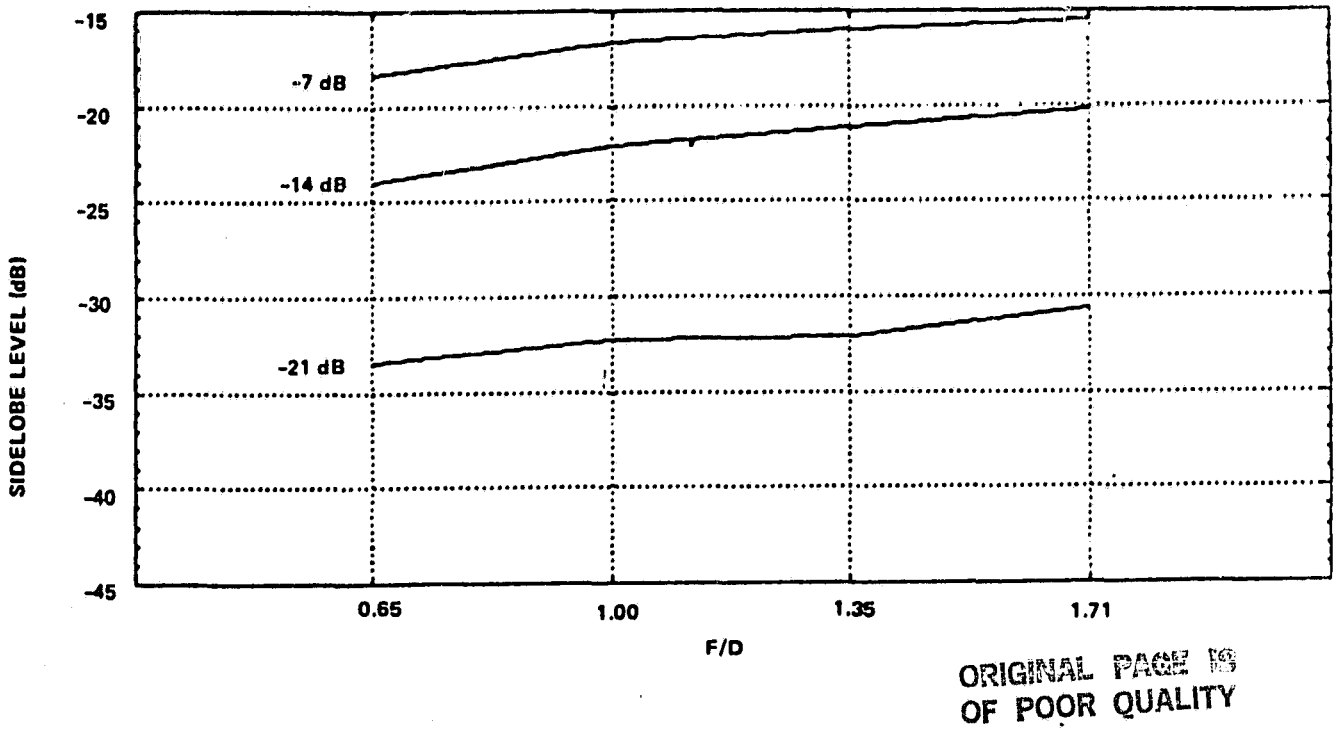

Maximum Sidelobes Level Vs F/D Ratio in an offset Cassegrain antenna. Feed offset along the "Focal Surface" corresponding to 8 beamwidths scan.

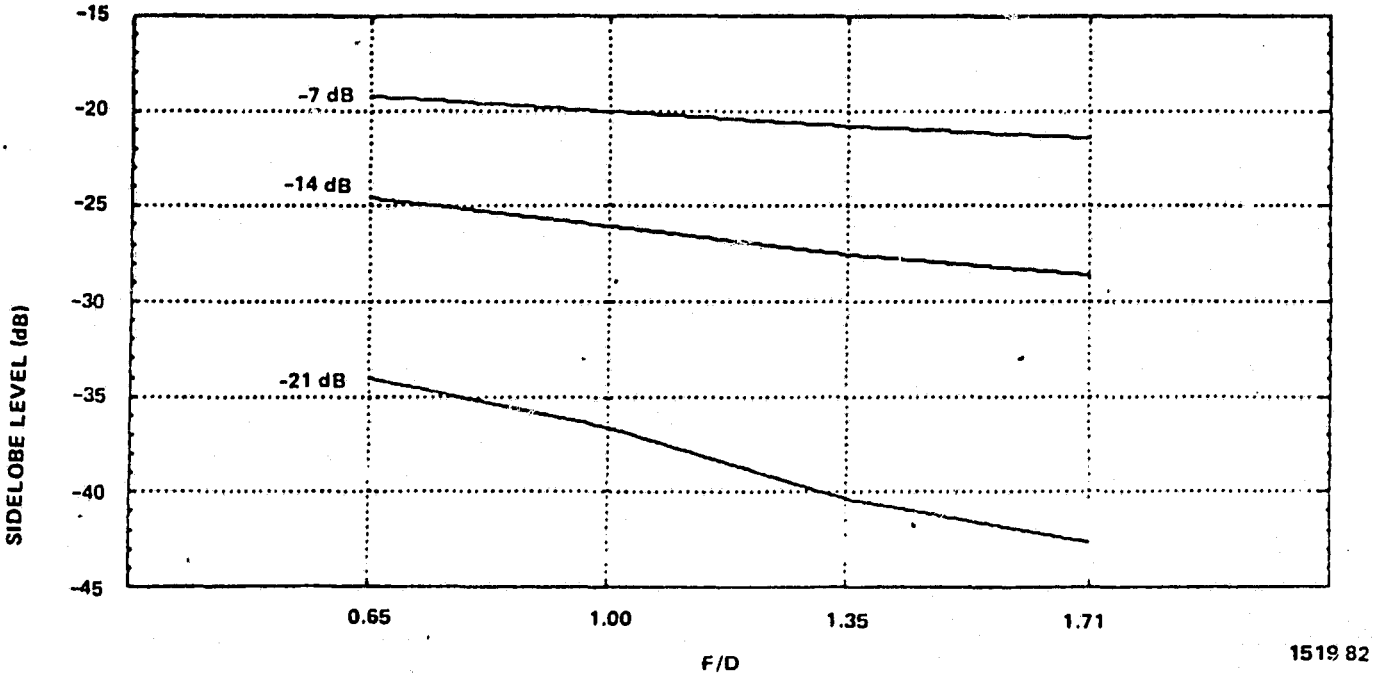

Figure 4.5-11.

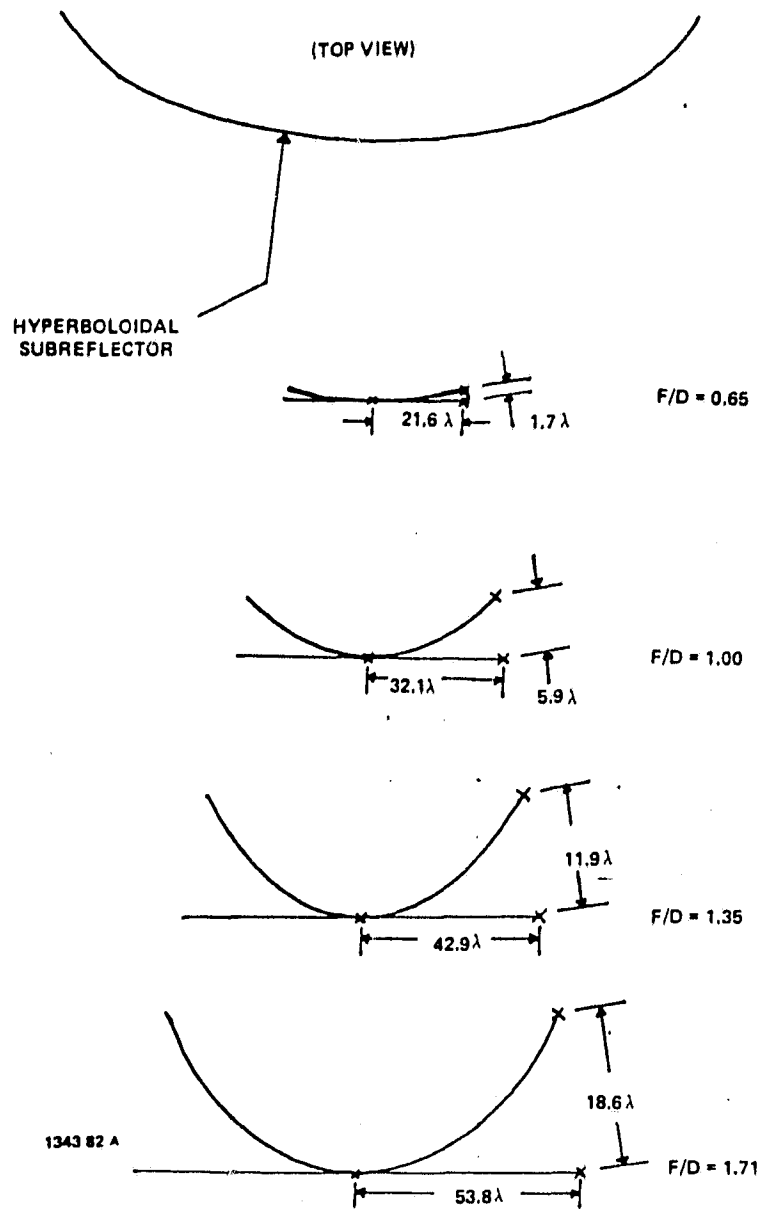

Figure 4.5-12. Feed Plane Versus Optimum Focal Surface

the feed is more out-of-focus for the higher F/D geometries, and in fact, is more than 18 wavelengths away for an F/D of 1.71. This figure shows that for low equivalent F/D geometries, the optimum surface is very well approximated by the focal plane. It also shows that the optimum focal surface deviates from the previously defined focal plane by a greater amount for higher F/D ratios. This indicates an inherent limitation of high equivalent F/D ratio offset Cassegrain reflector antennas and points to reflector shaping as an alternative for large scan and low loss reflector systems.

In selection of a best geometry, two things must now be considered. First, gain loss due to beam scanning must be maintained at a minimum. From Figure 4.5-10, for feeds on the focal surface, this loss decreases with increasing F/D ratio. Secondly, consider the design of eighteen cluster feed arrays, each lying on this highly curved focal surface, and as the equivalent F/D ratio gets higher, the angle subtended by the subreflector becomes smaller, making it more difficult to illuminate it efficiently. This will surely lead to troublesome hardware design considerations for higher F/D ratio systems.

Closer inspection of the focal surface graph in Figure 4.5-10 reveals that little improvement is obtained in gain loss reduction beyond an equivalent F/D ratio of 1.0. There is, so to speak, a "knee" in the curve at this value. For this reason, and the feed hardware design considerations discussed previously, multiple fixed spot beam configuration B (F/D = 1.0) is selected as the design choice.

4.6 Recommended Configurations

Based on the results of the parametric analysis, it is now possible to recommend two feed/reflector configurations for further refinement. These are outlined in Table 4.6, both utilizing the selected reflector geometry of Section 4.5, and differing only in the choice of MMIC modules.

Table 4.6.

CONFIGURATION C - MULTIPLE FIXED SPOT BEAM	
Main Reflector:	365.76 cm (12 foot) diameter paraboloid
Subreflector:	Hyperboloid
Feed:	7 to 19 element cluster for each spot beam on curved (optimum) focal surface
Elements:	Circular waveguide with MMIC modules
MMIC Modules:	Variable Phase Shift (VPS), Constant Gain Amplifier (CGA), Variable Power Amplifier (VPA)
Module Gain:	VPS, -3 dB; CGA, 19 dB; VPA, 20 dB
Module Phase:	3 bits phase shift used to adjust phase weighting to improve adjacent beam C/I
EIRP:	57 dBW
Output Power:	4 dBW (2.5 watts), 0.5 W maximum per element
Input Power Divider:	Amplitude weighting achieved by power dividers
CONFIGURATION D - MULTIPLE FIXED SPOT BEAM	
Same as Configuration C except:	
MMIC Modules:	Variable phase shift (VPS), Variable Power amplifier (VPA)
Module Gain:	VPS, -3 dB; VPA, 20 dB.

4.7 Typical Multibeam Cluster Design - Washington/New York/Boston

With the selection of reflector geometry completed, we turn to the design of individual feed clusters for the trunking beam application. To circumvent the time-consuming design of all 18 relatively similar clusters, a representative set of city locations is chosen that will demonstrate the applicability of the general cluster design procedure and the utility of the MMIC transmit modules in the multibeam antenna system. The Washington/New York/Boston locations are selected because of their proximity, indicating that it may be difficult to meet the 30 dB C/I specification with spatial separation and polarization diversity alone. In order to minimize phase errors and thereby maximize gain, feed clusters are positioned on the optimum focal surface as discussed in Section 4.5, and are oriented so as to most efficiently illuminate the subreflector and reduce spillover.

4.7.1 Cluster Design Procedure

Recall from Table 4.1.1 that the minimum gain of the antenna at the 20 GHz transmit frequency is 53 dB, and the power per beam requirement (EIRP) is 52-62 dBW. Gain and EIRP are related by the equation

$$EIRP_{dB} = Gain_{dB} + Feed\ Power_{dB}, \qquad (1)$$

where feed power is measured in watts for EIRP in dBW. Antenna gain[11] is given by

$$Gain_{db} = 10 \log\left[n \left(\frac{\pi D}{\lambda} \right)^2 \right], \qquad (2)$$

where

$\eta = \eta_p \eta_i \eta_s \eta_x \eta_b \eta_r$

η_p is phase error loss

η_i is illumination loss

η_s is spillover loss

η_x is cross-polarization loss

η_b is blockage loss

η_r is reflector surface error loss

D is the diameter of the antenna

Network losses are not included in the above calculations directly because the feed power is measured at the output of the MMIC amplifier modules (assuming one VPA per feed element). The feed power used in equation (1) can therefore be thought of as the output power of the feed cluster, thereby indirectly including BFN losses.

Assuming that the minimum gain requirement of 53 dB, calculated as in equation (2), is met, we find the required output power of the feed cluster becomes 0.8 watts for the low EIRP requirement of 52 dBW and 7.9 watts for the 62 dBW requirement. As a minimum, this necessitates the use of from 2 to 16 elements, respectively. We note, therefore, that the addition of more elements serves primarily to increase EIRP, and secondarily to improve discrete control of the focal field distribution.

The design procedure is therefore iterative, trading off improved beam performance and higher EIRP against increased complexity in the feed hardware with additional cost and weight. The procedure is briefly outlined below:

- As a starting point, select the minimum number of elements required to achieve the desired far field beam performance.

- Determine the element size and spacing based on the selected antenna geometry, the desired edge illumination, and number of elements.

- Determine element weighting coefficients by the conjugate matching technique[12] and check EIRP. Iterate with more elements until EIRP and desired beam performance is obtained.

Typical cluster arrangments that were considered are shown in Figure 4.7.1.1. Some are seen to be more readily applicable to clusters requiring overlapping elements, as is the case with the Washington/New York/Boston clusters, so careful consideration must be given to each city beam individually. It should be pointed out that an increase in the number of elements during this trade-off study does not increase the overall size of the feed cluster. More (smaller) elements are merely arranged within the same area in order to increase EIRP and improve beam performance. The element excitation coefficients were determined by the so-called conjugate matching technique where element weights correspond to the complex conjugate of the focal field distribution at the element aperture for the case of ideal plane wave reception through the reflector system. This technique is very easy to implement and produces optimum gain at the desired location for the given reflector/feed configuration.

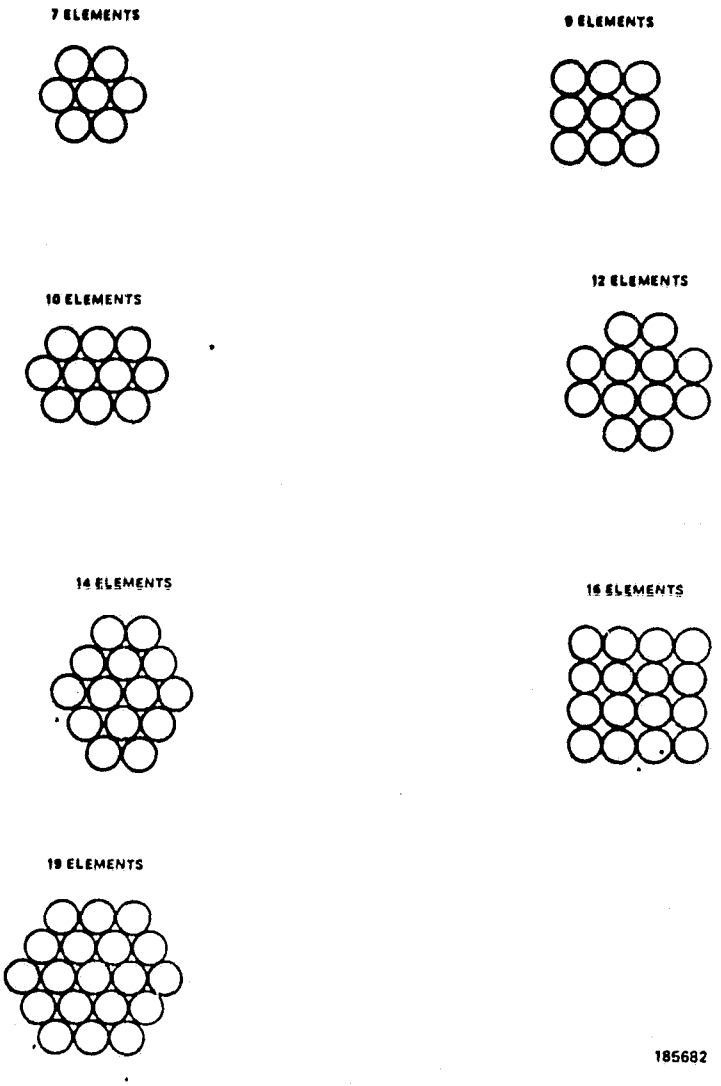

Figure 4.7.1.1

4.7.2 Washington/New York/Boston Beam Performance

A feed plane map appears in Figure 4.7.2.1, with each element's excitation shown in Table 4.7.2.1. The phase of each element has been quantized to the nearest level of phase available from the MMIC variable phase module. This configuration achieves the relative amplitude weights through a power dividing network, so the amplitude values are not affected by the discrete gain levels of the VPA modules. The computed far field performance of each beam is shown in Table 4.7.2.2, and 3-dimensional views of each beam displayed in Figures 4.7.2.3 through 4.7.2.5. The footprint of each of these beams on the Earth, or pattern contour, is shown in Figures 4.7.2.6 through 4.7.2.8.

The beam location from Table 4.7.2.2 is measured with respect to the antenna boresight, 38^{0} North latitude and 83^{0} West longitude. It is important to note that the gain specification is easily met for all three beams, and that the C/I ratio (interference includes only Washington/New York/Boston beams) is above the required 30 dB level. For the 7 element clusters designed, EIRP was consistently about 54 dBW. It appears, therefore, that spatial separation and polarization diversity alone may be sufficient to achieve the desired beam-to-beam isolation.

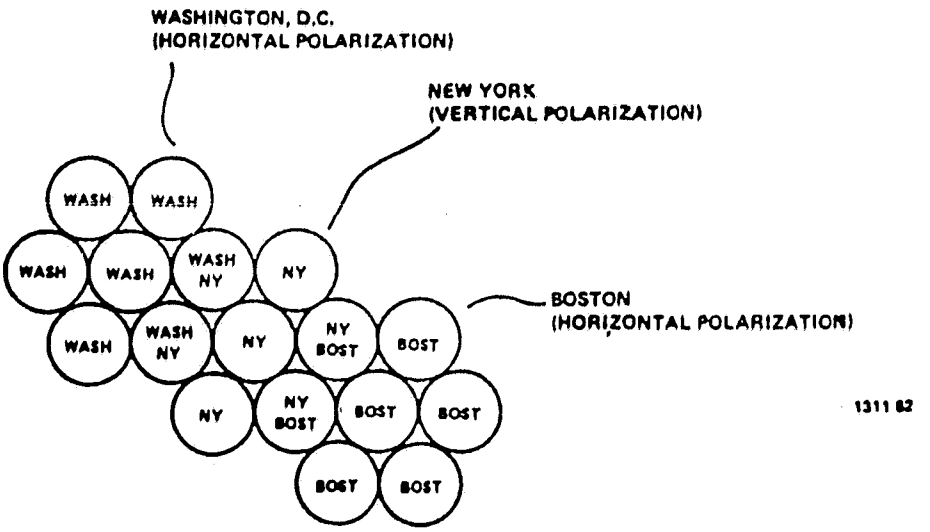

Figure 4.7.2.1. Washington/New York/Boston Feed Plane Map

Table 4.7.2.1. Element Excitation Coefficients for Washington/New York/Boston

Horn	Boston		New York		Washington	
	Relative Amplitude (dB)	Quantizied Phase (Deg)	Relative Amplitude (dB)	Quantizied Phase (Deg)	Relative Amplitude (dB)	Quantizied Phase (Deg)
1	-12.9	-22.50^{0}	-10.6	-11.25^{0}	-15.1	-11.25^{0}
2	-12.2	-33.75^{0}	-10.4	-22.50^{0}	-14.5	-33.75^{0}
3	-9.4	-22.50^{0}	-9.2	-11.25^{0}	-8.9	11.25^{0}
4	0.00	0.00^{0}	0.0	0.00^{0}	0.0	0.00^{0}
5	-7.8	0.00^{0}	-7.9	-11.25^{0}	-8.3	-22.50^{0}
6	-9.8	0.00^{0}	-12.1	-11.25^{0}	-8.4	0.00^{0}
7	-8.5	33.75^{0}	-11.1	-11.25^{0}	-7.8	-11.25^{0}

Table 4.7.2.2. City Beam Performance

City	(AZ, EL) Location	C/I Ratio	Peak Gain	Cross-Pol	EIRP
Washington	(0.65°, 0.1°)	33.9 dB	54.8 dB	-42.1 dB	54.0 dBW
New York	(0.95°, 0.25°)	44.3 dB	54.8 dB	-41.7 dB	54.0 dBW
Boston	(1.2°, 0.45°)	31.7 dB	54.9 dB	-37.9 dB	54.9 dBW

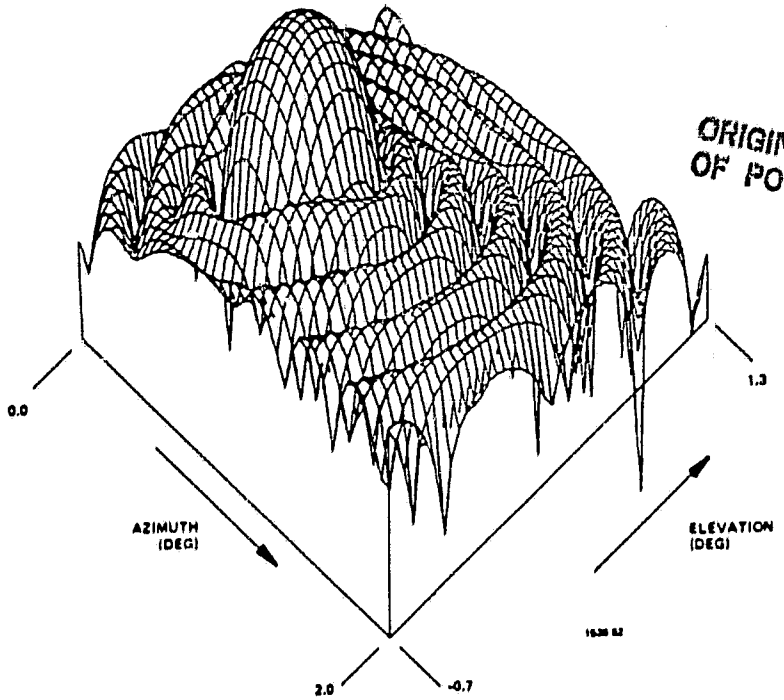

WASHINGTON

Figure 4.7.2.3.

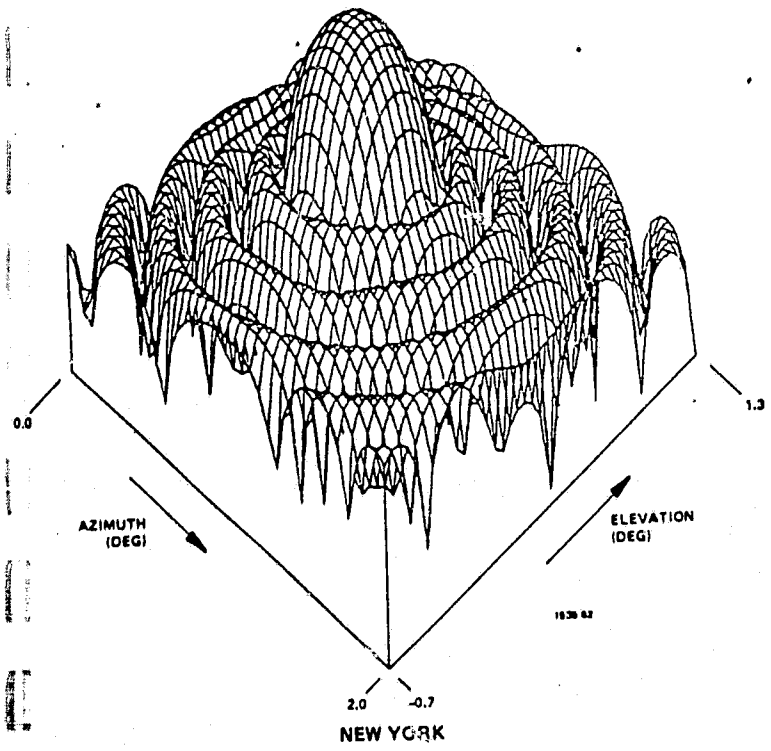

NEW YORK

Figure 4.7.2.4.

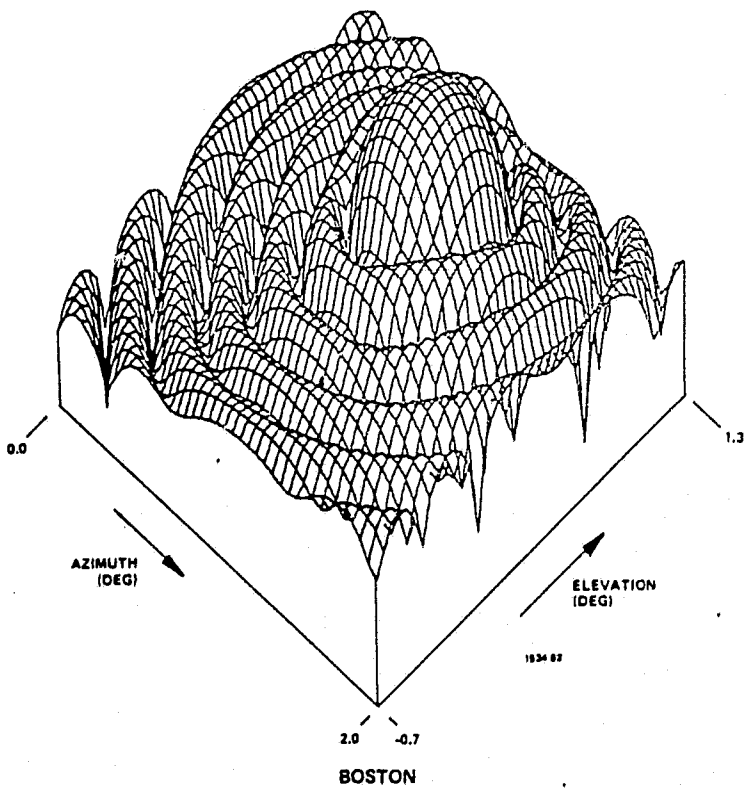

BOSTON

Figure 4.7.2.5.

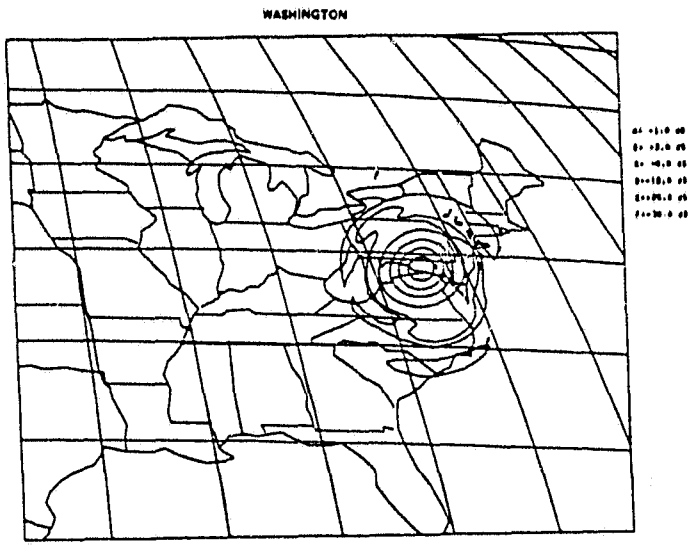

Figure 4.7.2.6. Washington Contour

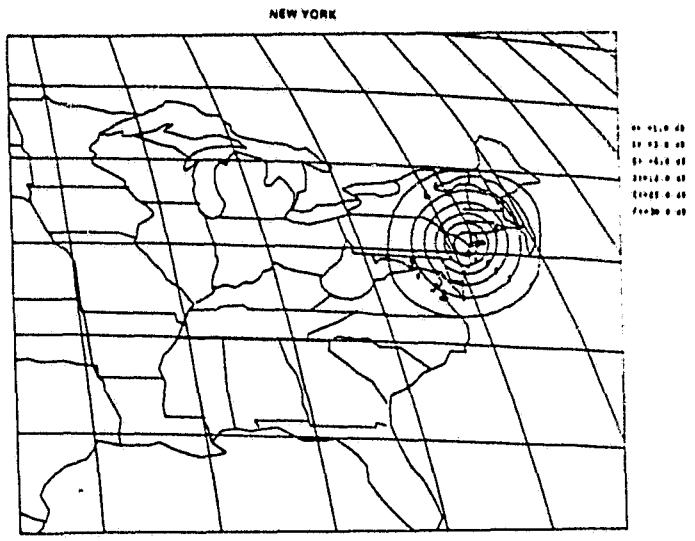

Figure 4.7.2.7. New York Contour

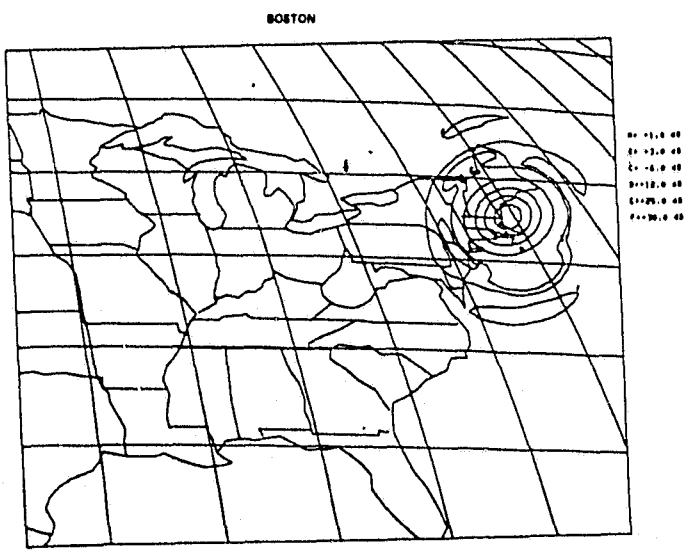

Figure 4.7.2.8. Boston Contour

4.7.3 Dynamic Beam Control

One obvious advantage of the MMIC modules is the capability to dynamically change the amplitude and phase weight of each element in the feed cluster. This may be required due to satellite mispointing, implementation of site diversity schemes because of rain-induced path attenuation, or simply in an attempt to improve the C/I performance at some other location. We concentrate here on the latter reason.

Note that the C/I performance at Boston, shown in Table 4.7.2.2, is 31.7 dB. This is slightly above the 30 dB design goal. The dominant interference component is from the Washington beam sidelobe levels, which are similarly polarized to the Boston beam. In an attempt to improve this C/I ratio, we reoptimize the Washington beam at new locations, resulting in a small amount of scan without significant degradation in beam performance. The original set of weights and two alternative sets are shown in Table 4.7.3.1, with the resulting beam performance listed in Table 4.7.3.2. Note that the C/I ratio at Boston improved to 34.3 dB and 32.9 dB, respectively for the two alternative beams with an increase in EIRP. The gain, however, is reduced, but is above the 53 dB specification in case A. Contours of each beam, shown in Figures 4.7.3.1 through 4.7.3.3, clearly demonstrate the beam movement with limited pattern degradation. The practical implementation of these new weights into the BFN will be discussed in Section 4.8.

Table 4.7.3.1. Three Sets of Weighting Coefficients for Washington

Horn	Original		A		B	
	Relative Amplitude (dB)	Quantizied Phase (Deg)	Relative Amplitude (dB)	Quantizied Phase (Deg)	Relative Amplitude (dB)	Quantizied Phase (Deg)
1	-15.1	-11.25^{o}	-4.4	11.25^{o}	-7.0	-11.25^{o}
2	-14.5	-33.75^{o}	-4.2	-11.25^{o}	-2.2	0.0^{o}
3	-8.9	11.25^{o}	-9.4	0.0^{o}	-15.5	-22.5^{o}
4	0.0	0.00^{o}	0.0	0.00^{o}	0.0	0.00^{o}
5	-8.3	-22.5^{o}	-8.5	-22.5^{o}	-3.6	-11.25^{o}
6	-8.4	0.00^{o}	-19.6	-67.5^{o}	-18.4	-90.0^{o}
7	-7.8	-11.25^{o}	-23.5	-56.25^{o}	-18.7	-33.75^{o}

Table 4.7.3.2. Computed Washington Beam Performance for Three Sets of Element Excitations

Weight	(AZ, EL) Location	C/I Ratio at Boston	Gain at Wasington	Cross-Pol	EIRP
Original	(0.65, 0.1)	31.7 dB	54.8 dB	-42.1 dB	54.0 dBW
A	(0.65, 0.0)	34.3 dB	53.2 dB	-41.9 dB	54.9 dBW
B	(0.7, 0.0)	32.9 dB	52.8 dB	-41.7 dB	55.5 dBW

(ORIGINAL)

ORIGINAL PAGE IS
OF POOR QUALITY

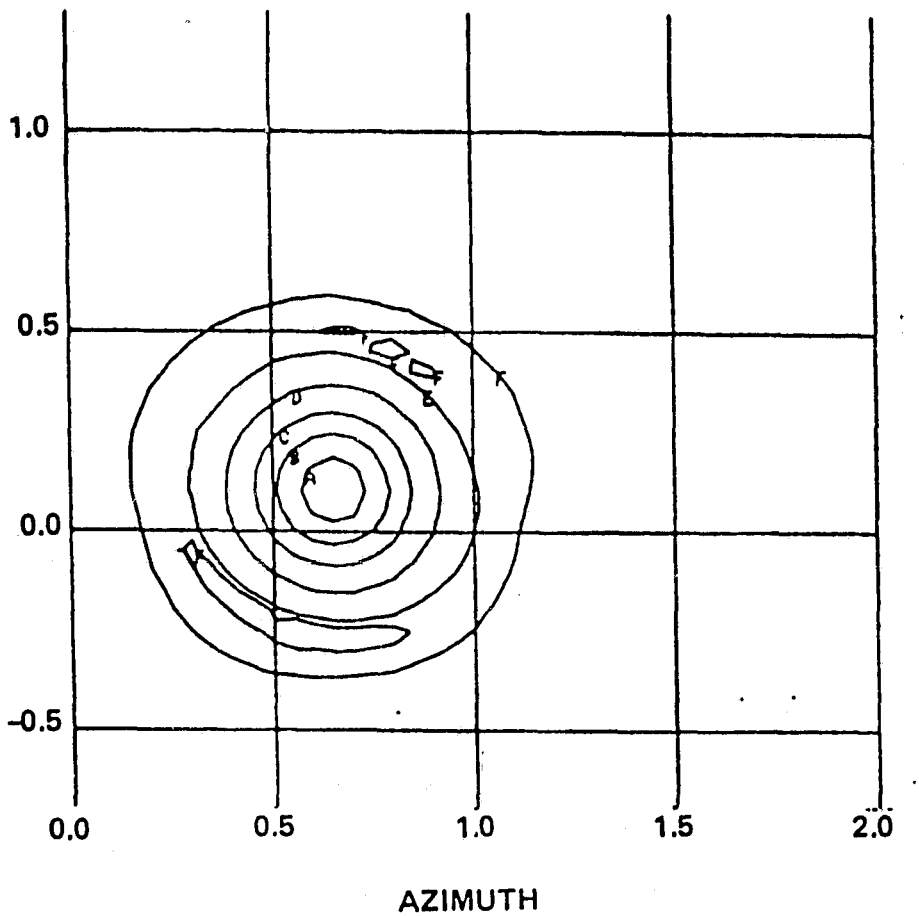

Figure 4.7.3.1. Contour of Original Beam

(ALTERNATE A)

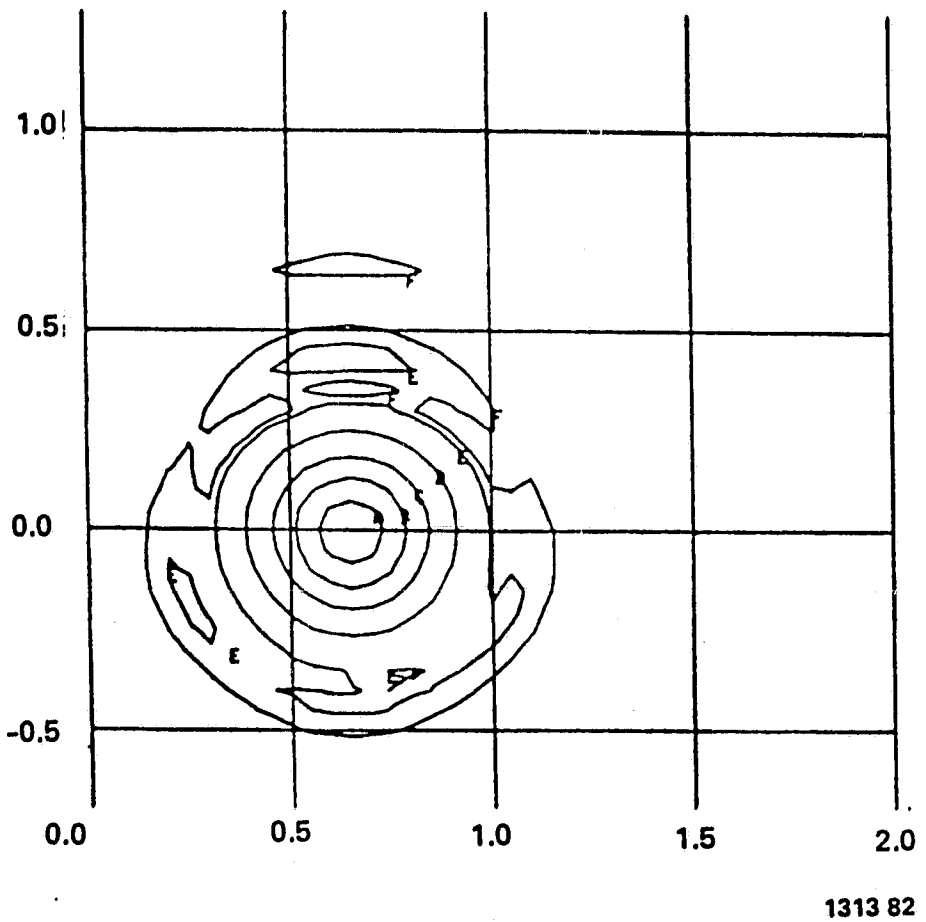

ELEVATION

AZIMUTH

Figure 4.7.3.2. Contour of Alternate A Beam

(ALTERNATE B)

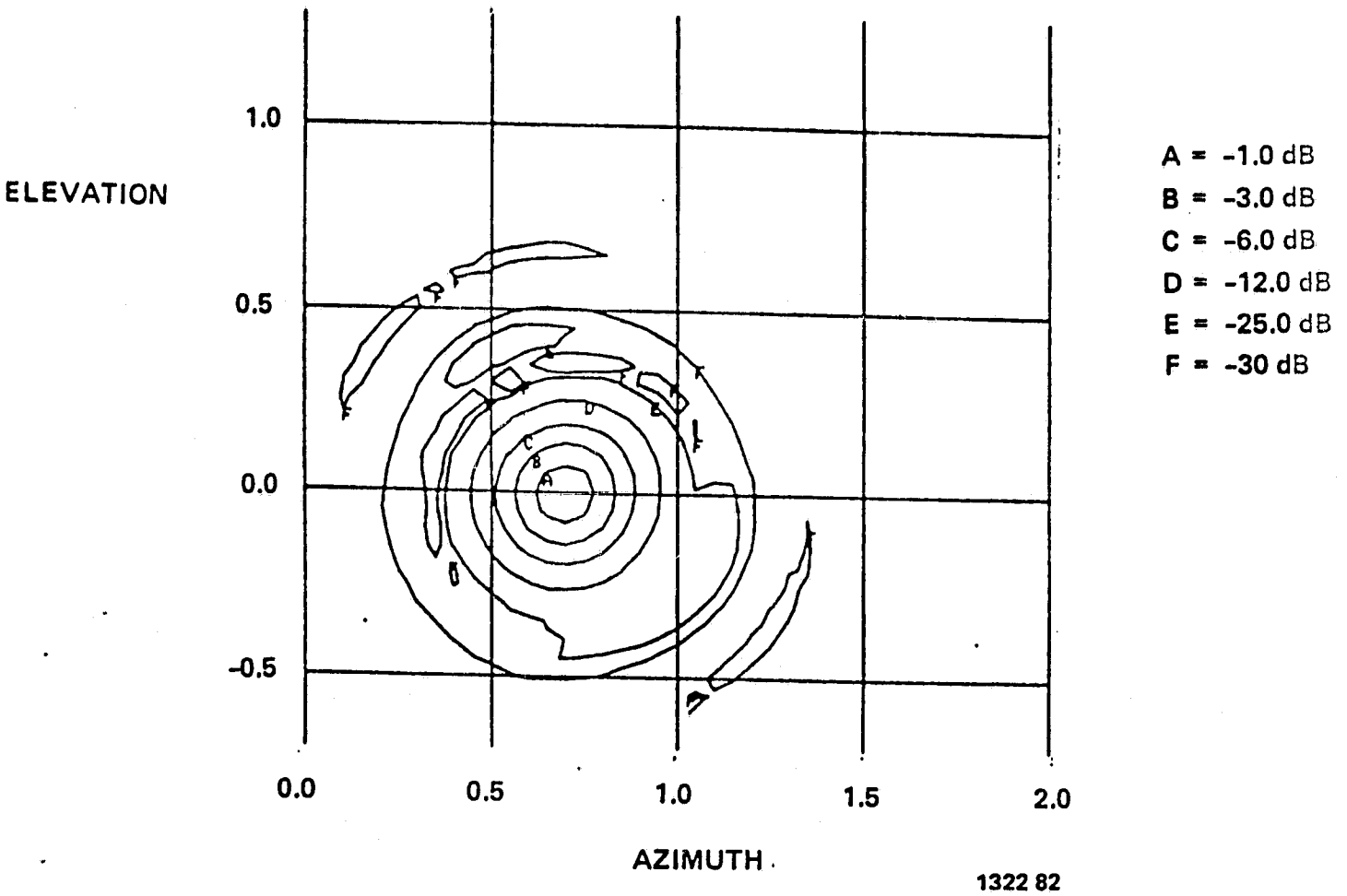

Figure 4.7.3.3. Contour of Alternate B Beam

4.8 Fixed Beam Cluster Design

Design of the fixed beam clusters for the multibeam antenna system is similar to that of the scanning beam phased array design in many respects. The three basic design tasks remain the same: radiating element selection, monolithic module integration and feed system design; however, differing design goals for the multibeam antenna system result in different design tradeoff considerations. Because of lower EIRP requirements, a typical fixed beam cluster requires only 7 elements implying that a corporate feed network may be more practical. The module mounting configuration developed for the scanning beam feed is directly applicable here, as are the transitions for carrying RF signals to and from the modules. An added complexity for the New York/Boston/Washington clusters is their use of shared elements. The hardware implementation thus requires orthomode transducers and two complete sets of modules behind each shared element.

4.8.1 Radiating Element Selection

Selection of the size of the radiating elements is based on city coverage requirements and reflector performance. Analysis showed a cluster of seven 2.57λ elements was required to achieve the specified performance. Circular elements are preferred because of their equal E and H-Plane beamwidths, reduced coupling, and multimode capability. A 2.57λ conical horn with 36^{o} maximum aperture phase error is shown in Figure 4.8.1.1.

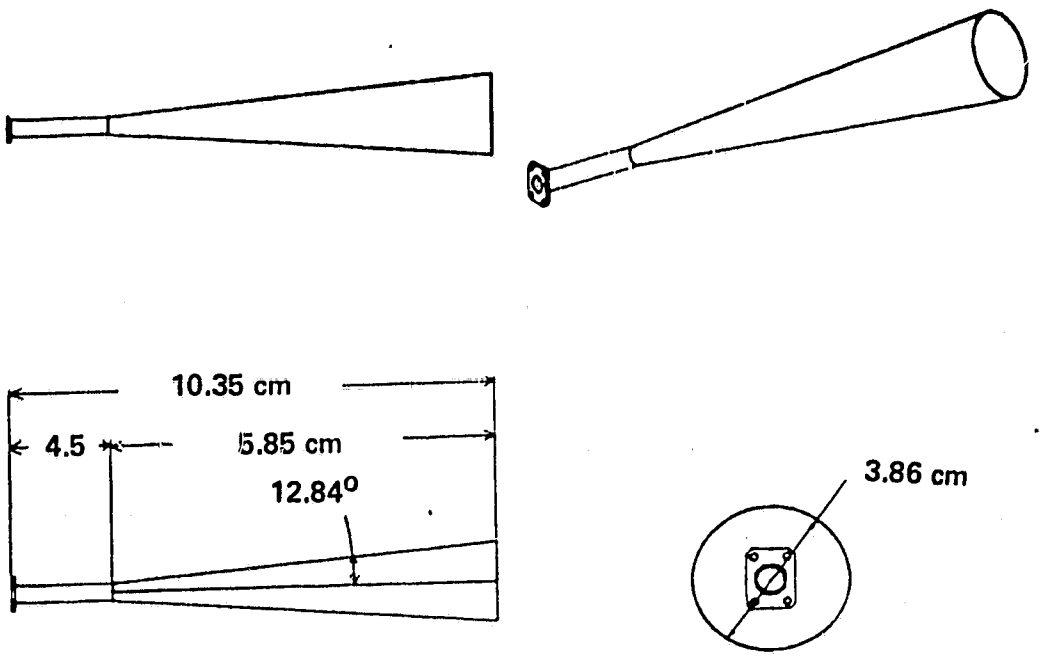

Figure 4.8.1.1. 2.57 Wavelength Conical Horn

4.8.2 Monolithic Module Integration

The monolithic module mounting configuration developed for the scanning beam phased array is directly applicable to the fixed beam cluster. Although size of the radiating element is different, the interface to the beam forming network is identical. Descriptions and diagrams for the mounting configuration are given in Section 3.10*. The completed transition and mounting configuration is shown in Figure 4.8.2.1.

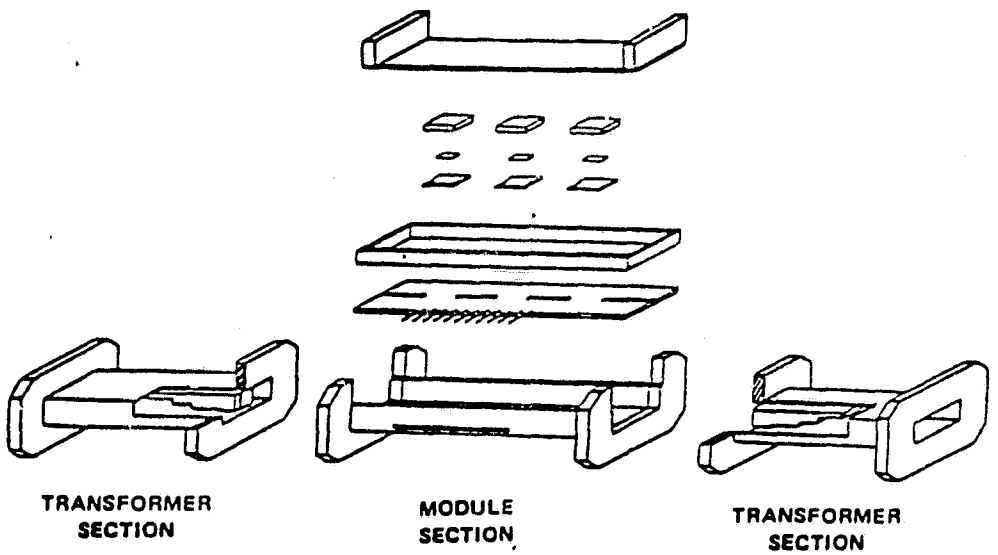

Figure 4.8.2.1. Monolithic Module Transition and Mounting Configuration

4.8.3 Feed System Design

A summary of the basic types of feed systems including discussion of advantages, disadvantages and tradeoff data is given in Section 3.11. A space feed system was chosen for the scanning beam array because it offered substantial cost and weight savings where a large number of elements (177) were involved. The fixed beam cluster, however, contains only seven elements. The close proximity of clusters within the feed and necessity of "sharing" some elements makes space feed difficult. Therefore, a corporate waveguide feed is preferred for the fixed beam cluster. A typical 7 element fixed beam cluster with corporate feed is shown in Figure 4.8.3.1.

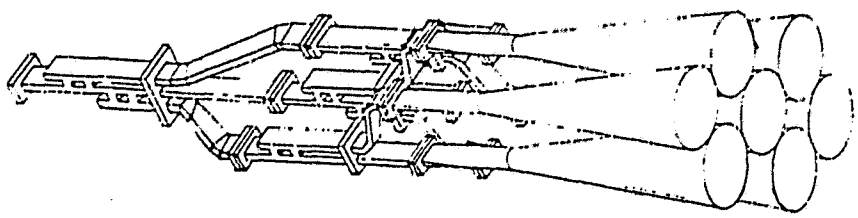

Figure 4.8.3.1. Typical 7 Element Cluster

4.8.3.1 Components

Components of the corporate beam forming network are power dividers, bends, twists, and in the case of shared elements, orthomode transducers. An ideal power divider for use in this application is the branch guide coupler. The branch guide coupler provides wideband performance with accurate power division ratios possible.

4.8.3.2 Losses

A loss budget for a 7 element corporate feed is given in Table 4.8.3.2.1.

Table 4.8.3.2.1. Losses for Seven Element Corporate Feed

Component	Loss
Power dividers (2 levels)	0.6 dB
Bends (5)	0.5 dB
Length (0.4m)	0.2 dB
Total	1.3 dB

4.8.3.3 Shared Elements

In the New York/Boston/Washington feed clusters, sharing of some elements is required to obtain required city coverage. Figure 4.8.3.3.1 shows a feed plane map indicating assignment of shared and nonshared elements. Because polarization isolation is used between adjacent beams, an orthomode transducer is required with two sets of modules. Each shared horn, then, has two inputs with orthogonal linear polarization, one for each beam. Because each input has its own module set, phase and amplitude for that elements contribution to each beam can be controlled independently. Figure 4.8.3.3.2 shows a single elements with OMT and two modules sets.

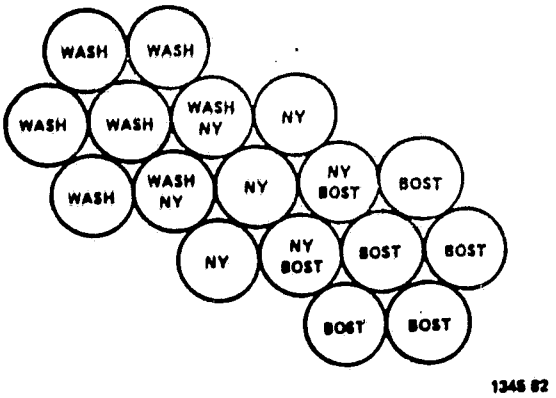

Figure 4.8.3.3.1. Washington/New York/Boston Feed Plane Map

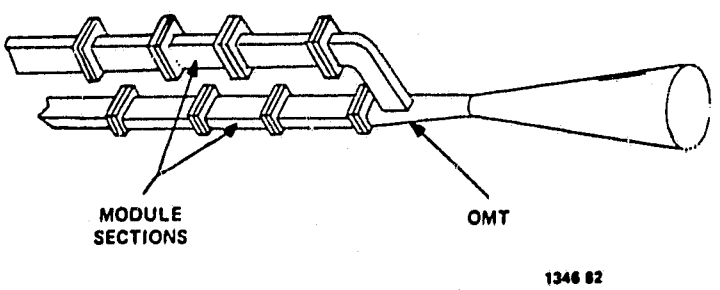

Figure 4.8.3.3.2. Shared Element Configuration

4.8.4 Obtaining Optimum Phase and Amplitude Weights

Section 4.8 presented a method for determining optimum phase and amplitude weights for any beam.

Using the variable phase and amplitude capabilities of the modules in combination with fixed phase and amplitude set by the corporate feed, any desired single set of phased and amplitude weights can be produced. Any trimming or adjustments required to that optimum set must be accomplished within the quantization constraints of the modules. However, by proper choice of feed system weights, it is possible to closely approach one or more alternate beam positions by trimming. As an example, assume that an optimum set and alternate sets have been obtained as in Table 4.7.3.1.

Table 4.8.4.1 shows the amplitude quantization levels in dB available with the VPS-VPA and VPS-VGA-VPA configurations. The 5 bit VPS module gives 11.25^{o} minimum phase quantization.

Table 4.8.4.1. Amplitude Quantization Levels

Power Quantization Level	dB
500 mW	0
125 mW	-6.02
50 mW	-10.0
12.5 mW	-16.02
6.25 mW	-19.03
1.5625 mW	-25.05
0.15625 mW	-35.05

By setting appropriate phase and amplitude levels in the corporate feed, the optimum weights can be obtained as shown in Table 4.8.4.2. Corporate feed levels are relative to element 4.

If proper choices are made for weights in the corporate feed, it is possible to closely approach one or more alternate beam positions by trimming using the modules only. Table 4.8.4.3 shows that alternate beam position A can be obtained with maximum amplitude error of 0.44 dB by changing module weights only. Feed weights are the same as in the original position. Table 4.8.4.4 shows that alternate beam position B can be obtained with maximum amplitude error of 3.27 dB.

The resulting beam performance, showing quantization effects, appears in Table 4.8.4.5. Notice the improvement in C/I ratio from 31.7 dB to more than 34 dB without a significant loss in gain at Washington.

Table 4.8.4.2. Washington Fixed Beam Cluster Corporate Feed and Module Weights

(Original Position)

	Corporate Amplitude (dB)	Weight Phase (Deg)	MMIC Amplitude (dB)	Weight Phase (Deg)	Resultant		Ideal Amplitude (dB)	Weight Phase (Deg)
					Element Amplitude (dB)	Weight Phase (Deg)		
1	-5.0	0.0	-10.0	-11.25	-15.0	-11.25	-15.1	-11.25
2	-4.2	0.0	-10.0	-33.75	-14.2	-33.75	-14.5	-33.75
3	-9.2	0.0	0.0	11.25	-9.2	11.25	-8.9	11.25
4	0.0	0.0	0.0	0.0	0.0	0.0	0.0	0.0
5	-2.5	0.0	-6.0	-22.5	-8.5	-22.5	-8.3	-22.5
6	-2.4	0.0	-6.0	0.0	-8.4	0.0	-8.4	0.0
7	-7.8	0.0	0.0	-11.25	-7.8	-11.25	-7.8	-11.25

Table 4.8.4.3. Washington Fixed Beam Cluster Corporate Feed and Module Weights

(Alternate Position A)

1	Corporate Amplitude (dB)	Weight Phase (Deg)	MMIC Amplitude (dB)	Weight Phase (Deg)	Resultant		Ideal Amplitude (dB)	Weight Phase (Deg)
					Element Amplitude (dB)	Weight Phase (Deg)		
1	-5.0	0.0	0.0	11.25	-5.0	11.25	-4.4	11.25
2	-4.2	0.0	0.0	-11.25	-4.2	-11.25	-4.2	-11.25
3	-9.2	0.0	0.0	0.0	-9.2	0.0	-9.4	0.0
4	0.0	0.0	0.0	0.0	0.0	0.0	0.0	0.0
5	-2.5	0.0	-6.0	-22.5	-8.5	-22.5	-8.5	-22.5
6	-2.4	0.0	-16.0	-67.5	-18.4	-67.5	-19.6	-67.5
7	-7.8	0.0	-16.0	-56.25	-23.8	-56.25	-23.5	-56.25

Table 4.8.4.4. Washington Fixed Beam Cluster Corporate Feed and Module Weights

(Alternate Position B)

	Corporate Amplitude (dB)	Weight Phase (Deg)	MMIC Amplitude (dB)	Weight Phase (Deg)	Resultant		Ideal Amplitude (dB)	Weight Phase (Deg)
					Element Amplitude (dB)	Weight Phase (Deg)		
1	-5.0	0.0	0.0	11.25	-5.0	11.25	-6.99	11.25
2	-4.2	0.0	0.0	0.0	-4.2	0.0	-2.2	0.0
3	-9.2	0.0	-6.0	-22.5	-15.2	-22.5	-15.5	-22.5
4	0.0	0.0	0.0	0.0	0.0	0.0	0.0	0.0
5	-2.5	0.0	0.0	-11.25	-2.5	-11.25	-3.6	-11.25
6	-2.4	0.0	-16.0	-90.0	-18.4	-90.0	-18.4	-90.0
7	-7.8	0.0	-10.0	-33.75	-17.8	-33.75	-18.7	-33.75

Table 4.8.4.5. Computed Washington Beam Performance for Three Sets of Element Excitations

Weight	(AZ, EL) Location	C/I Ratio at Boston	Gain at Wasington	Cross-Pol	EIRP
Original	(0.65, 0.1)	31.7 dB	54.8 dB	-42.1 dB	54.0 dBW
A	(0.65, 0.0)	34.3 dB	53.2 dB	-41.9 dB	54.9 dBW
B	(0.7, 0.0)	32.9 dB	52.8 dB	-41.7 dB	55.5 dBW

4.9 System Considerations

4.9.1 Extension of Multiple Beam Technology to 30 GHz

Extension of the technology developed from the 20 GHz multiple beam study to 30 GHz requires consideration of three basic problem areas. These areas are radiating element selection, feed system design, and integration of the monolithic modules.

The radiating element and feed systems design would be similar to the design utilized on the 20 GHz multiple beam study except scaled in frequency to 30 GHz. Beam-to-beam isolating is achieved with polarization diversity provided by OMTs on each element of the cluster array and spatial separation of the cluster arrays.

The problems associated with the monolithic module integration include the distribution of local oscillator signals, mounting configuration, bias and control line distribution, and conduction of heat from the modules. These problems were discussed in Section 3.13.4 and no significant problems were uncovered that would prevent the technology from being directly extended to 30 GHz.

In summary, the major difference in extending the technology to 30 GHz is the change in requirements from a transmitting beam configuration to a receiving beam configuration. As a result system noise temperature becomes an inportant consideration and care should be exercised in regard to the use of the MMIC modules in the system to reduce losses and system noise temperature.

4.9.2 Measurements Using 9-Foot Reflector

This section addresses the measurement of the multiple fixed beam antenna system at 20 GHz using a 9-foot main reflector. In order to maintain consistent beam performance with that predicted in Section 4.5, the eccentricity of the subreflector (and the corresponding magnification factor) should be held constant. On-focus gain will be lower (due to a smaller main reflector aperture) and the expected beamwidth is now about 0.4^{o}, but measured scan performance would be as computed in the parametric trade study.

4.10 Multiple Beam Antenna Summary and Conclusions

Throughout the study, it was assumed that two reflector antennas were to be utilized for the multiple fixed beam system; one for east-CONUS coverage and one for west-CONUS in order to reduce beam scan requirements. It was shown that feeds located on the optimum focal surface minimized gain loss as a function of scan and would be required to meet the objective requirements. Therefore, in order to utilize a single dual reflector system for multibeam operation, a highly contoured feed cluster arrangement or a shaped subreflector would be required.

It has also been shown that limited dynamic beam control can be effective using conventional beam forming networks and the MMIC modules to improve the C/I performance. Figure 4.8.4.5 shows a typical example of the improvment in C/I performance for the Boston beam cluster utilizing dynamic beam control. Dynamic beam control offers a new flexibilty for future communications system design in obtaining time on orbit beam control.

The present MMIC modules have sufficient phase quantization levels but finer control of amplitude is highly desirable to provide adequate beam tuning and improved C/I performance. It is recommended that additional studies be initiated to determine the hardware tradeoffs versus finer amplitude quantization levels.

REFERENCES

1. R. B. Gamble, M. Westheimer, H. R. Siltzer, and K. M. Speter, "30/20 GHz Fixed Communications Systems Service Demand Assessment," NASA Technical Report No. CR 159620, August 1979.

2. J. M. Bowyer, M. Frankfort, and K. M. Steinnagel, "Task II Report - Planning Assistance for the 30/20 GHz Program," NASA Technical Report No. 1-4-W-1-T11, June 1981.

3. R. Mittra, V. Galindo-Isreal, Y. Rahmat-Samii, and R. Norman, "Offset Paraboloidal Field Computations using an Efficient Series Expansion," presented at the IEEE Symposium on Antennas and Propagation, College Park, MD, May 1978.

4. Galindo-Isreal, R. Mittra, and A. G. Cha, "Aperture Amplitude and Phase Control of Offset Dual Reflectors," IEEE Trans. Antennas and Progation, Vol. AP-27, pp. 154-164, March 1979.

5. Reich, Ordang, Krauss, Skolnik; Microwave Theory and Techniques.

6. M.V. Schneider, B. Grance, and W.F. Bodtman, "Microwave and Millimeter Waves Hybrid Integrated Circuits For Radio Systems," Bell System Tech J., July-August 1969, pp. 1703-26.

7. Cohn, S. B., "Optimum Design of Stepped Transmission-Line Transformers," IRE Trans. on Microwave Theory and Techniques, MTT-3, No. 3 (April 1955), pp. 16-21.

8. Hopfer, S., "The Design of Ridged Waveguides," IRE Trans on Microwave Theory and Techniques, MTT-3, No. 5 (October 1955), pp. 20-29.

9. Peter W. Hannan, "Microwave Antennas Derived From The Cassegrain Telescope," IRE Trans. Antennas & Propagation, Vol. AP-9, pp. 140-153, March 1961.

10. Yahya Rahmat-Samii and Victor Galindo-Israel, "Shaped Reflector Antenna Analysis using the Jacobi-Bessel Series," IEEE Trans. on Antennas & Propagation, Vol. AP-28, No. 4, pp. 425-435, July 1980.

11. Peter J. B. Clarricoats, and Geoffrey T. Poulton, "High-Efficiency Microwave Reflector Antennas - A Review," Proceedings of the IEEE, Vol. 65, No. 10, October 1977, pp. 1470-1485.

12. Hung and R. Mittra, "Secondary Pattern and Focal Plane Distribution of Reflector Antennas Under Wide Angle Scanning," 1982 APS Symposium Digest, May 24-28, 1982, pp. 616-619.

APPENDIX A

MODULE THINNING

SUMMARY FOR MODULE THINNING TYPE A			
RF Output Power Per Element	Module Combination	Efficiency	DC Input Power Per Element
0.0625 mW	VPS	--	--
0.15625 mW	VPS-VPA	6%	1.5625 mW
0.625 mW	VPS-VPA	9%	6.25 mW
1.5625 mW	VPS-VPA	12%	12.5 mW
5 mW	VPS-CGA	15%	32.9 mW
6.25 mW	VPS-VPA	15%	41.25 mW
12.5 mW	VPS-CGA-VPA	15%-6%	157.9 mW
50 mW	VPS-CGA-VPA	15%-9%	532.9 mW
125 mW	VPS-CGA-VPA	15%-12%	1032.9 mW
500 mW	VPS-CGA-VPA	15%-15%	3332.9 mW

SUMMARY FOR MODULE THINNING TYPE B			
RF Output Power Per Element	Module Combination	Efficiency	DC Input Power Per Element
2.5 mW	VPS	--	--
6.25 mW	VPS-VPA	6%	62.5 mW
25 mW	VPS-VPA	9%	250 mW
62.5 mW	VPS-VPA	12%	500 mW
200 mW	VPS-CGA	15%	1316.7 mW
250 mW	VPS-VPA	15%	1650 mW

WEIGHTING SCHEME

- Assume cosine squared amplitude taper across the array
  - Provides good on focus performance
  - Some correction required at scan
- Apply allowed quantization levels to amplitude taper
- Calculate number of elements to be excited at each quantization level

AMPLITUDE TAPER

- The weighting of an element at a distance, R, from the center of the array is given by

$$A = A_{max} \cos^2 (\pi R / 2R_{max})$$

where

A_{max} = Maximum amplitude allowed

- Given the quantization levels allowed, this equation is used to calculate the radius at which each level falls

AMPLITUDE WEIGHTING FOR MODULE THINNING TYPE A

Output Quantization Level	Region Of Array	Percent of Elements Excited At Level
0.0625 mW	45.3 - 45.5 cm	1.42%
0.15625 mW	45.2 - 45.3 cm	0.82%
0.625 mW	44.7 - 45.2 cm	2.21%
1.5625 mW	44.1 - 44.7 cm	2.54%
5 mW	42.8 - 44.1 cm	5.35%
6.25 mW	42.5 - 42.8 cm	1.41%
12.5 mW	41.1 - 42.5 cm	5.44%
50 mW	36.3 - 41.1 cm	17.58%
125 mW	30.5 - 36.3	18.78%
200 mW		12.65%
500 mW	0 - 30.5 cm	31.8%

- Assumes a 91 cm array

AMPLITUDE WEIGHTING FOR MODULE THINNING TYPE B

Output Quantization Level	Region Of Array	Percent of Elements Excited At Level
2.5 mW	42.7 - 45.5 cm	12.35%
6.25 mW	41.1 - 42.7 cm	6.85%
25 mW	36.3 cm - 41.1 cm	17.58%
62.5 mW	30.3 cm - 36.3 cm	18.78%
200 mW	13.5 - 30.5 cm	35.73%
250 mW	0 - 13.5 cm	8.71%

- Assumes a 91 cm array

177 ELEMENT ARRAY MODULE THINNING TYPE A

0.125 mW RF INPUT POWER PER MODULE

Element RF Output Power	Module Type	Number Of Elements	Total DC Input Power	Total RF Output Power
0.625 mW	VPS	3	--	0.1875 mW
0.15625 mW	VPS-VPA	2	3.125 mW	0.46875 mW
0.625 mW	VPS-VPA	4	25 mW	2.5 mW
0.5625 mW	VPS-VPA	4	50 mW	6.25 mW
5 mW	VPS-CGA	9	296.1 mW	45 mW
6.25 mW	VPS-VPA	3	123.75 mW	18.75 mW
12.5 mW	VPS-CGA-VPA	10	1.579 W	125 mW
50 mW	VPS-CGA-VPA	31	16.520 W	1550 mW
25 mW	VPS-CGA-VPA	33	34.086 W	4125 mW
500 mW	VPS-CGA-VPA	78	259.9662 W	39 W
		177	312.65 W	44.873 W

- EIRP 69.52 dB (53 dB reflector gain)

177 ELEMENT ARRAY MODULE THINNING TYPE B

5 mW RF INPUT POWER PER MODULE

Element RF Output Power	Module Type	Number Of Elements	Total DC Input Power	Total RF Output Power
2.5 mW	VPS	22	--	55 mW
6.25 mW	VPS-VPA	12	750 mW	75 mW
25 mW	VPS-VPA	31	7750 mW	775 mW
62.5 mW	VPS-VPA	33	16500 mW	2062.5 mW
200 mW	VPS-CGA	63	82952 mW	12.6 mW
250 mW	VPS-VPA	16	26400 mW	4 mW
		177	134.352 W	19.5675 W

- EIRP 65.92 dB (53 dB reflector gain)

APPENDIX B
COMPUTER CODE VERIFICATION

APPENDIX B

COMPUTER CODE VERIFICATION

The software used for all parametric analysis and design tradeoffs was thoroughly checked against available data. Excellent agreement was found between the Harris offset Cassegrain codes (both AI and SCI) versions) and 1) the Numerical Electromagnetic Code (NEC), Ohio State University, using the equivalent parabola geometry and the aperture integration method, and 2) Raj Mittra, University of Illinois, current integration technique. The latter comparison is shown in Figures B.1 and B.2.

No data was available for the offset near field Cassegrain codes to be compared against. The codes are however, very similar to the two offset Cassegrain codes, differing primarily in the definition or subreflector shape, and have therefore been sufficiently verified.

		Gain		Maximum Sidelobe		Maximum X-Pol	
		OCR	MITRRA	OCR	MITTRA	OCR	MITTRA
ON	f/D = 0.652	55.66 dB	56.66 dB	27.51 dB @ 0.46° 27.61 dB @ 0.45°	27.49 dB @ 0.46°	21.14 dB @ 0.20° 21.18 dB @ 0.19°	21.17 dB @ 0.20°
FOCUS	f/D = 1.710	56.67 dB	56.66 dB	27.98 dB @ 0.46° 28.13 dB @ 0.45°	27.66 dB @ 0.46°	4.89 dB @ 0.18° 4.91 dB @ 0.19°	5.17 dB @ 0.18°
6 BW	f/D = 0.652	55.60 dB @ -1.86°	55.88 dB @ -1.86°	28.90 dB @ -1.42°	29.20 dB @ -1.42°	25.00 dB @ -1.82°	21.22 dB @ -1.68°
SCAN	f/D = 1.710	55.09 dB @ -1.80°	55.34 dB @ -1.80°	29.15 dB @ -1.36°	28.80 dB @ -1.36°	29.03 dB @ -1.80°	23.49 dB @ -1.80°

Gain	Δ Sidelobe	X-Pol
0.00 dB	0.02 dB	0.03 dB
0.01 dB	0.32 dB	0.28 dB
0.28 dB	0.30 dB	3.78 dB
0.25 dB	0.35 dB	5.54 dB

Figure B.1. Offset Cassegrain Code Comparison Aperture Integration Technique

		Gain		Maximum Sidelobe		Maximum X-Pol	
		OCR	MITRRA	OCR	MITTRA	OCR	MITTRA
ON	f/D = 0.652	56.65 dB	56.66 dB	27.61 dB @ 0.45°	27.49 dB @ 0.46°	21.29 dB @ 0.19°	21.17 dB @ 0.20°
FOCUS	f/D = 1.710	56.67 dB	56.66 dB	28.15 dB @ 0.45°	27.66 dB @ 0.46°	5.37 dB @ 0.19°	5.17 dB @ 0.18°
6 BW	f/D = 0.652	55.89 dB @ -1.86°	55.88 dB @ -1.86°	28.92 dB @ -1.42°	29.20 dB @ -1.42°	21.27 dB @ -1.68°	21.22 dB @ -1.68°
SCAN	f/D = 0.652	55.37 dB @ -1.80°	55.34 dB @ -1.80°	28.85 dB @ -1.37°	28.80 dB @ -1.36°	23.53 dB @ -1.79°	23.49 dB @ -1.80°

Gain	Δ Sidelobe	X-Pol
0.01 dB	0.12 dB	0.12 dB
0.01 dB	0.49 dB	0.20 dB
0.01 dB	0.28 dB	0.05 dB
0.03 dB	0.05 dB	0.04 dB

Figure B.2. Offset Cassegrain Code Comparison Surface Current Integration

APPENDIX C

RESULTS OF
ELEMENT WEIGHTING COEFFICIENT SYNTHESIS BY THE SYSTEM TRANSFORMATION MATRIX APPROACH

APPENDIX C

RESULTS OF ELEMENT WEIGHTING COEFFICIENT SYNTHESIS BY THE SYSTEM TRANSFORMATION MATRIX APPROACH

An initial investigation was conducted to determine the combination of MMIC modules needed to achieve optimum scanning beam performance. As the statement of work requested, three combinations were considered:

1. Constant Gain Amplifier (CGA)
   Variable Phase Shifter (VPS)

2. Variable Power Amplifier (VPA)
   Constant Phase

3. Variable Power Amplifier (VPA)
   Variable Phase Shifter (VPS)

To reduce computation time, all analysis was scaled to 2 GHz using half-wavelength elements with an assumed radiation pattern of $\cos^2\theta$. Weighting coefficients and corresponding far field radiation patterns were computed both on-focus and for one typical scan position. A flow diagram of the analysis is shown in Figure C-1. Element weighting coefficients were determined by the system transformation matrix method, described in Section 3.6.1.

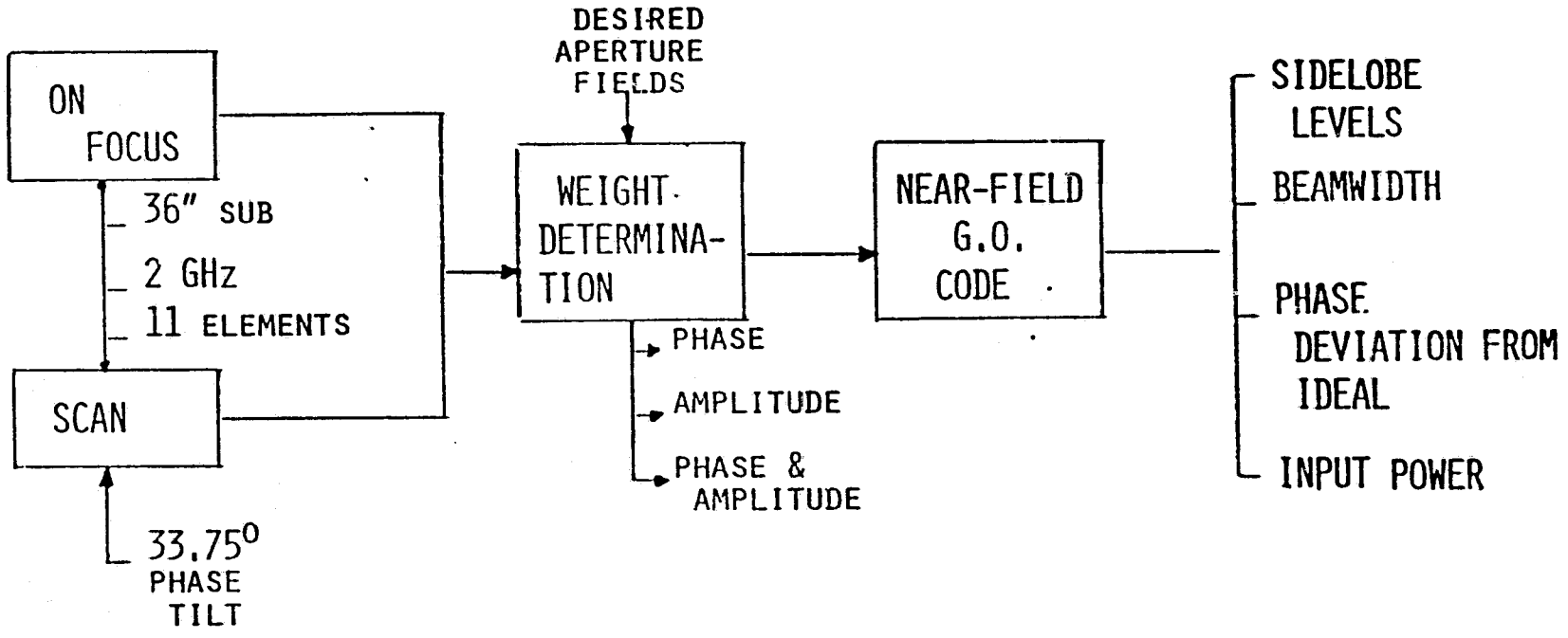

Figure C.1. Flow Diagram of Module Tradeoff

A detailed description of the flow plan is as follows:

CONFIGURATION 1 - CGA, VPS

On-Focus

Elements are initially weighted with tapered amplitude and zero relative phase. We then vary the phase of each element in order to improve the far field performance of the antenna.

Scanned

Elements are initially weighted with tapered amplitude and a constant ϕ_0 progressive phase shift between adjacent elements. ϕ_0 is 33.75^0 in order to produce approximately 2.2^0 of scan in the far field. We again attempt to improve beam performance by varying the phase excitation of each element.

CONFIGURATION 2 - VPA, Constant Phase

On-Focus

Our baseline element excitation is tapered amplitude and zero phase and we attempt to improve beam performance by varying only amplitude weights.

Scanned

Elements are excited with tapered amplitude and a fixed 33.75^0 phase shift between elements (this does not allow for dynamic beam positioning) and attempt to improve beam performance by varying only amplitude weights.

CONFIGURATION 3 - VPA, VPS

On-Focus

Baseline is tapered amplitude and zero phase. Both amplitude and phase weights are varied in order to improve beam performance.

Scanned

Baseline is tapered amplitude and a 33.75^{o} progressive phase shift between elements. Both amplitude and phase weights are varied in order to improve beam performance.

Results are shown in Tables C.1 and C.2. Both on-focus and scanned results indicate that significant improvement in beam performance can be achieved if both amplitude and phase are allowed to vary. It is therefore recommended that both the VPA and VPS modules be incorporated into the phased array design.

Table C.1. On-Focus Results

Parameters	Baseline	Phase Weighting Only	Amplitude Weighting Only	Phase and Amplitude Weighting
Sidelobe Level	-23.19 dB	-24.66 dB	-25.01 dB	-30.91 dB
Beamwidth @ 2 GHz	2.77^{o}	2.72^{o}	2.78^{o}	2.90^{o}
Maximum Phase Deviation From Ideal	11.5^{o}	7^{o}	8.4^{o}	6.5^{o}

Table C.2. Scanned Results

Parameters	Baseline	Phase Weighting Only	Amplitude Weighting Only	Phase and Amplitude Weighting
Sidelobe Level	-8.23 dB	-14.55 dB	-15.01 dB	-18.84 dB
Beamwidth @ 2 GHz	2.45°	2.59°	2.52°	2.73°
Maximum Phase Deviation From Ideal	38.1°	22.0°	27.3°	10.17°
Beam Peak	1.5°	1.45°	1.8°	2.25°